Development of Quantitative Risk Prediction Method of the Guerrilla Heavy Rainfall using Polarimetric Radars and its Application for the Flash Flood Guidance

KIM HWAYEON

2022

Development of Quantitative Risk Prediction Method of the Guerrilla Heavy Rainfall using Polarimetric Radars and its Application for the Flash Flood Guidance

A Dissertation Presented

by

KIM HWAYEON

Submitted to the Department of Civil and Earth Resources
Graduate School of Engineering, Kyoto University
for the degree of

DOCTOR OF ENGINEERING

2022

ACKNOWLEDGMENTS

I got to take a precious time that allowed me to experience many challenges and experiences until I completed this dissertation. I want to express my sincerest thanks and gratitude to the people who contributed to the process of achieving this outcome. It was almost impossible for me to finish this research without their tremendous help.

First of all, I want to express my sincere gratitude to my supervisor, Professor Eiichi NAKAKITA. I can say that even if I wrote thousands of thankful words to him, many words would still be left in my mind to express my gratitude to him. He taught me not only his passion and insight into research but also the necessary attitude to be a better person. I hope I can have his spirit and be a great person. I am also grateful to Professor Kosei YAMAGUCHI for helping me in all aspects, especially for material support and radiosonde experiment. In addition, I am exceedingly obliged to Professor Takahiro SAYAMA as the examiners of this dissertation who make it much better. I would like to thank and appreciate the encouragement of Professor Ying Hsin WU. They gave me meaningful advice from his sophisticated expertise and outstanding knowledge. Indeed, without support, I could not reach this stage.

I am deeply grateful to Professor Deghyo BAE from Sejong University, Seoul, South Korea. I was enrolled in his laboratory from a bachelor's course student to a master's student. He has motivated me with several challenges to continue research and encouraged me to go abroad to do further studies. Thanks to his advice, I could successfully finish my Ph.D. course.

I want to express my thanks to the Nakakita laboratory members. Even though they were busy with their work, they always spent time giving me some comments and cheering me up to be a good researcher. Ms. Mayumi TSUJI and Professor Yukari NAKA have kindly been helping me since I became a Kyoto University student. To the Students who have supported me since the beginning of my life as a student of Kyoto University, Ono AKIYIKI, Guilherme Mendoza Guimarães, Aoi NAKAMURA, Takao MITSUMASA, Ginaldi Ari Nugroho and all my colleagues were kind and enjoyable to help me during living in Japan. I am very sorry for not listing all the

members, especially the Nakakita laboratory members, but I owe to all of you. I also want to express my thanks to the Water Resources & GIS laboratory members. I would like to thank Dr. Jeongbae KIM, KIHS researcher Minkuk KIM, Dr. Moonhwan LEE, Dr. Jaemin SO, Dr. Seonho KIM, Jaeyeong HEO, Geonho MOON, Juhyun PARK, Byeongwook YU, and all my colleagues for giving me the confidence to conduct the study. Mainly, I am exceedingly obliged to Dr. Seongsim YOON. Even though she was very busy with her research, she always spent her time giving me lots of comments and teaching me the way to be a researcher.

My deepest gratitude goes to my family for their constant support and encouragement during my study. In particular, this achievement is for my grandparents Insoo KIM, Bunsun Jeong, parents Yongin KIM, Jeemi KIM, my sister Bomi KIM, and my brother Jaejung KIM and relatives. My special thanks go to my friends for their constant encouragement and to Gitaek LEE for helping me prepare for a job.

Lastly, I acknowledge and value the financial support from the Japan Society for the Promotion of Science for two years. They give me great support in managing my scholarship.

September 2022
Hwayeon KIM

ABSTRACT

Development of Quantitative Risk Prediction Method of the Guerrilla Heavy Rainfall using Polarimetric Radars and its Application for the Flash Flood Guidance

2022

KIM HWAYEON, Ph.D., KYOTO UNIVERSITY

Directed by: Professor Nakakita Eiichi

In Japan, a short period of isolated heavy rainfall that lasts only about 1 hour is referred to as Guerrilla heavy rainfall (GHR). The rapidly growing GHR has caused unpredictable damage to human life and property. Especially, the GHR is one of the triggering factors of flash floods in the small river basin. This is because it has occurred with a small spatiotemporal scale and suddenly appeared in a localized area. So, early detection of GHR is essential to prevent damage and save people's lives.

The Ministry of Land, Infrastructure, Transport and Tourism (MLIT) of Japan has been operating the X-band polarimetric RAdar Network (XRAIN) since 2010. The XRAIN can be used to identify the earlier detection of GHR and detect the precipitation particles in the development stage by three-dimensional observation. Using the XRAIN data, Nakakita et al. (2010) discovered that the first radar echo aloft named “baby rain cell” inside an isolated cumulonimbus cloud is an essential characteristic in the development stage. Then, Nakakita et al. (2017) proposed a methodology by analyzing the vertical vorticity to identify a baby rain cell of guerilla heavy rainfall. It has been proven that the cumulonimbus cloud grows vigorously when the pseudo vorticity is greater than or equal to $0.03s^{-1}$. Also, the early detection and qualitative risk prediction method of GHR is beginning to be used practically in various local governments. This previous research could secure a lead time of 10 minutes before the GHR occurs. The lead time is significant for evacuation and saving lives.

Even with this prediction and monitoring research, it is challenging to prevent disasters caused by GHR. In order to secure more lead time for warning alerts before the occurrence of flash floods, it is necessary to develop a quantitative risk prediction method according to the

development mechanism of GHR by utilizing XRAIN data. In addition, flash floods occur when meteorological and hydrological conditions coexist, so it is necessary to comprehensively consider the rainfall-runoff process through the sewer system. Therefore, this research shows originality in that it proposes a method to bridge the gap between the quantitative risk prediction of GHR and the flash flood prediction system.

In this research, the early detection and quantitative risk prediction method will be developed by using the radar observation variable. Chapter 3 proposes the early detection and quantitative risk prediction method using only radar observation data to minimize human casualties due to GHR. At the beginning of the process of a cumulonimbus cloud, the water vapor in the lower atmospheric layers rises and condenses to generate the precipitation particles which can be defined as the first radar echo or a baby rain cell. After a first rain stage is assigned, the rain stages from 2 to 6 are marked according to the process of convective cell development with a time interval of 5 minutes. When we assigned the rain stage, it is important to calculate the pseudo vorticity which is a measure of the rotation motion of the flow. Therefore, finding the relationship between the predicted risk level and pseudo vorticity is important within 30 minutes (from rain stage 1 to 6) before the maximum rainfall intensity occurs on the ground. To set the predicted risk level, the predicted risk categories (risk levels) are defined at the maximum rainfall intensity on the ground, such as Risk Level 1.0 (under 30 mm/hr), Risk Level 2.0 (between 30 mm/hr and 50 mm/hr), Risk Level 3.0 (between 50mm/hr and 70mm/hr), and Risk Level 4.0 (over 70mm/hr). Then, for predicting the risk levels using pseudo vorticity and reflectivity, the correlation can be represented using multilinear regressions.

It is necessary to make regressions depending on each rain stage because the reflectivity and pseudo vorticity hold different characteristics in different development rain stages of a cloud. To estimate the performance, the rain stage dependent regressions are compared with the total stage regression as a three-dimension scatter and surface plot. The surface plots are useful for showing the relationship of regression analysis among the dependent variable (i.e. predicted risk level) and two independent variables (i.e., reflectivity and pseudo vorticity). The total stage regression shows a positive correlation between the dependent variable and each independent variable. The stage dependent regressions from rain stages 1 to 6 represent the relationship among

the dependent variable and two independent variables. The correlation between predicted risk level and reflectivity shows more positive correlations as the rain stage develops, except for rain stage 1. The correlation between predicted risk level and pseudo vorticity shows positive correlations at the early rain stage. However, at the late rain stage, it becomes difficult to find correlations. So, it is necessary to estimate the risk level of GHR by the stage dependent regressions.

If this method is applied to the field, it is possible to secure lead time for disaster prevention and evacuation. However, even if the baby rain cell can be detected, it is difficult to predict which convective cell will develop. To discriminate the risk more precisely, Chapter 4 and 5 describe the method for improving the accuracy of the quantitative risk prediction. Chapter 4 considers the performance of added independent variables with different characteristics depending on the time. It has the potential to improve reliability and accurate risk prediction by adding more explanatory variables (i.e., reflectivity, vorticity, divergence, and updraft). In addition, Chapter 5 analyze the relationship and predict the risk level by reflecting on the physical mechanism. The accuracy of the quantitative risk prediction was considered according to the characteristics of the variables that have different characteristics depending on each rain stage and life cycle.

The quantitative risk prediction method has been improved to more accurately alert the risk of guerilla heavy rainfall by finding the best combination of variables. The multilinear regressions are expressed by combining the divergence and updraft based on reflectivity and vorticity. Using Pseudo radar analysis and multiple Doppler radar analysis, a part correlation coefficient shows how the explanatory variables explained the predicted risk level. The combinations of variables have conditions in common that the vorticity and reflectivity are very important at the early and late rain stage, respectively. We focus on the early rain stage for saving evacuation time to escape from danger because the GHR occurs within a few minutes. So, vorticity is the most explanatory variable to estimate the predicted risk level before the maximum rainfall reaches the ground. Then, the multilinear regression with the highest accuracy is chosen by using the Receiver Operating Characteristic (ROC) analysis and the Area Under ROC Curve (AUC) analysis among the combinations of variables. As a result of the highest accuracy, the multilinear regression of reflectivity, vorticity, divergence, and updraft has 83% accuracy (AUC= 0.83). Therefore, the risk

level of localized heavy rainfall could be predicted using the improved regression with high accuracy.

Flash floods occur depending on natural and human factors, including the duration and intensity of rainfall and watershed characteristics. Chapter 6 describes the flash flood guidance (FFG) (Georgakakos, 2006) was estimated to alert flash flood warnings for the watersheds of the Toga River basin in Japan. The FFG is the amount of precipitation needed in a specific period of time to initiate flooding in a watershed. In order to obtain FFG at a specific time (t), the estimation of threshold runoff (TR) and soil moisture deficit (SD) is needed as components of FFG. TR was estimated using topographic data (topographic data, land use, etc.), river, and watershed characteristic factors (watershed area, river width, river slope, etc.). Also, the soil moisture conditions were simulated by using the SWMM rainfall-runoff model. SWMM was set up by using hydrological and GIS data collected for the Toga River basin in which the rural and urban land uses affect the flood runoff analysis. The optimal rainfall value of threshold runoff was 13.42 mm per 10min on average. The advantage of this method is that after estimating the optimal rainfall values, flash flood warnings can be issued without the need to consider the entire hydro-meteorological models.

In conclusion, the GHR was predicted by comprehensively considering the rainfall-runoff process of flash floods affected by meteorological and hydrological conditions. Conclusions are detailed in Chapter 7, along with the limitations and further studies of this research.

Contents

List of Figures

List of Tables

CHAPTER 1

Introduction

1.1 Background

Recently due to the effects of climate change, localized heavy rainfall caused by convective cells have frequently occurred in Japan, which has not been experienced in the past. Especially, the guerilla heavy rainfall is one of the triggering factors of flash floods in the small river basin. The rapidly growing isolated single cumulonimbus cloud caused unpredictable damages to human life and property. On July 28 of 2008, fifty people have washed away and five people were killed by a tragic flash flood in Toga River, Kobe city. Figure 1.1 shows the change of water level in 10 minutes. The water level rose 1.34 meters just in 10 minutes.

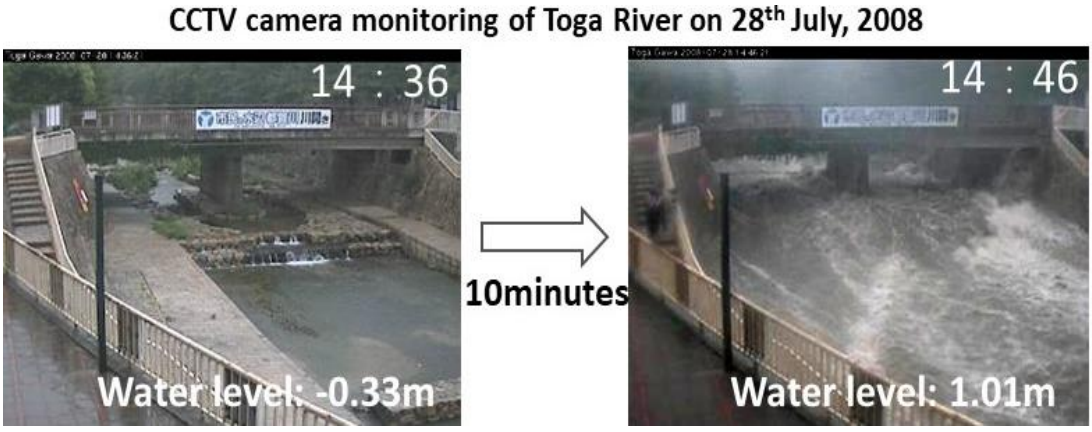

Figure 1.1 Flash flood occurrence in Toga River on 28th July 2008.

Weather radars predicted heavy rainfall observation during the Toga River disaster. However, some flow through the sewer system immediately occurred and brought a large amount of lateral inflow to the river after precipitation was detected by radars, so the conventional

prediction system could not detect the danger. To prevent the tragic disaster from happening again, it was emphasized the importance of securing a short lead time and the problem of disaster prevention in the monitoring system of the weather radar. It is necessary to consider the rainfall-runoff process comprehensively.

Guerrilla heavy rainfall is characterized by isolated and developing cumulonimbus clouds. Figure 1.2 conceptually represents the development process of an isolated cumulonimbus cloud. The development process is broadly divided into three stages: development, maturity, and dissipation. In the first development stage, unstable atmospheric conditions and moist air rise and condense to form clouds. The cloud particles are too small to be detected by weather radar, but the particles can be observed by using cloud radars. In the second development stage, cloud particles gather and precipitation particles are formed only in the sky. Weather radars can also detect these precipitation particles. These particles are called a baby rain cell of guerrilla heavy rainfall. In the first maturity stage, this baby rain cell develops and the height of the clouds gradually increases with the updraft. However, since precipitation only accumulates and develops in the sky, there is no precipitation on the ground around this stage. In the late maturity and early dissipation stage, cloud particles grow into raindrops, and the updraft turns into a downdraft as it pulls the surrounding air down. Eventually, the precipitation sufficiently accumulated inside the cloud is not supported by the updraft. The amount of precipitation is weakened in the dissipation stage. The development process occurs in 30 minutes to less than an hour. In this research, 'isolated cumulonimbus clouds that develop until rainfall of 50 mm/h or more occurs within 30 minutes on the ground' was selected as a target event criterion of the guerrilla heavy rainfall.

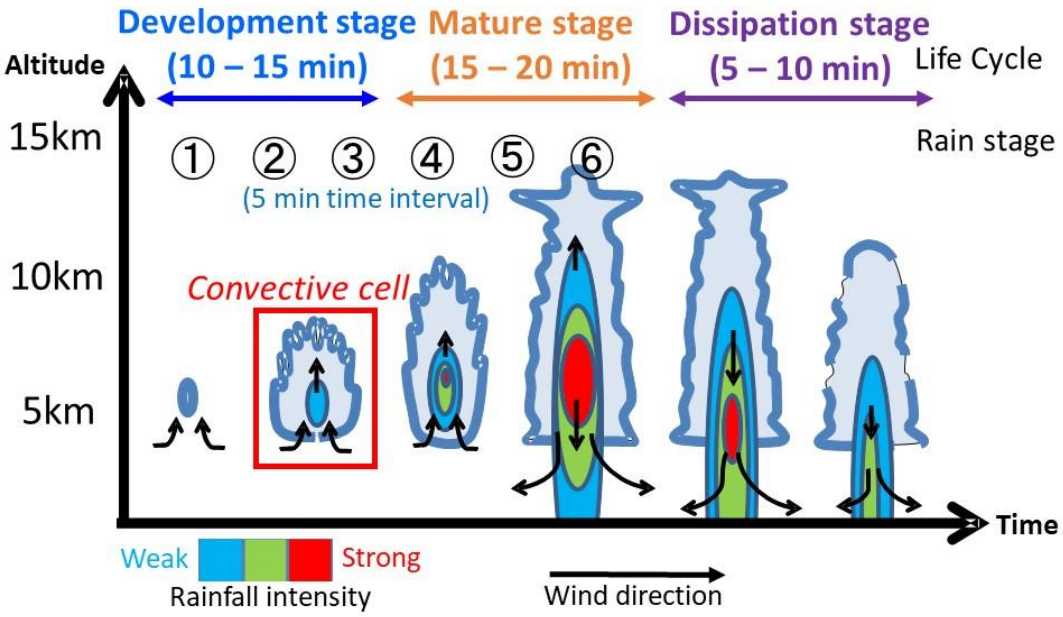

Figure 1.2 Guerrilla heavy rainfall occurrence process.

Early detection of guerilla heavy rainfall is an essential method to prevent damage and save people's lives. Research on heavy rainfall prediction and monitoring technology for disaster prevention purposes has been conducted for many years. However, the guerilla heavy rainfall has occurred with small spatiotemporal scale and suddenly appeared in a localized area. Even with these predictions and monitoring research, it is difficult to prevent disasters caused by guerilla heavy rainfall. So, the Ministry of Land, Infrastructure, Transport and Tourism (MLIT) of Japan has been operating the X-band polarimetric RAdar Network (XRAIN) since 2010. The XRAIN can be used to estimate the rainfall quantitatively and predict the earlier detection of guerilla heavy rainfall. In order to secure more lead time for warning alerts before the occurrence of a flash flood, it is necessary to investigate the mechanism of guerilla heavy rainfall and to develop a quantitative risk prediction method by utilizing the XRAIN data.

1.2 Literature Review

1.2.1 The early detection of guerilla heavy rainfall

For early detection of guerilla heavy rainfall, Nakakita et al., 2010 discovered that the first radar echo aloft named as “baby rain cell” inside an isolated cumulonimbus cloud is an important characteristic in the development stage. XRAIN data can be used to detect the precipitation particles in the development stage by three-dimensional observation. This became one of the chances for the MLIT to introduce the effectiveness of XRAIN data in the field (Figure 1.3).

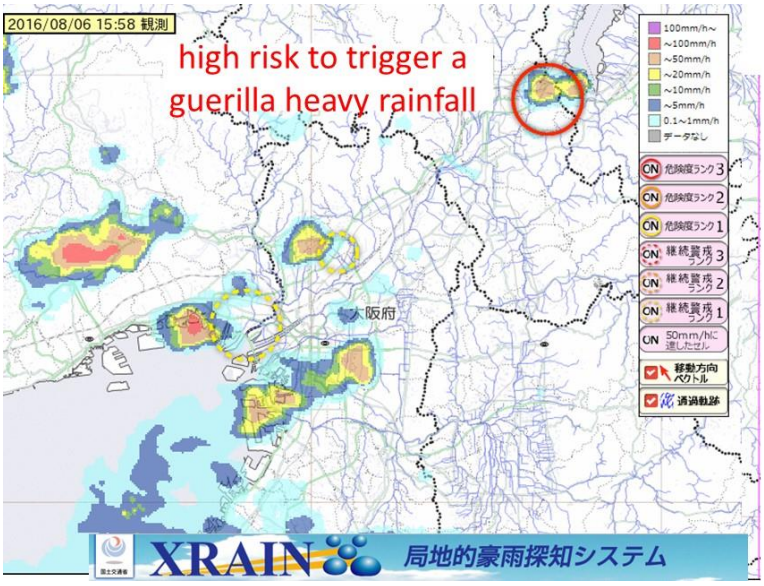

Figure 1.3 The real-time of early warning system based on baby rain cell detection.

Nakakita et al., 2014 have proposed a methodology by analyzing the vertical vorticity to identify the baby rain cell of guerilla heavy rainfall. A weak vertical shear formed a horizontal vortex, which was lifted by the buoyancy to form vertical vorticity. The vorticity has been shown to be very effective in the risk prediction of guerilla heavy rainfall. Also, it has been proven that

the cumulonimbus cloud grows strongly when the vorticity is greater than or equal to $0.03s^{-1}$. Katayama et al., 2015 and Nakakita et al., 2017 developed early detection system with auto-tracking and qualitative risk prediction. According to case studies, this system can detect baby rain cell an average of 23.6 minutes earlier before it rains on the ground with rain gauges (Figure 1.4). Also, the early detection and risk prediction of guerrilla heavy rainfall is beginning to be used practically in various local governments. This previous research could secure a lead time of 10 minutes in guerilla heavy rainfall. Although the lead time is about 10 minutes, the time is very important for evacuation and saving lives.

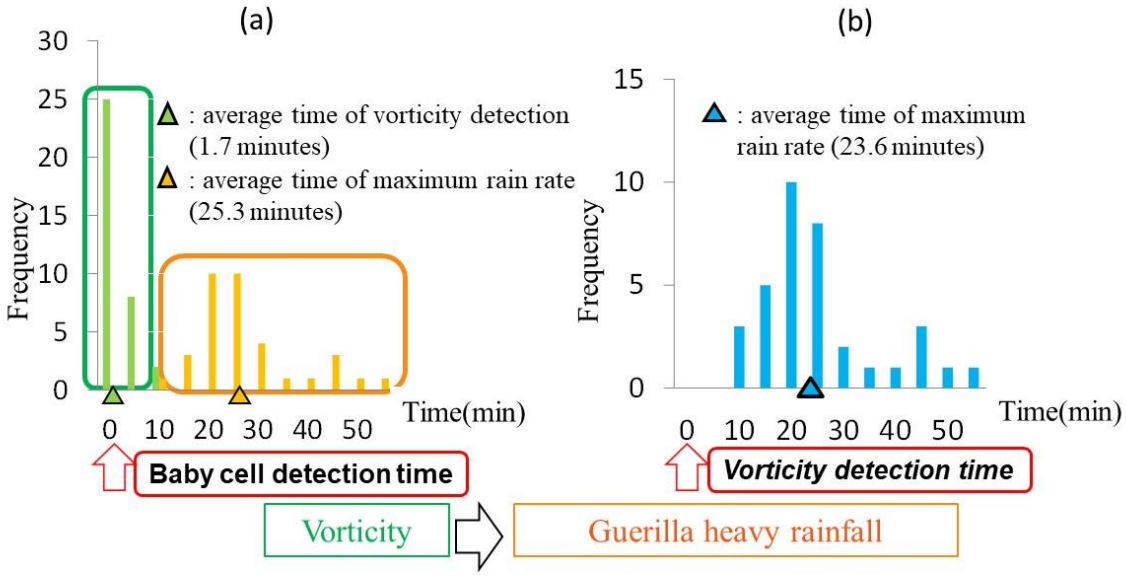

Figure 1.4 The statistics of the elapsed time since the first echo of a rain cell was detected: (a) green bars: the time interval between the vorticity detection and the first radar echo detection; orange bars: the time interval between the maximum rainfall intensity observation and the first echo detection; (b) blue bars: the time interval between the maximum rainfall intensity observation and the vorticity detection (Nakakita et al., 2017).

However, there are still unclear points about the physical cloud condition for guerrilla heavy rainfall development. The vorticity, divergence, and vertical wind are important variables at the beginning of isolated single cumulonimbus cloud development. The research has been conducted to analyze the relationship between the variables and the development process of cumulonimbus clouds. Especially, a strong updraft in the cloud not only inhibits the fall of the droplet (Ahrens, 2012) but also carries the droplet into the upper level, which will increase the probability of the growing size of the droplet (Zeng et al., 2000; Kim et al., 2012). Many of the updraft analyses are statically related to its intensity value. Still, some suggest that the position and its interaction with the surrounding flow properties of the updraft are also important for the process of precipitation development (Kim et al., 2012). Therefore, it is important to explicate the mechanism of how the variables (i.e., the vorticity, divergence, and vertical wind) is involved in the development process of cumulonimbus clouds. In order to predict the risk more accurately than the previous research, we aim to develop and improve the accuracy of quantitative risk prediction by considering the performance of variables with different characteristics depending on the development process. It could be used practically as information of risk prediction of guerrilla heavy rainfall.

1.2.2 Flash flood warning system

Flash floods are the deadliest natural disasters with significant socioeconomic effects and the highest average mortality rate among different types of floods (Jonkman, 2005). Flash floods are associated with localized, heavy rainfall events on small and medium watersheds. Due to the unusual short response time, there are some difficulties in controlling flash floods. Additionally, the climate change has increased the number of extreme rainfall events and the risk of flash floods

(Gregory and Mitchell, 1995; Palmer and Raisanen, 2002). Therefore, a reliable flash flood predicting model is necessary to respond the flash floods properly.

In order to decide the occurrence of flash floods, there are three methods: the flash flow comparison method, flood susceptibility assessment, and rainfall comparison method (Hapuarachchi et al., 2011). The flow comparison method has a criterion for determining whether flooding is expected by comparing the modeled flow rate with the observed flood threshold. Yoon and Nakakita, 2015 developed a nomograph (i.e., a lookup table) for the Toga River in Japan, which is a graphical representation of the peak flows. However, this approach requires long historical data and hydrological simulation to establish the observed frequency distribution. Also, the flash flood susceptibility assessment can be considered as a useful first step in determining the contributing factors to the flash flood vulnerability of a catchment using limited data (Collier and Fox, 2003). The rainfall comparison method does not compare the simulated flood with the flood flow but can compare the threshold rainfall that generates the flash floods. This method is needed as warn of the imminent flash flood. The typical method is Flash Flood Guidance (FFG) (Carpenter et al., 1999; Carpenter and Georgakakos, 1993). This method is easily understood by the general public and is widely used in flash flood forecasting. This study derives the variables that have the greatest influence on the determination of flash floods related to topographical information and the importance of soil moisture estimation. The Flash Flood Guidance could be an important method for issuing flash flood warnings based on rainfall information only.

Over the past few years, increased public and governmental attention to improving flash flood warnings has been called for in many parts of the world including the United States, the European Union, and Australia (Handmer, 2001, Penning-Rowsell et al., 2000). As the need for countermeasures to reduce flash flood damage is increasing, studies for flash flood warnings have

been conducted, such as flash flood warning systems, flash flood index, and flood risk. Among them, in the case of the flash flood warning systems, the Flash Flood Guidance was mainly conducted to develop flash flood warning systems. The National Weather Service (NWS) first introduced the basic concept of Flash Flood Guidance in the mid-1970s by using the Geographic Information System (GIS) on watersheds. Recently, the National Weather Service Meteorological Development Lab (MDL) collected and managed various weather data such as ground observation networks, GOES satellites, and radars with a large-capacity Advanced Weather Interactive Processing System (AWIPS). In addition, a Flash Flood Monitoring and Prediction (FFMP) model was proposed using AWIPS. Such as the European Flood Warning System (EFAS), the Malaysian Monsoon Flood System (GEOREX), and the Thailand Flood Forecast Design Support System (DSS), various flash flood warning systems which are developed by NWS have been introduced and used. In Korea, Bae and Kim (2007) developed the Korea Flash Flood Guidance (KoFFG) by using hydrological and radar meteorological components by considering the topographical characteristics of the watershed. This previous research could provide accurate information to prepare for flash flood damage. Therefore, there is a need for a method that can easily estimate and judge whether a flash flood has occurred so that people can escape more quickly.

1.3 Research Aims and Objectives

This study aimed to predict the flash floods on the guerilla heavy rainfall by comprehensively considering the rainfall-runoff process affected by meteorological and hydrological conditions. The objectives of this study as follows:

1) To accurately predict the risk level of guerrilla heavy rainfall, this research aims to develop the quantitative risk prediction method by using the variables. The early detection and

quantitative risk prediction method will be developed using pseudo vorticity and reflectivity. To discriminate the predicted risk level precisely, it is necessary to consider the performance of variables that have different characteristics depending on the development process of guerilla heavy rainfall over time.

2) The accuracy of the quantitative risk prediction has been improved when the risk level was predicted by adding the variables which are reflectivity, vorticity, divergence, and vertical wind with Pseudo and multiple Doppler radar analysis.
3) In chapter 3 and 4, the method can predict the risk of guerilla heavy rainfall with a time interval of 5 minutes. However, the process from a rain cell into the guerilla heavy rainfall takes about 30 minutes to an hour and varies according to each case. In order to be generally applied to the guerrilla heavy rainfalls, the life cycle, which is the development stage of guerrilla heavy rainfall based on a physical description, was considered. It is expected to analyze the relationship and predict the risk level by reflecting the physical mechanism.
4) The rainfall-runoff process affected by meteorological and hydrological conditions has to be considered to predict flash floods comprehensively. The flash flood guidance method is applied in the Toga River basin to prevent flash floods. The advantage of the method is that after estimating the optimal rainfall values, flash flood warnings can be issued without the need to consider the entire hydro-meteorological models.

1.4 Outline of Dissertation

This dissertation consists of seven chapters. The main analysis from chapter 3 to chapter 5 contains the development of a quantitative risk prediction method according to the development mechanism of guerrilla heavy rainfall by utilizing XRAIN data. In chapter 6, the analysis has been

conducted by applying the flash flood guidance to the watersheds in the Toga River basin. Figure 1.5 shows the roadmap of this dissertation. The rectangles represent each chapter's title and objective, and the arrow represents the relation between the chapters. A brief explanation of each chapter is following;

Chapter 2 introduces the study area, data, and target event. Kinki region is the study area. Especially, the Toga River basin is a metropolitan city with many residents. To consider the sewage systems, the quantitative risk prediction and flash flood warning system are necessary to alert the occurrence of guerrilla heavy rainfall. The four X-band polarimetric RAdar Network (XRAIN) are used: Rokko, Katsuragi, Juubusan, and Tanokuchi. The Digital Elevation Model (DEM) was downloaded from the Geospatial Information Authority of Japan. Also, the flow observation data from MLIT and a cross-section of the Toga River from Hyogo prefecture were collected.

In Chapter 3, the early detection and quantitative risk prediction method was developed by using only radar observation data to minimize human casualties due to guerrilla heavy rainfall. It shows the relationship among the predicted risk level, reflectivity, and pseudo vorticity within 30 minutes (from rain stage 1 to 6) before the maximum rainfall intensity occurs on the ground. Since reflectivity and pseudo vorticity have different characteristics depending on the rain stage, it is shown that the relationships are required for each rain stage. The correlation between predicted risk level and reflectivity shows more positive correlations as the rain stage develops, except for rain stage 1. The correlation between predicted risk level and pseudo vorticity shows positive correlations at the early rain stage.

To discriminate the risk more precisely, chapter 4 and 5 describe the method for improving the accuracy of the quantitative risk prediction. Chapter 4 considers the performance of added

independent variables that have different characteristics depending on the time. It has the potential to improve reliability and accurate risk prediction by adding more explanatory variables (i.e., reflectivity, vorticity, divergence, and vertical wind). In addition, chapter 5 analyze the relationship and predict the risk level by reflecting on the physical mechanism. The accuracy of the quantitative risk prediction was considered according to the characteristics of the variables that have different characteristics depending on each rain stage and life cycle. The combinations of variables have conditions in common that the vorticity and reflectivity are very important at the early and late rain stage, respectively. We focus on the early rain stage for saving evacuation time to escape from danger because the guerrilla heavy rainfall occurs within a few minutes. So, vorticity is the most explanatory variable to estimate the predicted risk level before the maximum rainfall reaches the ground.

Chapter 6 describes the flash flood guidance (FFG) was estimated to alert flash flood warnings for the watersheds of the Toga River basin in Japan by using hydrological and GIS data. The FFG is the amount of precipitation needed in a specific period of time to initiate flooding in a watershed. The optimal rainfall values for the flash flood warning threshold were between 9.97 and 23.89 mm per 10min. The advantage of this method is that flash flood warnings can be issued after estimating the optimal rainfall values without considering the entire hydro-meteorological models.

Finally, Chapter 7 summarizes this research with the conclusion, limitations, and further research relevant to this study.

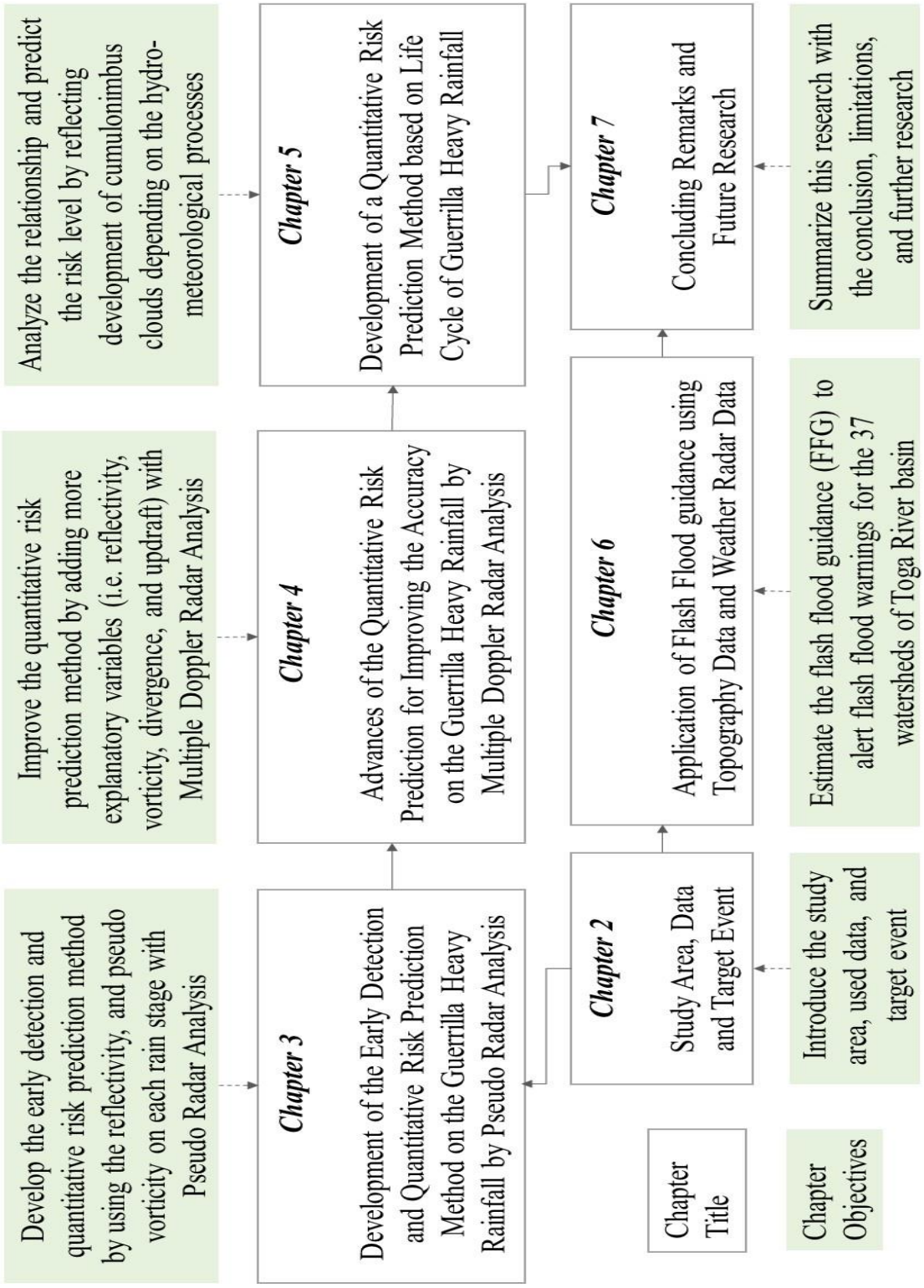

Figure 1.5 Roadmap of this thesis.

CHAPTER 2

Study Area, Data and Target Event

2.1 Study Area

This research's study area is the Kinki region, referred to as the Kansai region. This region is located in the middle south of the Japanese island of Honshu. There are seven prefectures in the Kinki region: Hyogo, Kyoto, Mie, Nara, Osaka, Shiga, and Wakayama. Kyoto, Osaka, and Kobe in Hyogo are metropolitan cities with many residents. So, it is necessary to consider the sewage systems for flash flood warning systems. Especially, the Toga River in Kobe has two small tributary streams: the Rokko and Somatani rivers. The length of the Toga River is 1.79 km, and according to MLIT, the total basin area is 10.98 km^2. As a role of the hydrophilic River, the side stairs were installed, and the walls of the riverfront are fixed with concrete. The residential houses and paved streets are occupied mostly from the lower Toga River basin up to the foot of the mountains. Although the duration of the guerrilla heavy rainfall lasted only about 20 minutes, the Toga River has been affected from upstream of the river and a large amount of lateral inflow to the river through the sewer system. So, as a previous study, Fujita and Kunita 2010 installed a storm drainage system to prevent inland floods and most of the inland water is conveyed to the main river via pipes or ducts. Therefore, it is very necessary to develop a risk prediction system considering the occurrence of guerilla heavy rainfall and flash floods. This is the reason why the Kinki area was chosen as the study area.

2.2 Data

2.2.1 Weather radar data

To provide high spatiotemporal observation data throughout Japan, the Ministry of Land, Infrastructure, Transport, and Tourism (MLIT) of Japan has been operating the X-band polarimetric RAdar Network (XRAIN) since 2010. As of now, the MLIT has installed 39 X-band multi-parameter (X-MP) radars. X-band multi-parameter RAdar Network is especially designed for estimating rainfall quantitatively. It is expected that XRAIN can be used to predict the occurrence of flash floods on small river basins. Figure 2.1 illustrates the positions of the radar sites and their observation ranges in the Kinki region among 39 XRAIN radars. The detailed specification of XRAIN can be tabulated in Table 2.1.

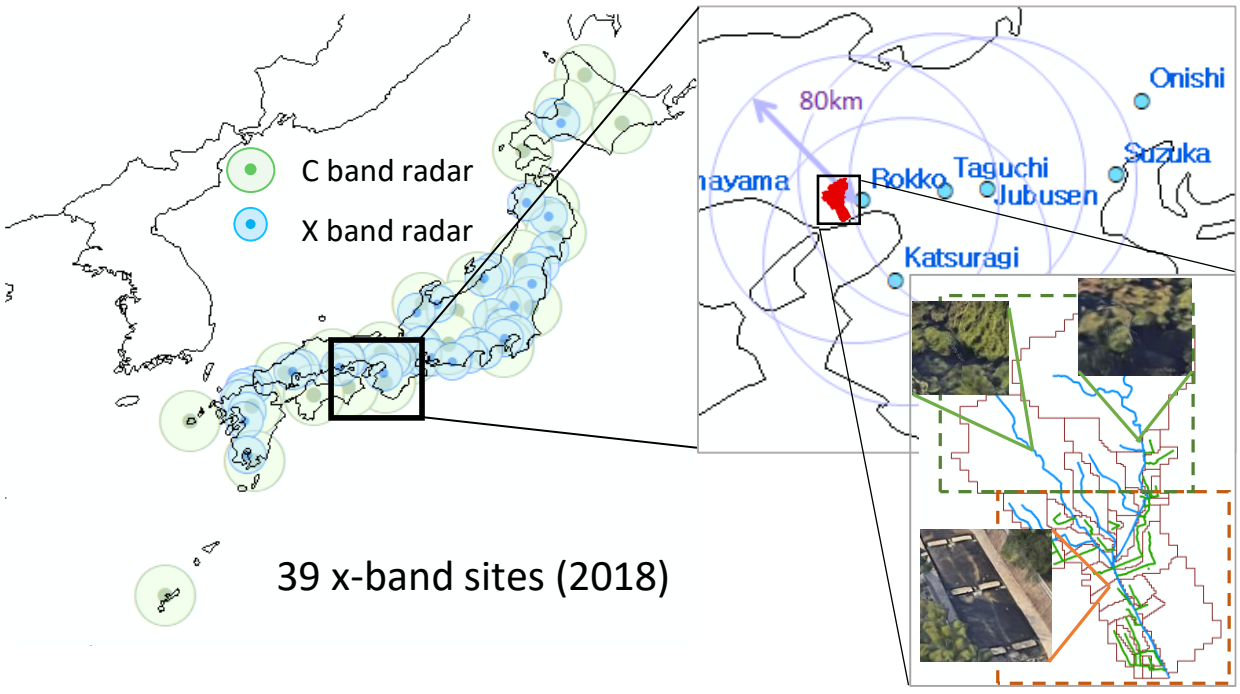

Figure 2.1 The detection range of radars, study area of guerrilla heavy rainfall and flash flood.

Table 2.1 Detailed specifications of X-band multi-parameter RAdar Network

Features	**Specifications**
Microwaves amp.	Klystron or solid state device
Frequency	9700 MHz – 9800 MHz
Transmit power	100 kW
Pulse width	1.0 μ sec.
Occu. bandwidth	≤ 4 MHz
Pulse Rep. Freq.	1200 Hz – 1800 Hz
Antenna	Parabola, ϕ ≤ 2.2 m
Antenna gain	≥ 42 dBi
Beam width	≤ 1.2o
Polarization	H & V, Simultaneous transmit/reveive
Min. Sensitivity	≤ -110 dBm
Observation range	80 km
Elevation angle	12
Polarization	Dual polarization
Wavelength	3 cm
3D scan time	5 minutes (12 PPI scans)
Data resolution	150 m (range) 1.2o (azimuth)
Sampling number	100 (approximately, at PRF=1800 Hz
Output parameters	PrH,nor, PrV,nor, PrH,mti, PrV,mti, V, W, ϕDP, ρHV (Reflectivity, Doppler velocity, polarimetric parameters,)

The four radars of XRAIN in the Kinki region are in Rokko, Katsuragi, Juubusan, and Tanokuchi. Scanning for each radar takes 20 seconds. It means that three different angle scanning are possible in one minute. More specifically, to obtain three-dimensional volume scan data, a one-time scanning at a low angle and two-times high angle scanning are performed every minute. The 12 different angles were divided to complete the volume scan up to the highest angle. The XRAIN of the Kinki region could produce composite radar images for every one minute and provides complete volume scan data every 5 minutes.

Horizontal reflectivity and Doppler velocity, which are the two types of observation data, are used for the three-dimensional volume scan data. First, to get formatted data from the raw volume scan data, the cylindrical coordinate system of the raw data is converted into a three-dimensional rectangular coordinate system. Considering that the beam pulse resolution of the XRAIN is 150m, the cylindrical coordinate data is interpolated and extrapolated to generate three-dimensional cubic grid data with 200m resolution. For the reflectivity data only, with noise reduction, the reflectivity data is smoothed again to 250m horizontal resolution and 500m vertical resolution. Then, the reflectivity and differential reflectivity (ZDR) of volume data taken over five minutes from each radar are corrected using the specific differential phase (KDP). Detailed specifications of three-dimensional data can be seen in Table 2.2.

Table 2.2 XRAIN three-dimensional data

Horizontal grid spacing	250 m
Vertical grid spacing	500 m
Maximum altitude	10 km

2.2.1 Topographical data

In this research, the topographical data affecting the flash floods are Digital Elevation Model (DEM), land use, and soil. The topographical data of watersheds are combined with the crust of the earth's surface, the slope of flows and hollow filling, elevation and position of slopes, etc. Indeed, the process of infiltration in delta watersheds will be greater than in hilly watersheds. The steeper the watershed, the higher the flow coefficient and the lower the surface flow loss. Especially, the direct influence on the river is especially evident in small watersheds where mostly

surface water supplies to the rivers, and groundwater is negligible. However, in different topography areas, the dependence of the above factors on the watershed is very different. It is affected by regional variations in factors such as groundwater depth, evaporation, etc. In addition, vegetation cover has the ability to change the structure and hydraulic properties of the soil. Thus, the topographical characteristics of watersheds are closely related to flash floods.

The climate mostly affects soil conditions. The soil conditions with different physical and chemical properties on the watersheds affect the flow through evaporation and soil properties. In particular, soil moisture is often considered the most important property for flash floods. Once the soil is saturated, there is no space for additional rainfall to infiltrate. On the other hand, when the soil is dry, large amounts of rainfall infiltrate rather than runoff. Surface runoff occurs when rainfall exceeds the infiltration capacity. Therefore, it is necessary to predict flash floods in consideration of topographical data.

2.3 Target Event

In this research, the target event is localized heavy rainfall caused by a single cumulonimbus cloud known as guerilla heavy rainfall (GHR) in Japan. The guerilla heavy rainfall occurs in the area of around 10 km^2 and less than one hour. Especially, the guerilla heavy rainfall frequently occurs around the summer season (June-August) in the climate of Japan. Due to the heating from the sunlight and the highest temperature, the convection causes the guerilla heavy rainfall. So, from August 2013 to August 2018, 7 GHR events were selected in the Kinki region. Additionally, from July 2012 to July 2020, 4 flash flood events were selected in the Toga River basin.

CHAPTER 3

Development of the Early Detection and Quantitative Risk Prediction Method on the Guerrilla Heavy Rainfall by Pseudo Radar Analysis

Abstract Guerrilla heavy rainfall occurs in 30 minutes to less than an hour until rainfall of 50 mm/h or more occurs on the ground. The guerrilla heavy rainfall causes a disadvantage of a very short lead time for early warning and evacuation. For predicting disasters triggered by guerrilla heavy rainfall, it is necessary to develop an early detection and quantitative risk prediction method. By using the early detection method, the existence of the first echo of hydrometeors in a convective cell was identified. Then, to predict the risk of guerrilla heavy rainfall, the risk prediction is categorized into four risk levels based on the maximum rainfall intensity of the rain cell. The relationship among the predicted risk level, reflectivity, and vorticity within 30 minutes (from rain stage 1 to 6) was considered depending on the total and each rain stage to investigate the performance. The multilinear regression equations for risk levels are fitted by 7 guerrilla heavy rainfall events. A Receiver Operating Characteristic (ROC) analysis verifies the most appropriate multilinear regression equation. As a result, it is possible to quantitatively predict the risk based on the different characteristics according to the development of the convective cell with high accuracy of 84% at the early rain stage.

3.1 Introduction

Recently, localized severe heavy rainfalls, which have not been experienced in the past, have frequently occurred in Japan due to the effects of climate change (Miyasaka et al., 2020). Especially, the guerilla heavy rainfall by isolated rapidly growing single cumulonimbus is one of the phenomena triggering flash floods in a small river basin and has caused huge damage to human

life and property. In this study, guerilla heavy rainfall is defined as a target event with 50 mm/hr or more precipitation observed on the ground within 30 minutes. In 2008, fifty people have washed away and five people were killed by a tragic flash flood caused by guerilla heavy rainfall in Toga River, Kobe city. It is quite difficult to observe and forecast the cells which rapidly developed and disappeared within several minutes to hours with a small spatiotemporal scale. Therefore, it is important to identify the risk of heavy rainfall in advance. In the previous studies, Nakakita et al., 2014 developed a qualitative risk prediction method based on the early detection of the aloft cells as the radar first echo and an automatic cell tracking of the further developing convective cells. This method can predict whether the early detected cells become heavy rainfall or not, and it has been practically utilized in real-time prediction in Japan by the Ministry of Land, Infrastructure and Tourism (Kim and Nakakita, 2020).

However, even with the prediction and monitoring system, it is difficult to prevent disasters caused by guerilla heavy rainfall with a small spatiotemporal scale. Also, the current system could predict the risk level of only two risk categories, i.e., heavy rainfall with maximum rainfall intensity of more than 50 mm/h or not. This is still not enough to discriminate the risk precisely. Therefore, for more accurate and efficient prediction, this research aims to develop a quantitative risk prediction method by using risk levels. The risk level was classified by the maximum rainfall intensity at the height of 2 km close to the ground surface. In addition, Nakakita et al., 2017 discovered the relationship between the growth of the rain cell and vorticity behavior. So, in this research, the early detection and quantitative risk prediction method will be developed by using vorticity and radar reflectivity.

3.2 Data and Methodology

3.2.1 Reflectivity and pseudo vorticity from X-band multi-parameter (X-MP) radar data

In this research, four X-band multi-parameter radars are used in the Kinki region by the Ministry of Land, Infrastructure and Transport. Radio Detection And Ranging (Radar) detects distant objects and measures the distance by emitting electromagnetic waves. The electromagnetic wave emitted from the radar antenna hits the objects, and some of the scattered electromagnetic waves are received. The received electromagnetic wave measures the position of the target and the time for the round trip of the electromagnetic wave. The intensity of the reflected wave or the change in phase could measure the characteristics or size of the target. Depending on the length of the wavelength of the electromagnetic wave, the size of the object is different. The X-MP radar corresponds to a wavelength of about 3 cm in the frequency band of 9 GHz. It is suitable for the observation of precipitation with a diameter of 0.1 to several mm. The X- MP radars do the scanning while changing the elevation angles and three-dimensional observation once every 5 minutes.

Among the radar observation data, the radar reflectivity is expressed by the following equation,

$$Z = \int N(D) D^6 \, dD. \tag{3.1}$$

where Z [$mm^6 m^{-3}$] is the radar reflectivity factor, $N(D)$ is the number of drops with a given diameter, and D [mm] is the drop size. As can be seen from Equation (3.1), the radar reflectivity

is a function of drop size, and the amount of radar reflectivity increases when it rains heavily or the drop size is big.

The X-MP radar is a Doppler radar and captures the motion of observation with the Doppler mechanism. The wind velocity observed with the Doppler radar is called the Doppler wind velocity and is calculated from the radar wavelength and the Doppler frequency. The Doppler frequency is a change in frequency that occurs in a received signal as the object moves. v [m/s] is Doppler wind velocity. If the direction away from the radar is positive, f_d [/s] is the Doppler frequency and λ [m] is the wavelength. It is expressed as

$$v = -\frac{\lambda f_d}{2} . \tag{3.2}$$

Using the Doppler wind velocity, the pseudo vorticity was estimated as follows by Nakakita et al., 2011. In the Northern Hemisphere, vertical vorticity (referred to as vorticity) assumes positive values of low pressure rotation (counterclockwise). The vertical vorticity (ζ) in a Cartesian coordinate system can be expressed as

$$\zeta = \frac{\partial v}{\partial x} - \frac{\partial u}{\partial y} . \tag{3.3}$$

where u [m/s] and v [m/s] represent the horizontal wind velocities of each x and y direction. In the polar coordinate system, the vertical vorticity (ζ) can be written as

$$\zeta = \frac{1}{r}\left\{\frac{\partial}{\partial r}\left(r v_{\varphi}\right) - \frac{\partial v_r}{\partial \varphi}\right\} . \tag{3.4}$$

where v_r and v_{φ} are the wind velocities of each r and φ direction. The Doppler wind velocity can be detected only in the direction of the radar beam. So, the information on the right-hand side of Equation (3.4) can be obtained. Nakakita et al., 2011 proposed a method to approximate the vorticity by using the different wind velocity directions of the radar beam. The different wind velocity direction assumes that vorticity exists. In this study, the vertical vorticity was calculated by dividing the different directions of wind velocity by distance. The vertical vorticity can be expressed by the following equation,

$$\zeta = \frac{v_a - v_b}{\Delta x} \ . \tag{3.5}$$

where v_a [m/s] and v_b [m/s] are the Doppler velocity between adjacent cells. Nakakita et al., 2017 found the relationship between the growth of the rain cell and vorticity. To fully understand the structure of guerilla heavy rainfall, the radar observation data were visualized as Constant Altitude Plan Position Indicator (CAPPI). The detailed reason is described in Appendix A.

3.2.2 The development of the quantitative risk prediction method

For predicting the risk triggered by guerilla heavy rainfall, it is necessary to identify a first radar echo. At the beginning of the process of an isolated cumulonimbus cloud, the water vapor in the lower atmospheric layers rises in an atmospheric instability condition. Also, the precipitation particles are condensed to generate the first radar echo or a baby rain cell. Then, a first rain stage

is assigned. In this research, the rain stages from 2 to 6 are marked according to the process of isolated convective cell development with a time interval of 5 minutes. When we find out the existence of the first echo, it is important to calculate the vorticity which is a measure of the rotation motion of the flow. Because not every first radar echo develops into a severe heavy rainfall, Nakakita et al., 2017 have proposed that the behavior of the vorticity is related to the growth of rain cell. They have found that a rain cell that caused guerilla heavy rainfall had vertical vorticity values greater than or equal to $0.03s^{-1}$. Also, it has been clarified that the first echo was detected about 25 minutes on average before the maximum rainfall occurred on the ground. Flash floods occur in 30 minutes to less than one hour. Therefore, finding the relationship between the predicted risk level and vorticity is important within 30 minutes (from rain stage 1 to 6) before the maximum rainfall intensity occurs on the ground. From August 2013 to August 2018, 7 guerilla heavy rainfall events were selected and tabulated in Table 3.1.

Table 3.1 List of guerrilla heavy rainfall events

No.	Date	No.	Date
1	2013-08-06	5	2016-08-03
2	2013-08-07	6	2016-08-25
3	2015-08-07	7	2018-08-13
4	2015-08-29		

To set the predicted risk level, the predicted risk categories (risk levels) are defined at the maximum rainfall intensity on the ground, such as Risk Level 1.0 (under 30 mm/hr), Risk Level 2.0 (between 30 mm/hr and 50 mm/hr), Risk Level 3.0 (between 50mm/hr and 70mm/hr), and Risk Level 4.0 (over 70mm/hr). The risk of terminology represents the severity of the localized heavy rainfall intensity. To predict the risk levels by using radar observation data, we need to select an appropriate set of explaining variables. Referring to previous research, the vorticity and radar

reflectivity were selected as explaining variables. Then, for predicting the risk levels by using the observed and calculated variables, the correlation can be represented by using multilinear regressions. The variables would be extracted depending on each rain stage (Figure 3.1).

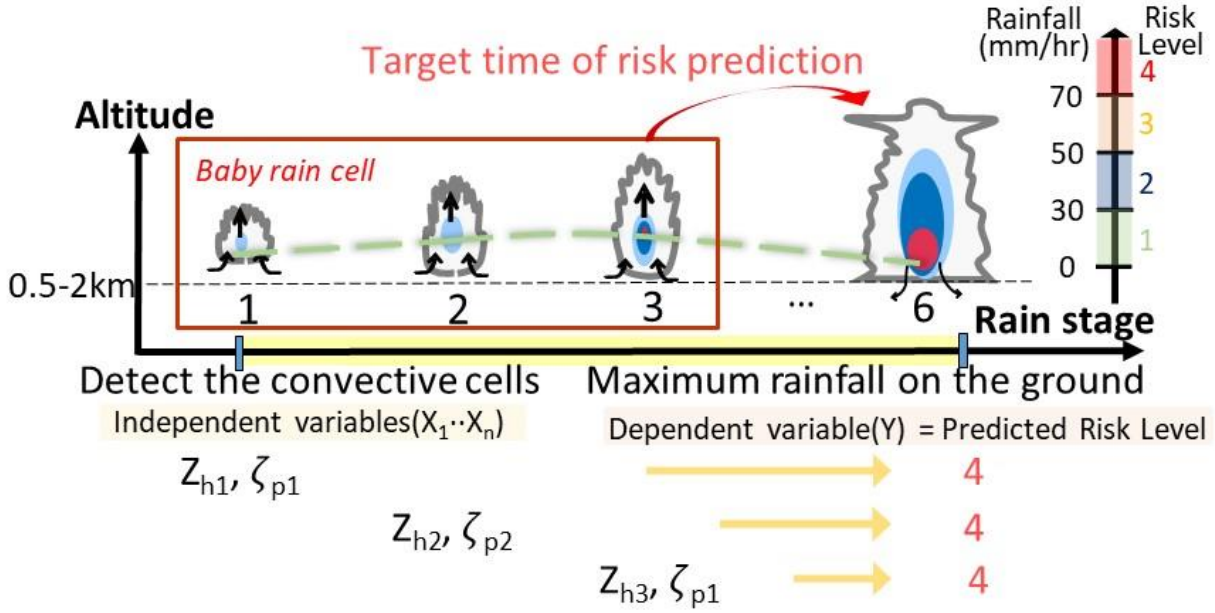

Figure 3.1 Early detection of the isolated convective cell until the maximum rainfall occurs on the ground. Extraction of variables depending on each rain stage.

3.2.3 The Receiver Operating Characteristic (ROC) analysis

To find the most appropriate multilinear regression equation, we applied the Receiver Operating Characteristic (ROC) analysis and examined the obtained Area Under ROC Curve (AUC). The ROC analysis is used as a quantitative evaluation method to assess the accuracy of the multilinear regression equation. It divides values into observation and prediction as a contingency (Table 3.2) and estimates the ability of how much the analysis reflects the observation.

Table 3.2. ROC matrix for RP_{RD}(Risk Prediction by radar observation data) and RP_{RG}(Risk Prediction by multilinear regression)

		Observed Value (RP_{RD})	
		GHR occurred	GHR not occurred
Predicted Value (RP_{RG})	GHR occurred	Hit (H)	False (F)
	GHR not occurred	Missing (M)	Negative hit (N)

The ROC curve plots the *hit rate* (*HR*) against the *false alarm rate* (*FAR*), which are computed as Equations 3.6 and 3.7:

$$Hit\ rate\ (HR) = \frac{H}{H + M}\,, \tag{3.6}$$

$$False\ alarm\ rate\ (FAR) = \frac{F}{F + N}\,, \tag{3.7}$$

where *H* and *M* represent hits and misses when guerilla heavy rainfall occurred. *F* and *N* represent false and negative hits when guerilla heavy rainfall did not occur. The resulting pairs of (*FAR*, *HR*) from the contingency table are plotted and connected by line segments from the origin point (0, 0), which corresponds to never prediction of the guerrilla heavy rainfall, and to the point (1, 1), which corresponds to always prediction of the guerrilla heavy rainfall. The AUC can represent the accuracy of the multilinear regression equations with a range of 0.5 to 1. When the AUC value approaches unity, the ROC curve goes up to the upper-left corner of the ROC diagram and reflects

better discrimination performance. By using the ROC curve, the accuracy was analyzed at the early and late rain stages as well to reveal specific characteristics of variables during each rain stage. Therefore, the most appropriate multilinear regression equation is chosen by the highest AUC value between the total rain stage and rain stage dependent regressions.

3.3 Results and Discussion

3.3.1 The development process of convective cell and the characteristics of variables

Figure 3.2 shows the development process of the convective cell with the variables of the altitude in which the maximum precipitation occurs every 5 minutes. The pseudo vorticity is calculated with the method described above by using the Doppler velocity. The method was proposed to approximate the vorticity by using the different wind velocity directions of the radar beam. The rain cells first appeared at 15:30. The different wind velocity directions showed that vorticity existed. The vorticity was calculated by dividing the different directions of wind velocity by the distance between adjacent cells. The relationship between the growth of rain cell and vorticity is proven in Figure 3.2. The rain cells have vorticity values greater than or equal to $0.03s^{-1}$ and reflectivity values greater than 10 dBZ. As shown in Figure 3.2, while the rain cell developed into guerrilla heavy rainfall, the vorticity and reflectivity values increased accordingly. Figure 3.2 proves that the vorticity and reflectivity were correlated with the risk of guerrilla heavy rainfall.

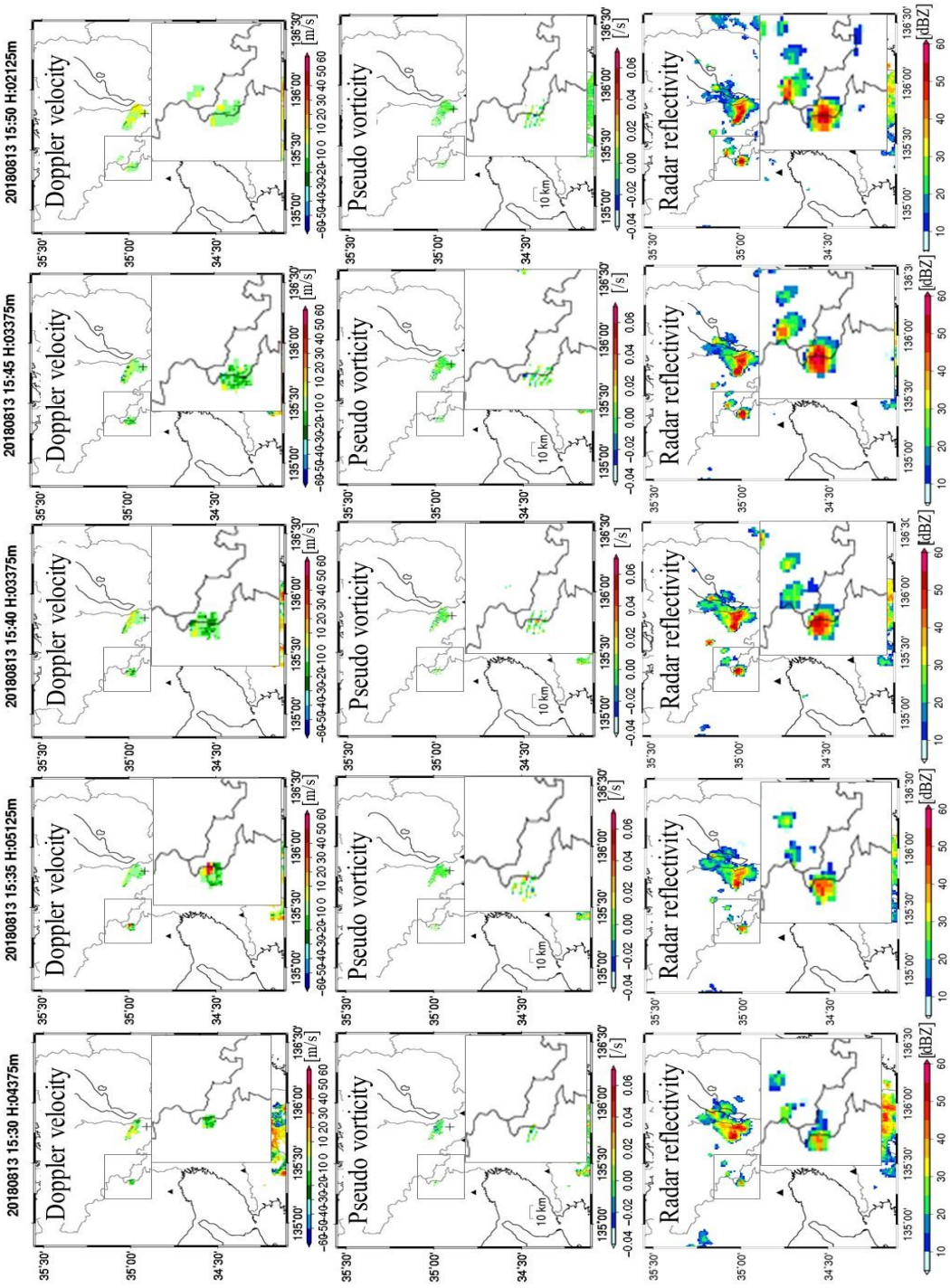

Figure 3.2 The development process of convective cell with variables (Upper: Doppler velocity, Center: Pseudo vorticity, Bottom: radar reflectivity).

3.3.2 Accuracy comparison between total rain stage regression and rain stage dependent regressions

3.3.2.1 Accuracy comparison by using the three-dimension Scatter and Surface plots

To predict the occurrence of guerrilla heavy rainfall is quite easy when the maximum rainfall reaches the ground. However, it doesn't have enough lead time to escape from the disaster of guerilla heavy rainfall. So, it is important to predict guerilla heavy rainfall earlier for a longer lead time. In order to select the most accurate multilinear regression for predicting the risk before the maximum rainfall occurs, an accuracy comparison is needed between total rain stage regression and rain stage dependent regressions. Firstly, the performance of rain stage dependent regressions is compared with the total rain stage regression as a three-dimension scatter and surface plot. The three-dimension scatter plot shows the amount of each variable. The surface plots are useful for showing the relationship of regression analysis among the dependent variable (i.e., predicted risk level) and two independent variables (i.e., reflectivity and vorticity). The warmer color of the surface plot, which is closer to the risk level 4.0, corresponds to more severe risk levels. The total rain stage regression (Figure 3.3, blue dashed box) shows a positive correlation between the dependent variable and each independent variable. Especially, the vorticity has a strong positive correlation. The rain stage dependent regressions (Figure 3.3, red dashed box) from rain stages 1 to 6 represent the relationship among the predicted risk level, reflectivity and vorticity. The correlation between predicted risk level and reflectivity shows more positive correlations as the rain stage develops, except in the early rain stage. The correlation between predicted risk level and vorticity shows strong positive correlations at the early rain stage. However, at the late rain stage, it seems to find low correlations. The pseudo vorticity is an important factor in determining the guerrilla heavy rainfall at the early rain stage. Therefore, to develop the quantitative risk prediction

method, it is necessary to make regressions depending on each rain stage because reflectivity and vorticity have different characteristics in the development process of the convective cell.

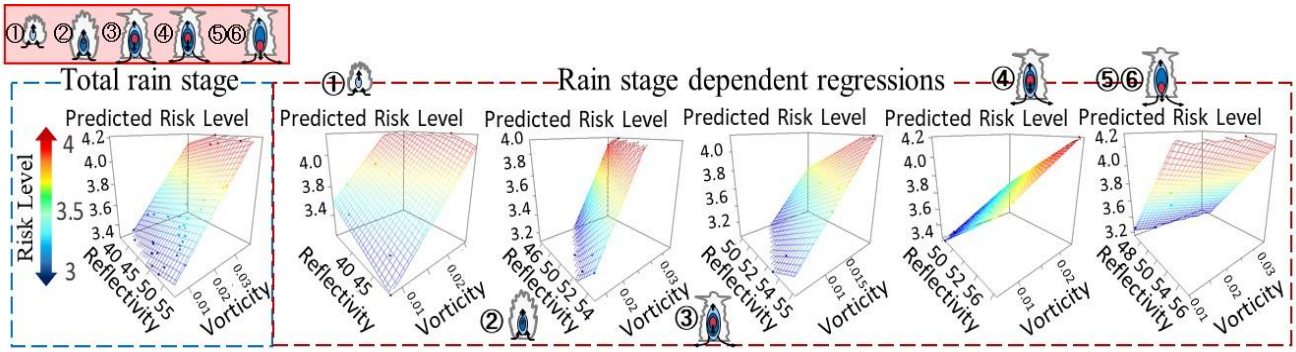

Figure 3.3 The performance of rain stage dependent regressions is compared with the total rain stage regression by three-dimension scatter and surface plots.

Statistically, the number of cases about rain stage dependent regressions is smaller than the total rain stage regression. It is possible that the stage dependent regressions deviate from the limited number of cases. The rain stage dependent regressions are strongly affected by cases, so the regressions have less statistical stability than total rain stage regression relatively. However, if we collect more events, the problem could be solved. Physically, the variables show different characteristics according to the development process of the convective cell. Also, the rain stage dependent regressions calculate higher accuracy at the early rain stage. For saving lives by alerting the warning at the beginning of guerilla heavy rainfall, this research is focused on the accuracy of the quantitative risk prediction by considering the performance of variables that have different characteristics depending on each rain stage.

3.3.2.2 Accuracy comparison according to the characteristics of the variables

To identify the characteristics of the variables (i.e., reflectivity, pseudo vorticity), a part correlation coefficient is used. The partial correlation coefficient shows a similar explanation with the part correlation coefficient. However, in this chapter, we use the part correlation coefficient of variables because the part correlation coefficient shows how the explanatory variables explained the predicted risk level. The part correlation coefficient is the correlation between the independent variable (i.e., vorticity (ζ)) and the dependent variable (i.e., predicted risk level (j_{PRL})) after the linear effects of the other independent variables (i.e., reflectivity (Z_h)) have been removed from the independent variable (i.e., vorticity (ζ)) only. It indicates the amount of unique explanatory power in predicted risk level explained by vorticity. Figure 3.4 illustrates the part correlation coefficient of variables affecting the predicted risk level depending on each rain stage by pseudo radar analysis. It represents that the most explanatory variable is changed depending on each rain stage. The vorticity and reflectivity are very important at the early and late rain stage, respectively. We focus on the early rain stage for saving evacuation time to escape from danger because the guerrilla heavy rainfall occurs within a few minutes. So, vorticity is the most effective explanatory variable to estimate the predicted risk level before the maximum rainfall reaches the ground.

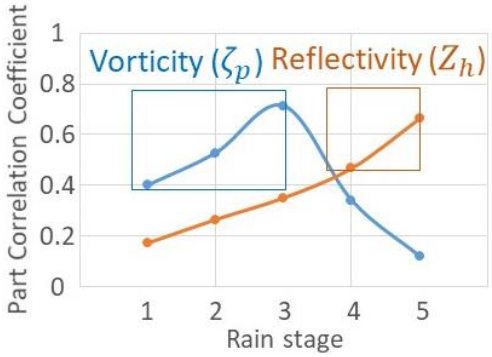

Figure 3.4 The impact of variables affecting the predicted risk level by pseudo radar analysis.

3.3.2.3 Accuracy comparison by using the Receiver Operating Characteristic (ROC) analysis

The accuracy is evaluated by using the ROC and AUC analysis to find the most appropriate multilinear regressions. For each event, the risk level was classified by using multilinear regressions. The observed value defined whether the guerilla heavy rainfall occurs or not by the radar observation data which is maximum rainfall intensity near the ground within 30 minutes. Then, the Hit Rate (HR), False Alarm Rate (FAR), and Area Under ROC Curve (AUC) were estimated. Figure 3.5 represents the ROC curves at the early (i.e., rain stage 1 to 2) and late rain stages (i.e., rain stage 3 to 6), which are estimated by the total rain stage and rain stage dependent regressions with vorticity and reflectivity. The regression with high accuracy has AUC close to unity. The accuracy of rain stage dependent regressions is 75% (AUC=0.75), which is higher than the total rain stage regression (AUC=0.74). There is no significant difference in accuracy. However, the AUC analysis of rain stage dependent regressions gets higher accuracy (84% accuracy) at the early rain stages than total rain stage accuracy (76% accuracy). It is necessary to use the rain stage dependent regressions because the higher accuracy at the early rain stage can secure the lead time required for evacuation and saving lives.

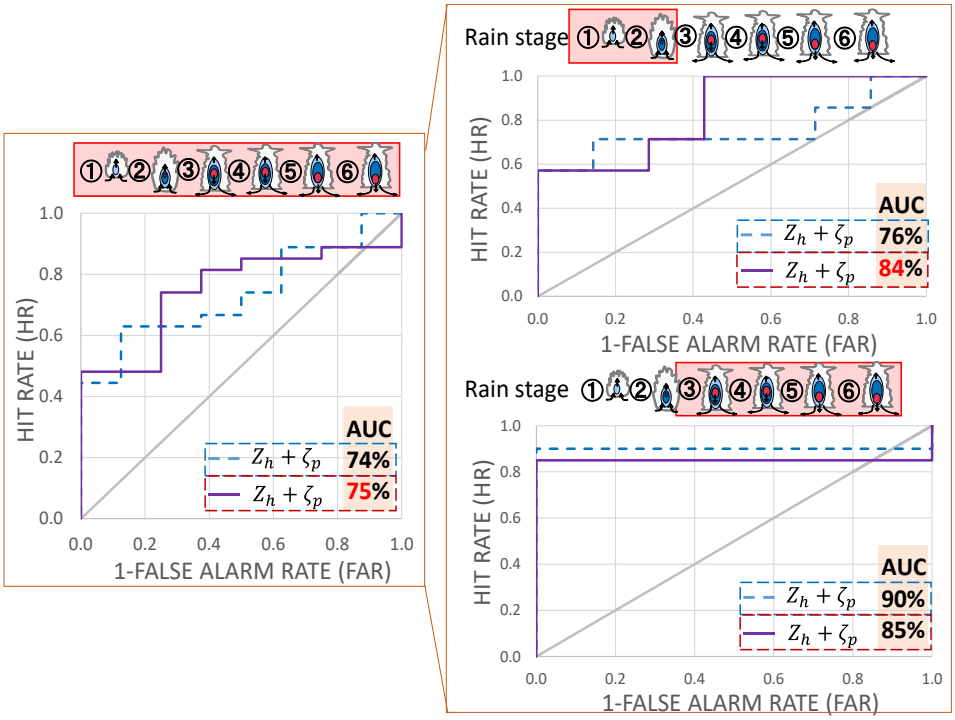

Figure 3.5 The comparison between total rain stage regression and rain stage dependent regressions is conducted at the early and late rain stages based on the accuracy by ROC curve.

3.4 Conclusion

In this study, the early detection and quantitative risk prediction method was proposed using only radar observation data to minimize human casualties such as isolation, death, and disappearance due to heavy rainfall. As the multilinear regressions can predict the risk intuitively by using only the radar observation data, it is easy to identify the danger of guerilla heavy rainfall. Therefore, the quantitative risk prediction method has the reliability to predict the risk before the maximum rainfall occurs. If this method is applied to the field, it is possible to secure sufficient time for disaster prevention and evacuation with high accuracy. However, the actual occurrences of guerilla heavy rainfall were missed, when the risk of the multilinear regressions received an

unexpected value of variables as input data. Also, even if the baby rain cell can be detected, it is difficult to be predicted in which direction the rain cell will move and in which area the rain cell will cause guerrilla heavy rainfall. Besides, it remains unclear which convective cell will develop. It has the potential to improve reliability and accurate risk prediction by adding more explanatory variables. In the next chapter, additional research and analysis will be conducted by adding variables such as reflectivity, Doppler wind velocity, vertical vorticity, divergence, convergence, and vertical wind, etc. Also, developing the quantitative risk prediction method can contribute to the improvement of the flash flood prediction system.

CHAPTER 4

Advances of the Quantitative Risk Prediction for Improving the Accuracy on the Risk of Guerrilla Heavy Rainfall by Multiple Doppler Radar Analysis

Abstract It is necessary to predict the risk of guerrilla heavy rainfall precisely for reducing the damage to human life and property. To better alert the risk triggered by guerrilla heavy rainfall, we aim to propose an advanced quantitative risk prediction method in this research. By multiple Doppler radar analysis, the variables (i.e., the vorticity, divergence, and vertical wind) were estimated with real wind field data. Then, the multilinear regression was used for finding the relationship between the predicted risk level and the variables with the pseudo and multiple Doppler radar analysis. The accuracy of multilinear regression was estimated by a Receiver Operating Characteristic (ROC) analysis. As a result, the most appropriate regression among the relevant variables was composed of reflectivity, vorticity, divergence, and vertical wind by multiple Doppler radar analysis. It is possible to predict the risk quantitatively with high accuracy of 90% at the early rain stage.

4.1 Introduction

Recently, localized severe heavy rainfalls, which have not been experienced in the past, have frequently occurred in Japan due to the effects of climate change (Miyasaka et al., 2020). In particular, the guerilla heavy rainfall, which is a rapidly growing isolated single cumulonimbus cloud, could trigger flash floods in watersheds and cause extensive economic damages and casualties. It is quite difficult to observe and predict the rapidly developed guerilla heavy rainfall. If the risk of heavy rainfall can be identified and alerted in advance, it would be possible to safely

evacuate people in danger. Nakakita et al., 2013, Kim and Nakakita, 2020 developed qualitative and quantitative risk prediction methods based on the early detection of the rain cells aloft. These methods can predict the risk of the guerilla heavy rainfall and track the development of convective cells. The risk of terminology represents the severity of the localized heavy rainfall intensity. In this research, to discriminate the risk more precisely compared with the previous research, we aim to improve the accuracy of the quantitative risk prediction by adding the explaining variables with the pseudo and multiple Doppler radar analysis. In addition, this method considers the performance of variables that have different characteristics depending on the development process of guerilla heavy rainfall over time.

4.2 Data and Methodology

To provide high spatiotemporal observation data throughout Japan, MLIT has been operating the X-band polarimetric RAdar Network (XRAIN) since 2010. As of now, the MLIT has installed 39 X-band multi-parameter (X-MP) radars. In this research, four X-band multi-parameter radars are used in the Kinki region by the Ministry of Land, Infrastructure and Transport. The four X-MP radars are named Rokko, Katsuragi, Juubusan, and Tanokuchi. The XRAIN in the Kinki region produces composite radar images every 1 minute and provides complete volume scan data every 5 minutes. The three-dimensional volume scan data has a resolution of 250 and 500 m in the horizontal and vertical directions, respectively. Also, to retrieve the three-dimensional wind field, especially at upper levels, background information (i.e., Sounding data) is required. From August 2013 to August 2018, 7 guerilla heavy rainfall events were selected as the same events in chapter 3.

4.2.1 Multiple Doppler radar analysis

Multiple Doppler radar analysis is an analysis method that estimates the three-dimensional wind velocity field using the Doppler velocity observed by the Doppler radars. The multiple Doppler radar analysis could retrieve the three-dimensional wind field. This analysis can improve the understanding of the physical mechanisms behind guerrilla heavy rainfall and forecasting severe weather. There are various methods for multiple Doppler radar analysis, including the methods of Gao et al., 1999 and Protat et al., 1999. In methods, it is common to simultaneously estimate the wind velocity field (u, v, w) that minimizes the evaluation function using the three-dimensional variational method. However, the cost function that needs to be minimized is different. Gao et al., 1999 minimize the cost function (J) with the variational method. The cost function is defined as the sum of squared errors due to discrepancies between observations and analysis with additional constraint terms. It is expressed as follows,

$$J = J_o + J_d + J_s + J_b, \tag{4.1}$$

where J_o represents the difference between the observed radial velocity and the analyzed radial velocity, J_d is the mass continuity equation constraint term, J_s is the smoothness constraint term, and J_b is the background constraint term. To obtain an optimal solution, the cost function is derived with respect to the control variables: two horizontal wind components (u, v) and a vertical wind component (w).

$$J_o = \frac{1}{N} \sum_{i,j,k,m} \lambda_o (Vr_m - u\,cos\,A - v\,cos\,B - (w + w_t)\,cos\,C)^2, \tag{4.2}$$

$$J_d = \frac{1}{2}\sum_{i,j,k} \lambda_d \, D^2, \tag{4.3}$$

$$D = \frac{\partial \overline{\rho} u}{\partial x} + \frac{\partial \overline{\rho} v}{\partial y} + \frac{\partial \overline{\rho} w}{\partial z}. \tag{4.4}$$

where J_o is defined as the observation value of the Doppler wind velocity V_r on a specified Cartesian grid, where *i*, *j*, and *k* indicate the spatial location in the *x*, *y*, and *z* directions, respectively. *N* is the total number of observations, *m* indicates the m-th radar, w_t is the falling velocity of the precipitation particles, *cosA*, *cosB*, and *cosC* are the direction as cosine from the radar position, $\overline{\rho}$ is the average air density, and λ_o and λ_d are the reciprocal of the mean squared error. Protat et al., 1999 minimized J_o under the condition that J_d equals zero. J_o and J_d represent the observation error of the Doppler wind velocity and the error of the continuous equation.

To allow the measurement error, the Doppler velocities as weak constraints and the continuity equation as strong constraints are used in the cost function. The weak constrain appropriately accepts the observation errors from the radar data or assumptions in equations. On the contrary, the strong constraint demands all of the analyzed and retrieved variables satisfy the equation exactly. Since the collected radar observation data could be affected by noise, in the Cartesian coordinates, the horizontal wind components (*u*, *v*) are used as weak constraints. By using the continuity equation, the vertical wind component (*w*) in multiple Doppler analysis is estimated. The continuity equation is expressed as follows:

$$\partial u/\partial x + \partial v/\partial y + \partial w/\partial z = kw, \tag{4.5}$$

where (u, v, w) are the three wind components in Cartesian coordinates, $k=-\partial(\ln \rho)/\partial z$, and ρ is the air density. With the continuity equation, the vertical wind component (w) is calculated by a weighted average of upward and downward integrations. The variational method minimizes the cost function, which is the sum of discrepancies between observations and analysis with weighting matrices that depend on the strength of the constraint. In summary, the procedures are to 1) set initial control variables (u, v); 2) estimate the vertical wind component; 3) calculate the gradient of the cost function concerning control variables; 4) finish if the predefined condition of cost function was satisfied; otherwise, set new control variables and return to the step 2.

4.2.2 The advances of the quantitative risk prediction method

To discriminate the risk more precisely compared with the previous chapter, we aim to improve the accuracy of the quantitative risk prediction by considering the performance of variables (i.e., vertical vorticity, reflectivity, divergence, and vertical wind) that have different characteristics depending on each rain stage. Ulanski and Garstang, 1978 have proved that the updraft, downdraft, upward flux of water vapor, maximum divergence, vorticity, and rainfall are presented in the convective cell. So, the variables are collected to find the correlation between the variables and the predicted risk level of guerilla heavy rainfall. Especially, the vorticity, divergence, and vertical wind are important variables at the beginning of an isolated cumulonimbus cloud. The vorticity and divergence can be estimated by using pseudo radar analysis and multiple Doppler radar analysis. On the other hand, the vertical wind can be calculated by multiple Doppler radar analysis only because the analysis can retrieve a three-dimensional wind field. Pseudo radar analysis uses only a single Doppler radar observation which is a radial component of the wind field that flows toward or away from the radar. To predict the risk level more accurately, it is necessary

to estimate the three-dimensional wind field using multiple Doppler radars. Therefore, an advanced quantitative risk prediction method is proposed in this chapter. This research can determine the multilinear regression with the highest accuracy by finding the best combinations of the variables (i.e., reflectivity, vorticity, divergence, and vertical wind) with pseudo and multiple Doppler radar analysis. Figure 4.1 shows how to calculate the vertical vorticity by pseudo and multiple Doppler radar analysis. In the previous chapter, only pseudo vertical vorticity and reflectivity were used to find the regression. The pseudo vertical vorticity is roughly estimated by applying the method proposed in Nakakita et al., 2017 with the radial velocity. From the radial velocity, the vorticity can be calculated by the following equation. $\zeta=(V_2-V_1)/\Delta X$, where V_1 and V_2 are moving toward and away from the radar in the Cartesian coordinates and ΔX is the distance between the center of the mesh. Because the volume scanning observation using a single Doppler radar could not measure horizontal wind velocities but the radial velocity. If we estimated the horizontal wind velocities by multiple Doppler radar analysis, the vertical component of vorticity could be calculated by $\zeta = \partial v/\partial x - \partial u/\partial y$, where (u, v) are the horizontal wind velocities in the Cartesian coordinates.

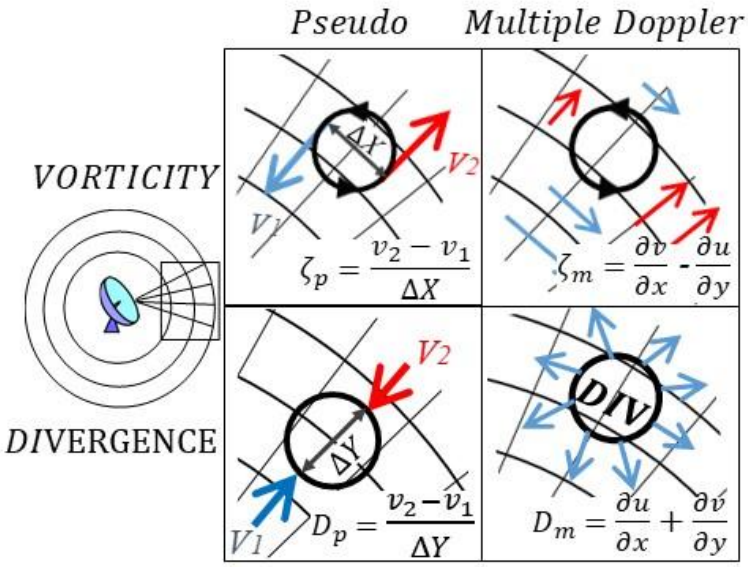

Figure 4.1 Conceptual diagram of calculating vorticity and divergence by pseudo and multiple Doppler radar analysis.

For predicting the risk triggered by guerilla heavy rainfall, it is necessary to identify a first radar echo. At the beginning of the process of a cumulonimbus cloud, the water vapor in the lower atmospheric layers rises and condenses to generate the precipitation particles which can be defined as the first radar echo or a baby rain cell in an atmospheric instability condition. Then, a first rain stage is assigned. In this research, the rain stages from 2 to 6 are marked according to the process of convective cell development with a time interval of 5 minutes. When we find out the existence of the first echo, it is important to calculate the vorticity which is a measure of the rotation motion of the flow. Because not every first radar echo develops into a severe heavy rainfall, Nakakita et al., 2017 have proposed that the value of the vorticity greater than or equal to 0.03 s^{-1} is related to the growth of rain cells. Also, they clarified that the first echo was detected about 25 minutes on average before the maximum rainfall near the ground occurred. Therefore, finding the relationship

between the predicted risk level and vorticity is important within 30 minutes (from rain stage 1 to 6) before the maximum rainfall intensity occurs on the ground. Figure 4.2 illustrates the process of how to find the relationship among the variables with the predicted risk level. This research can improve the quantitative risk prediction accuracy.

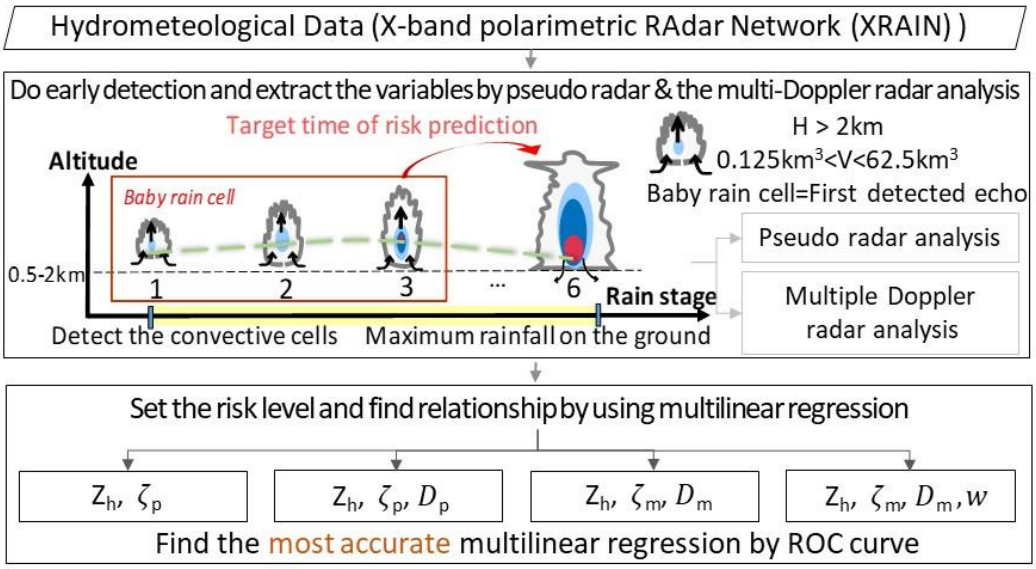

Figure 4.2 Flowchart of improvement of the quantitative risk prediction accuracy. Z_h : reflectivity, ζ_p : pseudo Vorticity, D_p: pseudo divergence, ζ_m: vorticity of multiple Doppler radar analysis, D_m: divergence of multiple Doppler radar analysis and w: vertical wind.

To set the predicted risk level, the predicted risk categories (risk levels) are defined when the maximum rainfall reached on the ground, such as Risk Level 1.0 (under 30 mm/hr), Risk Level 2.0 (between 30 mm/hr and 50 mm/hr), Risk Level 3.0 (between 50mm/hr and 70mm/hr), and Risk Level 4.0 (over 70mm/hr). Then, for predicting the risk level by using the observed and calculated variables, the correlation can be represented by using multilinear regressions. Figure 4.3 shows the

extraction of variables depending on each rain stage. Then, the formulation of the multilinear regression becomes;

$$j_{PRL}(i) = C_{0_i} + C_{1_i} \cdot Z_{hi} - C_{2_i} \cdot \zeta_i + C_{3_i} \cdot w_i + C_{4i} \cdot DivCon_i \,, \tag{4.6}$$

where $j_{PRL}(i)$ is predicted risk level from rain stage i. Z_h, ζ, w, $DivCon$ are reflectivity, vorticity, vertical wind, and divergence and convergence, respectively. $i \in [1, 6]$ is the number of rain stage which represents the development of a cumulonimbus cloud over time. Since the variables have characteristics depending on each rain stage, the stage dependent regressions are considered to improve the accuracy of risk prediction among the variables.

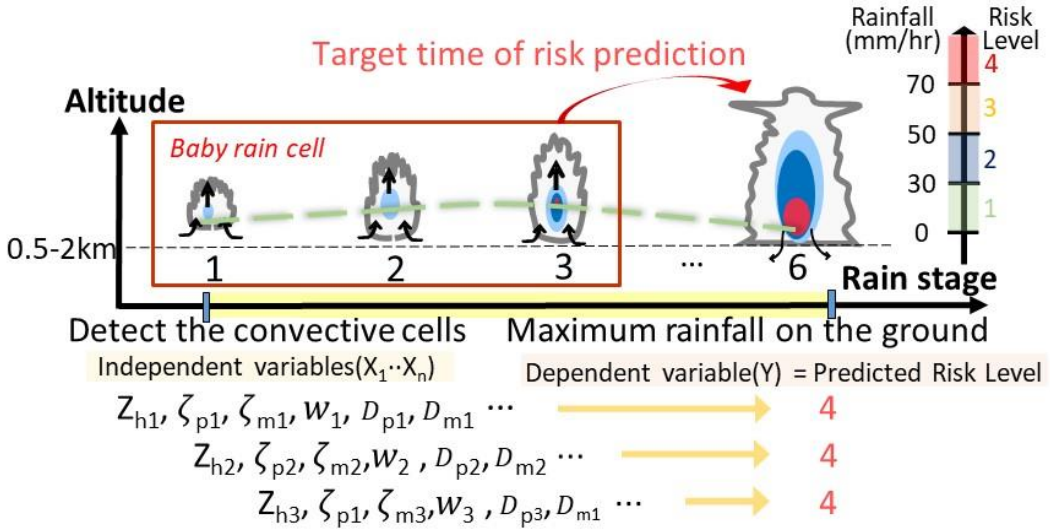

Figure 4.3 The early detection of the isolated convective cell until the maximum rainfall occurs on the ground. Extraction of variables depending on each rain stage.

4.3 Results and Discussion

4.3.1 The development process of convective cell and the characteristics of variables by pseudo and multiple Doppler radar analysis

The development processes of the convective cell from the rain stage 1 to 6 are plotted in Figure 4.4 with the variables calculated by pseudo and multiple Doppler radar analysis. The three-dimensional vorticity and divergence are calculated depending on each rain stage. Then the pair of vorticity and divergence and convergence increase while the rain cell developed into guerilla heavy rainfall. The divergence and convergence can be an explanatory variable because the strong convergence occurred at the lower layer at the beginning of the cumulonimbus cloud. This was confirmed by Ulanski and Garstang, 1978. In addition, when the vorticity is detected in the development of a cumulonimbus cloud, a vertical vortex tube is formed by the strong updraft to bring the water vapor. The reflectivity is important at the late rain stage. According to the results, we consider that the variables (i.e., reflectivity, vorticity, divergence and convergence, and vertical wind) are related to the predicted risk level of guerilla heavy rainfall.

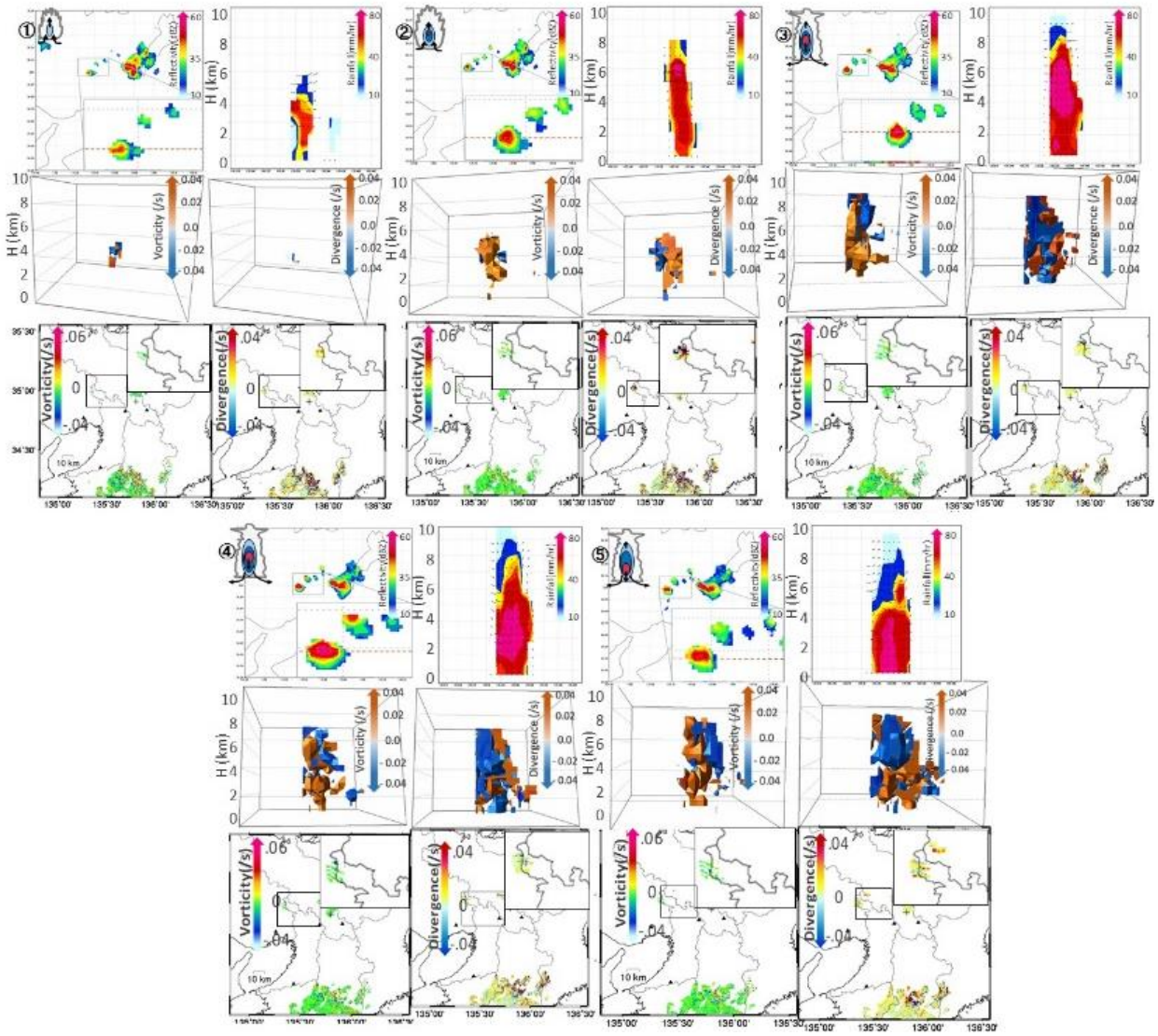

Figure 4.4 The variables on 13th August 2018 (Upper: reflectivity, rainfall, and vertical wind, Center: vorticity, divergence, and convergence calculated by multiple Doppler radar analysis, Lower: vorticity, divergence, and convergence calculated by pseudo radar analysis).

4.3.2 The relationship among the predicted risk level and the variables by pseudo and multiple Doppler radar analysis

The three-dimension scatter plots and surface plots can represent the relationship among the dependent variable (i.e. predicted risk level) and independent variables (i.e. reflectivity, vorticity, divergence, convergence, and vertical wind). For each rain stage, the relationships between the predicted risk level and variables are expressed. The points are predicted risk levels according to the value of each variable. Surface plots are diagrams of three-dimensional data and show the relationship of the variables. Rather than showing the individual data points, surface plots show a functional relationship between a designated dependent variable (predicted risk level) and two independent variables. Figure 4.5 illustrates the relationship among the predicted risk level and the variables. By pseudo radar analysis, the combinations of (a) reflectivity, pseudo vorticity and (b) those with added pseudo divergence show the relationship with the predicted risk level. By multiple Doppler radar analysis, the combinations of (c) reflectivity, vorticity, divergence and (d) those with the added vertical wind show the relationship. The combinations of variables have in common that the vorticity and reflectivity are very important at the early and late rain stage, respectively. Especially, at the first rain stage of (c) and (d), the relationship between the vorticity and the predicted risk level has a high correlation. Additionally, the vertical wind and vorticity are strongly correlated with the predicted risk level over time at the early rain stage.

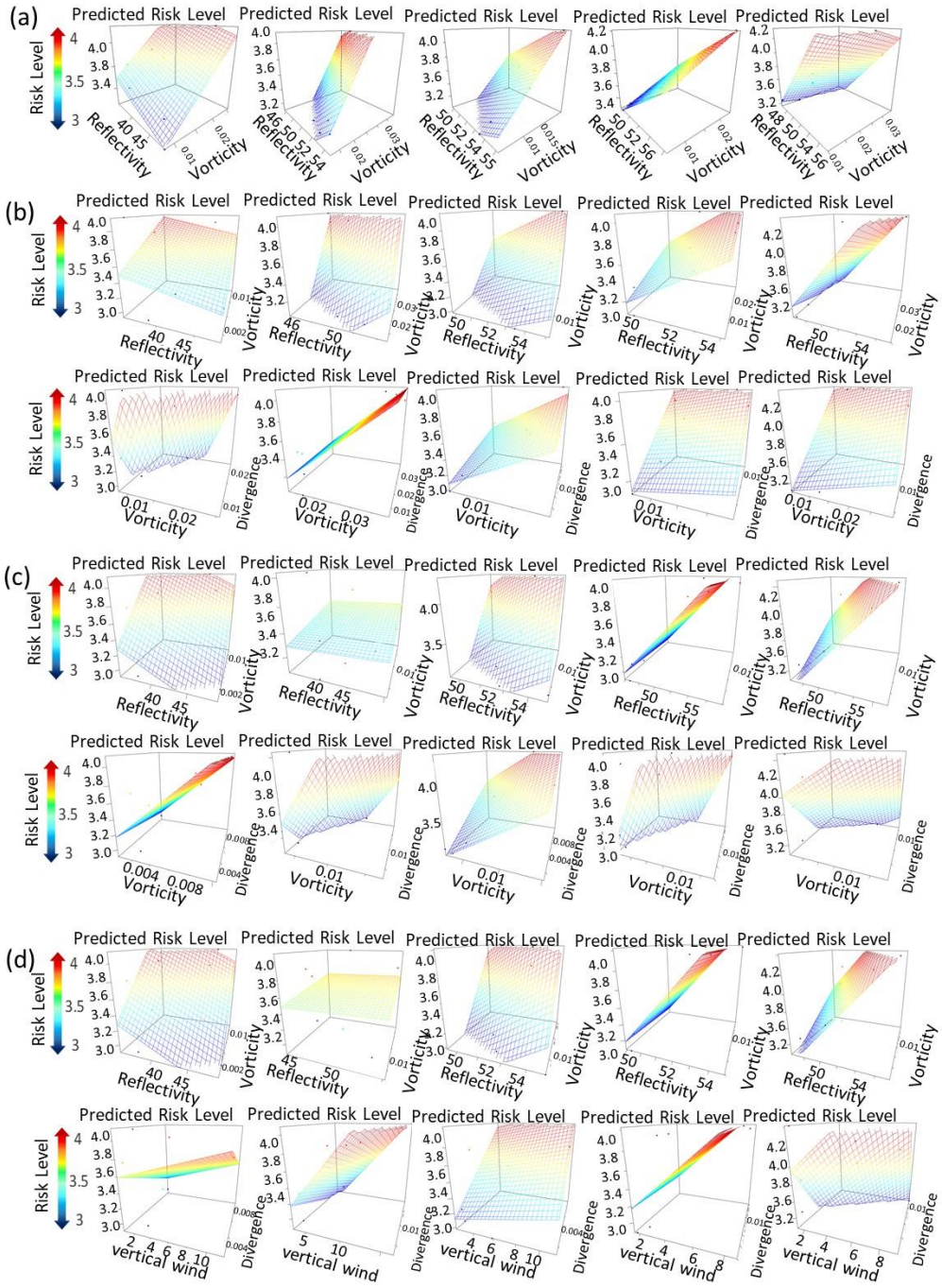

Figure 4.5 The performance of rain stage dependent regressions by three-dimension scatter and surface plots. By pseudo radar analysis, the combinations of (a) reflectivity, pseudo vorticity and (b) those with added pseudo divergence. By multiple Doppler radar analysis, the combinations of (c) reflectivity, vorticity, divergence and (d) those with the added vertical wind.

4.3.3 Determination of the most appropriate regression among the variables

4.3.3.1 The most appropriate regression according to the characteristics of the variables

To discriminate the risk more precisely, the accuracy of the quantitative risk prediction was improved by considering the performance of variables that have different characteristics depending on each rain stage. Also, divergence and vertical wind were included to find the correlation with the predicted risk level in addition to the vertical vorticity and reflectivity. Especially, the vorticity, convergence, and vertical wind are important variables at the beginning of an isolated single cumulonimbus cloud. The divergence, convergence, and vorticity can be estimated by using pseudo radar analysis and multiple Doppler radar analysis. On the other hand, the vertical wind can be calculated by multiple Doppler radar analysis only because the analysis can retrieve the three-dimensional wind field. Pseudo radar analysis uses only a single Doppler radar observation which is a radial component of the wind field that flows toward or away from the radar. So, the multilinear regressions are expressed by combining the divergence and vertical wind based on reflectivity and vorticity to analyze the characteristics of variables depending on each rain stage.

A part correlation coefficient shows how the explanatory variables explained the predicted risk level. This is because the part correlation coefficient indicates that only the variable (e.g., vorticity) by eliminating the influence of the other variables can explain the dependent variable (i.e., predicted risk level). Figure 4.6 illustrates the part correlation coefficient of variables affecting the predicted risk level depending on each rain stage by pseudo and multiple Doppler radar analysis.

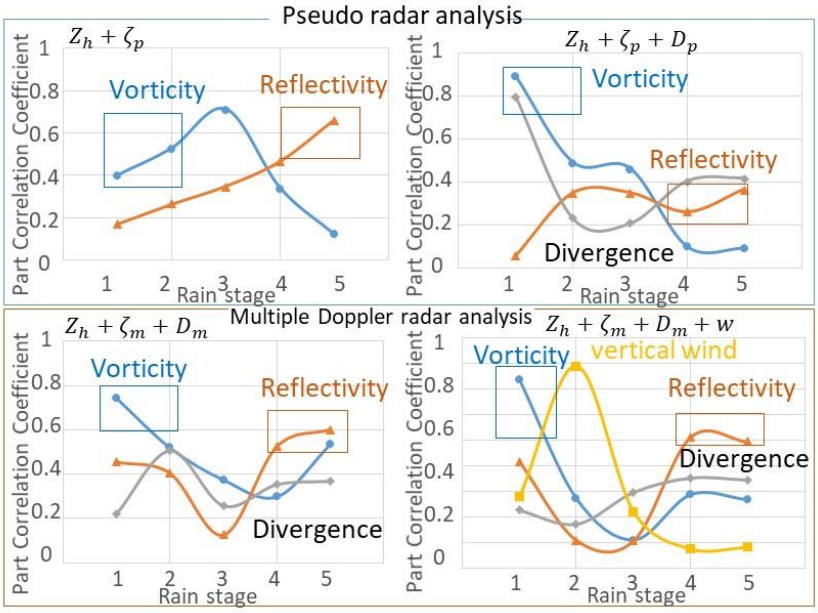

Figure 4.6 The part correlation coefficient of variables affecting the predicted risk level by pseudo and multiple Doppler radar analysis.

It represents that the most explanatory variable is changed depending on each rain stage. In pseudo and multiple Doppler radar analysis, the combinations of variables have conditions in common that the vorticity and reflectivity are very important at the early and late rain stage, respectively. We focus on the early rain stage for saving evacuation time to escape from danger because the guerrilla heavy rainfall occurs within a few minutes. So, vorticity is the most explanatory variable to estimate the predicted risk level before the maximum rainfall reaches the ground. By the way, the part correlation coefficient of vertical wind suddenly increases at rain stage 2. The reason is that updrafts condense water vapor in the lower atmosphere at the early rain stage, creating convective cells in atmospheric instability. The results were consistent with the description of the development process of cumulonimbus clouds.

4.3.3.2 The most appropriate regression by using the Receiver Operating Characteristic (ROC) analysis

The ROC analysis is applied to select the most appropriate multilinear regression with the highest accuracy. The predicted risk level is defined when the maximum rainfall reached on the ground according to the predicted risk categories from Risk Level 1 to Risk Level 4. To make the ROC curve, the Hit Rate, False Alarm Rate, and AUC are estimated among the combinations of independent variables of the multilinear regression. The equation with high accuracy has AUC near 1. Figure 4.7 represents the ROC curves of the rain stage dependent regressions. As a result of the highest accuracy, the multilinear regression of reflectivity, vorticity, convergence, divergence, and vertical wind has 83% accuracy (AUC= 0.83). The regression by using multiple Doppler radar analysis and adding more independent variables has brought notable improvement. Moreover, the inclusion of convergence, divergence, and vertical wind can better describe the predicted risk level. The AUC analysis is conducted at the early and late rain stages and confirms higher accuracy at the early rain stage (90% accuracy). Therefore, using the improved regression, the predicted risk level of guerrilla heavy rainfall could be predicted with high accuracy.

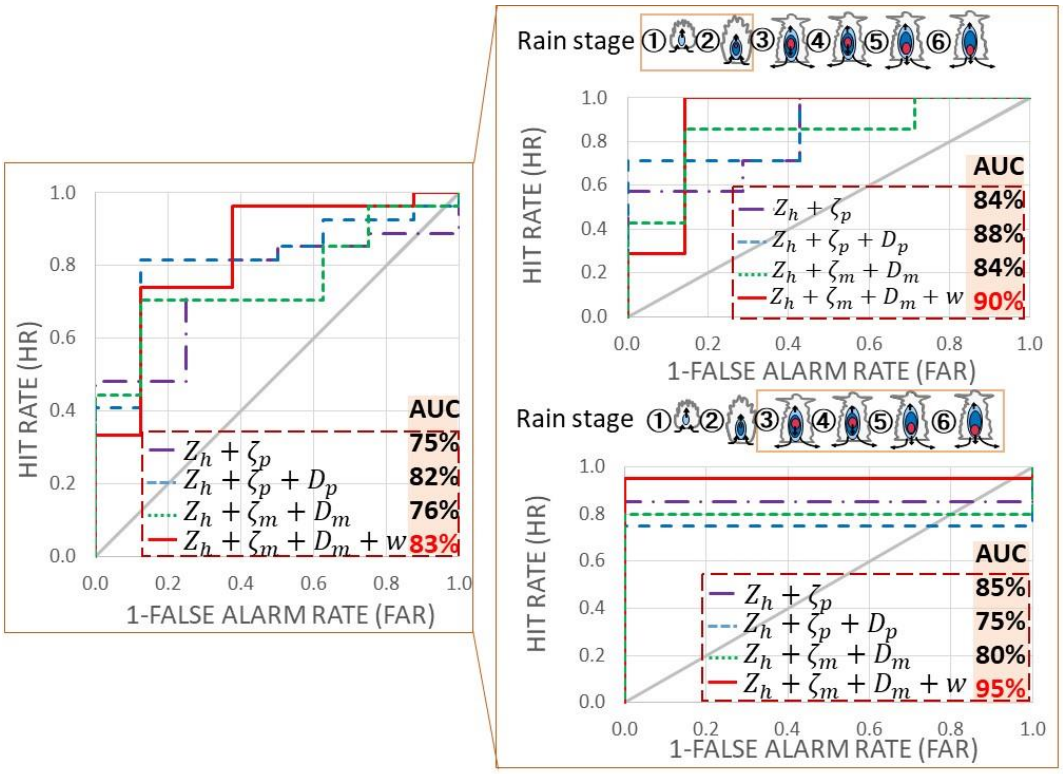

Figure 4.7 The accuracy of multilinear regression among the combination of dependent variables by AUC. By pseudo radar analysis, the purple and blue lines were the regressions of 1) reflectivity, pseudo vorticity and 2) those with added pseudo divergence. By multiple Doppler radar analysis, the green and red lines were the regressions of 3) reflectivity, vorticity, divergence and 4) those with the added vertical wind.

4.4 Conclusion

In this chapter, the predicted risk level was discretized when the maximum rainfall was reached on the ground by isolated cumulonimbus clouds. Also, the quantitative risk prediction method has been improved to accurately alert the risk triggered by guerilla heavy rainfall. By using pseudo radar analysis and multiple Doppler radar analysis, the multilinear regression with the

highest accuracy is chosen among the combinations of variables. If this regression is applied to the field, it is possible to secure more evacuation time and predict the disasters with high accuracy. However, there still exists some points to improve the method. When the rain stage dependent regressions were formulated, the number of cases was still insufficient to be used in various conditions. This could cause the rain stage dependent regressions to be over-fitted due to data insufficiency. If more cases are included, this problem should be resolved. Furthermore, it is still unclear to determine which convective cell would be developed. Even if a baby rain cell can be detected, it is difficult to predict in which direction the rain cell would move and where guerilla heavy rainfall would occur. So, it is necessary to find the variables affecting the heavy guerilla rainfall. In addition, the research will be conducted to secure the lead time by predicting the movement of convective cells judged to be dangerous with the rainfall forecasting model.

CHAPTER 5

Development of Quantitative Risk Prediction Method based on the Life Cycle of Guerrilla Heavy Rainfall

Abstract To predict the risk triggered by guerrilla heavy rainfall based on a physical mechanism, the applicability of the quantitative risk prediction method was analyzed according to the development process (i.e., life cycle). By multiple Doppler radar analysis, the variables (i.e., reflectivity, vorticity, divergence, convergence, and vertical wind) were estimated. Then, the correlation between the predicted risk level and the variables was founded on the multilinear regression. The usefulness of the life cycle could be described both physically and statistically by comparing rain stage. The vorticity and vertical wind are important variables as they are related to the initial growth of guerrilla heavy rainfall. In this research, the vorticity and vertical wind show a stronger correlation with the predicted risk level in the development and early maturity life cycle than in the early rain stage. Therefore, the quantitative risk prediction method based on the life cycle can be possible to generally predict the guerrilla heavy rainfall.

5.1 Introduction

Kim and Nakakita, 2021 has been developed and advanced the quantitative risk prediction method by finding the relationship among the predicted risk level and the variables (i.e., the vorticity, divergence, and updraft). In the previous chapter, to discriminate the risk more precisely, the accuracy of the quantitative risk prediction has been improved depending on the development of guerilla heavy rainfall over time. The method can predict the risk triggered by guerilla heavy rainfall with a time interval of 5 minutes. However, the process from rain cell into guerilla heavy

rainfall needs to be considered on a physical basis. In this chapter, using the method of Masuda and Nakakita, 2014, the risk can be predicted by classifying the development process into the development, early maturity, late maturity, and dissipation stages. By using X-band multi-parameter data, the classification is conducted based on the hydrometeor type estimation. It is expected to analyze the relationship and predict the risk level by reflecting the physical mechanism.

5.2 Data and Methodology

To find the correlation between the predicted risk level and the variables (i.e., reflectivity, vorticity, divergence, convergence, and vertical wind), four X-band multi-parameter radars are used in the Kinki region by the Ministry of Land, Infrastructure, and Transport. The four X-band radars are named Rokko, Katsuragi, Juubusan, and Tanokuchi. Seven events of guerilla heavy rainfall, which is a rapidly growing isolated single cumulonimbus cloud, were selected from August 2013 to August 2018 as in Chapter 3. In particular, multi-cells that overlap with neighboring cells were excluded. Three-dimensional data with a horizontal resolution of 250 m, a vertical resolution of 500 m, and a maximum altitude of 10 km is created at 1 minute interval using the observation values (Polar coordinate system).

5.2.1 Life cycle discrimination using X-band multi-parameter radar

The multi-parameter data of XRAIN can be used to identify the life cycle of the cumulonimbus cloud (Masuda and Nakakita 2014). There are two procedures to generate a life cycle. Firstly, the estimation of the vertical distribution of hydrometeor type. The hydrometeor type is classified into eight categories (i.e., hail, big drop, rain, heavy rain, graupel, wet snow, dry snow, and ice crystal). The categorization of hydrometeor type is proceeded by using a fuzzy logic

classification (Park et al. 2009). The hydrometeor type is verified with the observation of video sonde. Secondly, the hydrometeor types are used to classify the life cycle into four categories (i.e., development, early maturity, late maturity and dissipation stages). The categorization of the life cycle is proceeded by using a fuzzy logic classification (Masuda and Nakakita 2014). For the five elements (i.e., dry snow + rain, big drop, heavy rain + rain / hail, grupel ratio and vertical rainfall intensity ratio), the membership functions were obtained by frequency of occurrence.

Many studies have been conducted on the use of precipitation particle discrimination. In this research, the precipitation particle discrimination method of Masuda and Nakakita, 2014 used. Masuda and Nakakita, 2014 applied the Park et al., 2009 method, which used fuzzy theory to S-band radar and discriminated particles to X-band MP radar. The XRAIN observes not only the Doppler velocity but also the polarimetric radar parameters (i.e., reflectivity (Z_H), differential reflectivity (Z_{DR}), Specific differential phase (K_{DP}), differential propagation phase (Φ_{DP}), and correlation coefficient (ρ_{HV})). The polarimetric radar parameters show different values depending on the shape, mixing ratio, and particle size of the precipitation particles. The details of the precipitation particle discrimination method are described in Masuda and Nakakita, 2014. The polarimetric radar parameters and the precipitation particles i are expressed by the membership function ${\mu_i}^x$, and the evaluation value Q_i is expressed by Equation 5.1,

$$Q_i = \frac{1}{4}({\mu_i}^{Z_H}(Z_H) + {\mu_i}^{Z_{DR}}(Z_{DR}) + {\mu_i}^{\rho_{HV}}(\rho_{HV}) + {\mu_i}^{K_{DP}}(K_{DP})) \,. \tag{5.1}$$

The evaluation value is calculated for each precipitation particle, and the largest evaluation value is selected as the hydrometeor type.

Then, Masuda and Nakakita, 2014 has discriminated the life cycle of each rain cell based on hydrometeor discrimination results. The stage of cumulonimbus clouds consists of four life cycles: development stage, early maturity stage, late maturity stage, and the dissipation stage. First, when the second derivative with the time of rainfall intensity at 2 km is negative, it is defined as the maturity stage. Then, the period before the maturity stage is defined as the development stage, and the stage after the maturity stage is defined as the dissipation stage. By using the 55 cases, Masuda and Nakakita, 2014 created the membership function of the life cycle with the hydrometeor discrimination results and applied it to the life cycle discrimination method. With these membership functions, the evaluation value Q_j is calculated for each cell every 1 minute as follows:

$$Q_j = \frac{\sum_{k=1}^{5} {\mu_j}^k(V_k) \cdot {w_j}^k}{\sum_{k=1}^{5} {w_j}^k}, \tag{5.2}$$

where ${\mu_j}^k$is the membership function, V_k is the 5 elements as input to the membership function, and ${w_j}^k$ is the weighting coefficient considering the overlap of the frequency of each element. The life cycle with the highest evaluation value is selected as the life cycle of the cell.

5.2.2 Definition of life cycle and rain stage discrimination

The life cycle is the process of cumulonimbus clouds by reflecting the physical mechanism. For selected seven events of guerilla heavy rainfall, the discrimination of life cycle is determined by using the Masuda and Nakakita, 2014 method from the radar polarimetric parameters (Cartesian coordinate data). First, the hydrometeor discrimination method is determined every 1 minute. The detailed procedure is presented with the event of August 13, 2018 in Figure 5.1. It represents the

vertical distribution of the hydrometeor discrimination result. Rainfall intensity in the horizontal section at the altitude of 2 km was investigated for tracking the precipitation cell. Also, the life cycle discrimination is performed every one minute by using the result. Figures 5.1 show the life cycle determination results in different colors. The blue line indicates the development stage, the green line indicates the early maturity stage, the red line indicates the late maturity stage, and the purple line indicates the dissipation stage, respectively.

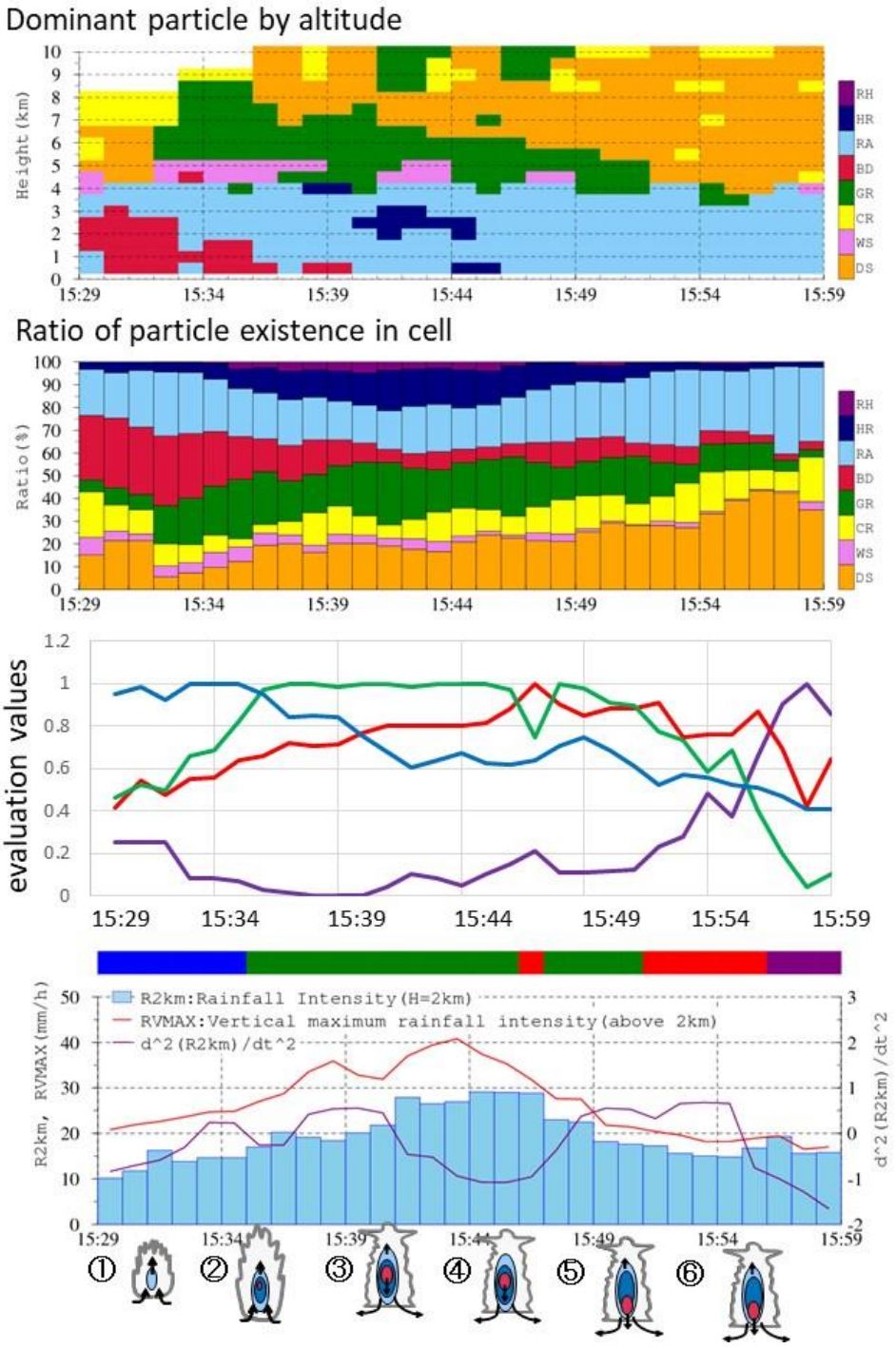

Figure 5.1 The method to identify the life cycle of cumulonimbus cloud (Masuda and Nakakita 2014).

The rain stage is the process of cumulonimbus clouds over time. Through multiple Doppler radar analysis, the research has been conducted. So, the time resolution is every 5 minutes. To analyze the process of cumulonimbus clouds between life cycle and rain stage, it is necessary to perform life cycle discrimination every 5 minutes. For example, the output of multiple Doppler analysis from 15:30 to 15:34 is the result at 15:30. In order to compare the rain stage and life cycle, it is necessary to determine the life cycle representing 5 minutes based on the life cycle discriminations from 15:30 to 15:34. We set that 1 indicates the development stage, 2 indicates the early maturity stage, 3 indicates the late maturity stage, and 4 indicates dissipation stage, respectively. When the majority of life cycle results were obtained (i.e., three or more) among the five life cycle determination results during 5 minutes, the life cycle was set as the majority for the 5 minutes. If there is no majority of life cycle results, the average among the five life cycles was taken, and the life cycle corresponding to the closest value was taken as the life cycle for 5 minutes. The example is in Figure 5.2. Then, the result shows the 5 minutes life cycle of each event in Figure 5.3. The development of cumulonimbus clouds occurs depending on the hydro-meteorological processes. Therefore, the life cycle based on the physical mechanism is necessary to analyze the relationship among the variables and predict the risk level.

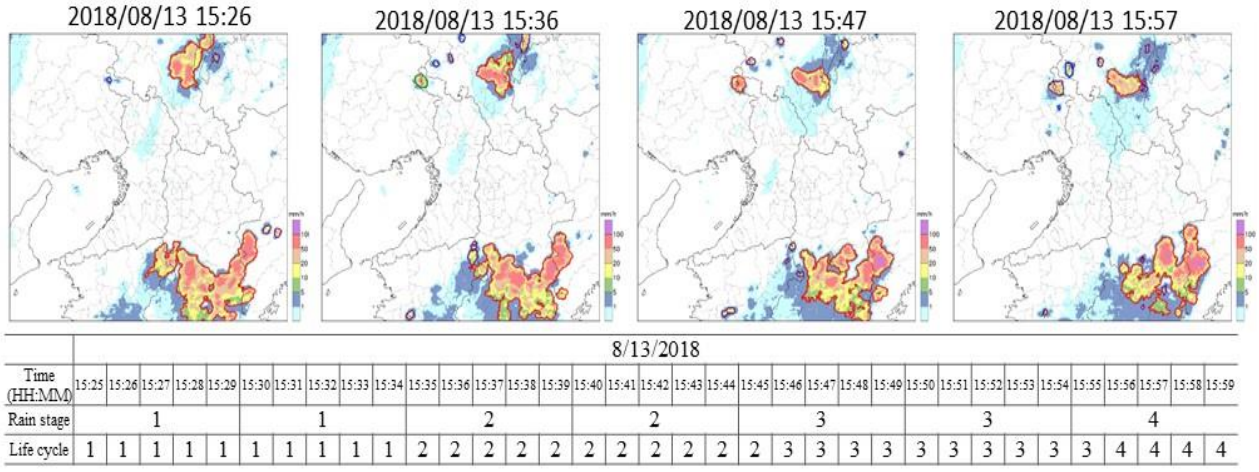

	8/13/2018																																								
Time (HH:MM)	15:25	15:26	15:27	15:28	15:29	15:30	15:31	15:32	15:33	15:34	15:35	15:36	15:37	15:38	15:39	15:40	15:41	15:42	15:43	15:44	15:45	15:46	15:47	15:48	15:49	15:50	15:51	15:52	15:53	15:54	15:55	15:56	15:57	15:58	15:59						
Rain stage	1					1					2					2					3					3					4											
Life cycle	1	1	1	1	1	1	1	1	1	1	2	2	2	2	2	2	2	2	2	2	2	3	3	3	3	3	3	3	3	3	3	4	4	4	4						

Figure 5.2 The discrimination of the life cycle into the 5 minutes life cycle on 13th August 2018.

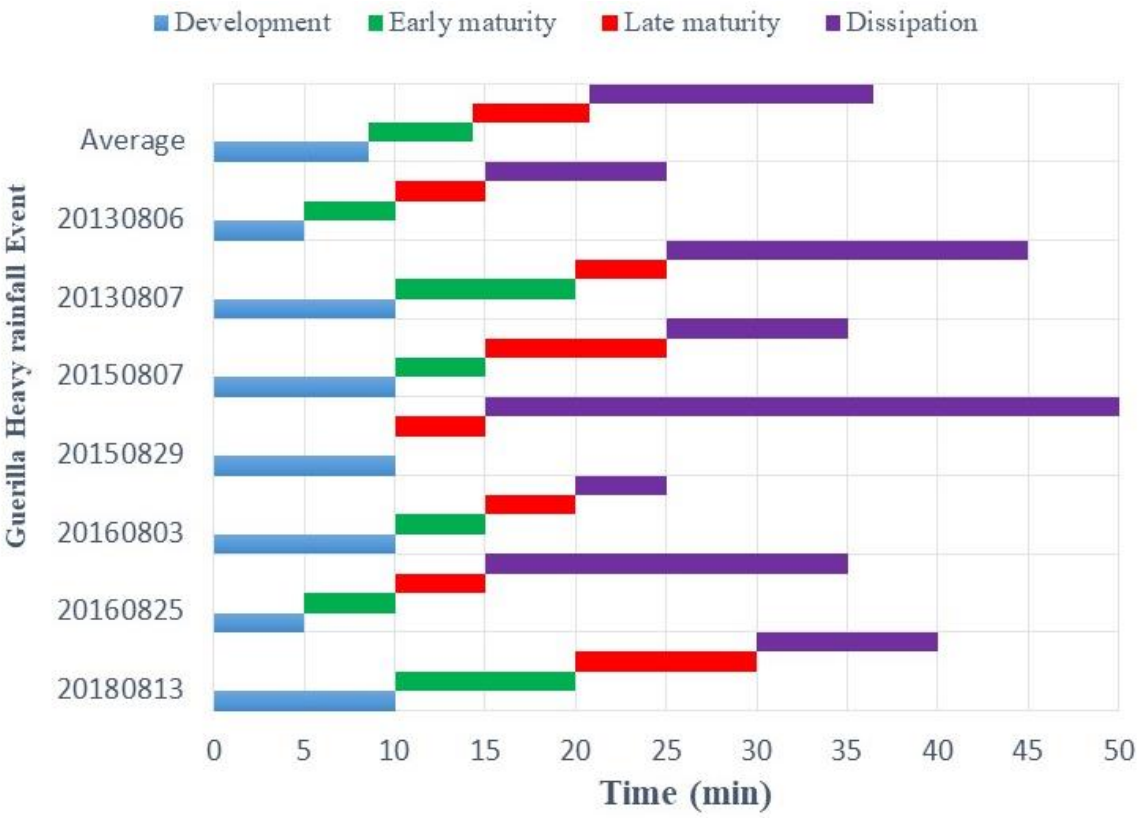

Figure 5.3 The 5 minutes life cycle discrimination on the guerrilla heavy rainfall events.

5.3 Results and Discussion

In this chapter, by using the variables (i.e., the reflectivity, vertical vorticity, divergence, convergence, and vertical wind) obtained through multiple Doppler radar analysis, the physical and statistical comparisons between the life cycle and rain stage are performed to predict the risk quantitatively with high accuracy.

5.3.1 Analysis physically on the development process of convective cell and the characteristics of variables according to the life cycle

The development processes of the convective cell every 5 minutes along with the variables calculated by multiple Doppler radar analysis are shown in Figure 5.4 on 13th August 2018 rainfall event. The blue, green, and red lines are the development, early maturity, and late maturity life cycle, respectively. The development processes of the convective cell for the other guerrilla heavy rainfall events can be seen in Appendix B. The three-dimensional reflectivity, vorticity, divergence, convergence, and updraft are represented as 5 minutes intervals. Then, the value of vorticity pairs, divergence, and convergence increase while the convective cell develops into guerilla heavy rainfall. The divergence and convergence can be an explanatory variable because convergence occurs in the lower layers at the beginning of the cumulonimbus cloud. The updraft and convergence could bring the water vapor from the lower layers to the upper layers. In addition, a pair of vertical vorticity is formed in the development of the cumulonimbus cloud. According to the results, we consider that the vorticity, divergence, convergence, and vertical wind are related to the predicted risk level of guerrilla heavy rainfall. Especially, on the development process, the discrimination of the life cycle reflects the physical aspects clearly. It represents that the pair of vertical vorticity are maturing as a strong updraft occurs. It could be confirmed that the risk

triggered by guerrilla heavy rainfall could be expressed on the life cycle better than the rain stage with a time interval of 5 minutes.

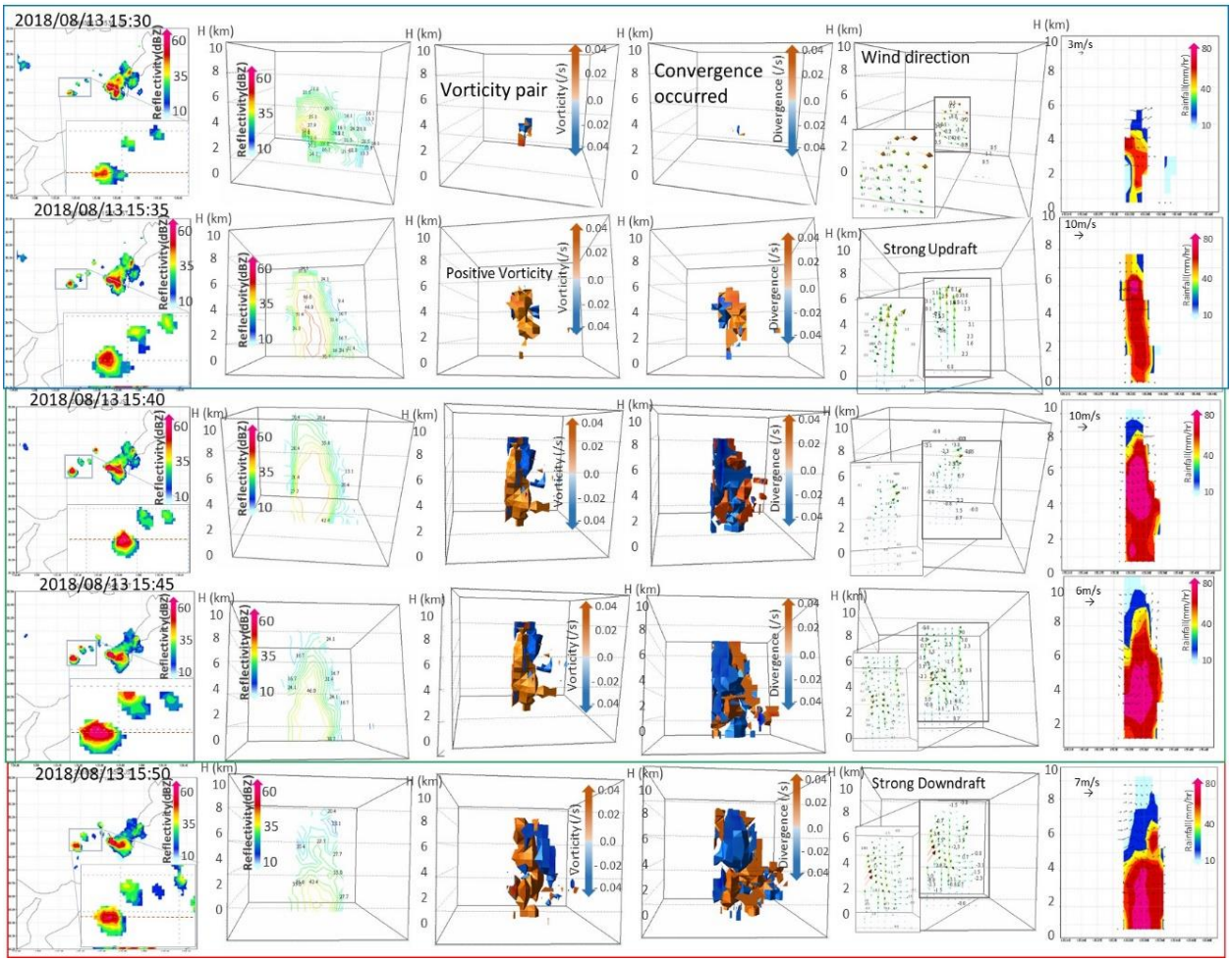

Figure 5.4 The characteristics according to the development of the convective cell according to the variables (i.e. radar reflectivity, the vorticity, divergence, convergence, and vertical wind) on 13th August 2018. The blue, green, and red lines are the development, early maturity, and late maturity life cycle, respectively.

5.3.2 Analysis statistically in comparison between life cycle and rain stage according to the three-dimension scatter and surface plots

For each rain stage and life cycle, the relationships between the predicted risk level and variables are expressed with the three-dimension scatter and surface plots in Figure 5.5 and Figure 5.6, respectively. The three-dimension scatter and surface plots can represent the relationship among the predicted risk level and the variables (i.e., reflectivity, vorticity, divergence, convergence, and vertical wind). The point is the predicted risk level according to the value of two variables. The surface plots show the functional relationship among the predicted risk level and the two variables. In addition, the table shows the correlation between the predicted risk level and each variable. The upper part of the diagonal represents the correlation as an ellipse shape. On the other hand, the lower part shows the correlation as a number. This research focuses on the early rain stage and life cycle for saving evacuation time to escape from danger because the guerrilla heavy rainfall occurs within a few minutes. On the late rain stage and life cycle, the reflectivity and rainfall are observed as large value, so that the risk of guerrilla heavy rainfall can be identified. To see the explanatory ability of variables on the early rain stage and life cycle, Figure 5.5 and Figure 5.6 was compared. In the development and early maturity life cycle, the vorticity, convergence, and vertical wind have a stronger correlation with the predicted risk level than in the early rain stage. The variables are important to predict the risk level triggered by guerilla heavy rainfall. This is because a vertical vortex tube is formed by the strong updraft to bring the water vapor when the vorticity is detected in the development of the cumulonimbus cloud. Therefore, it is useful to consider the relationship between predicted risk level and variables (i.e., reflectivity, vorticity, divergence, convergence, and vertical wind) of the life cycle.

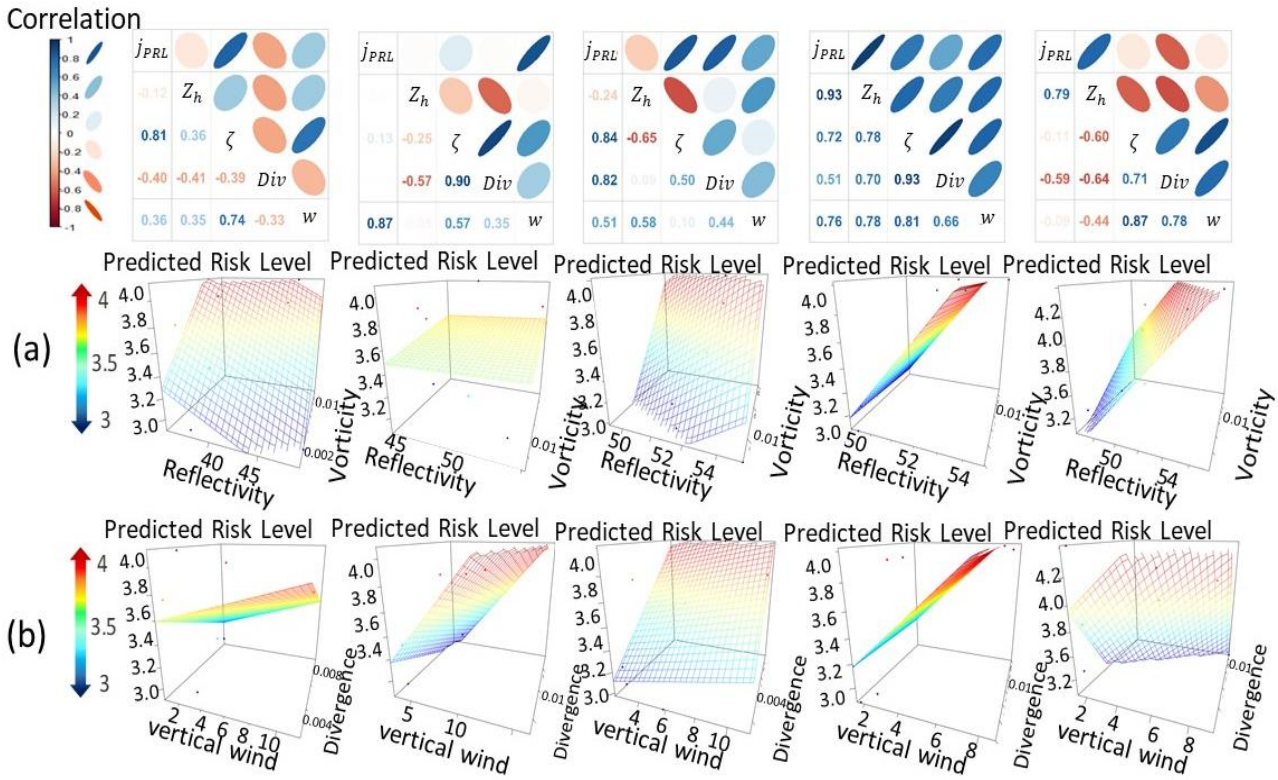

Figure 5.5 The performance of rain stage dependent regressions by correlation, three-dimension scatter and surface plots. By multiple Doppler radar analysis, the relationship between (a) the reflectivity and vorticity, and (b) divergence and vertical wind.

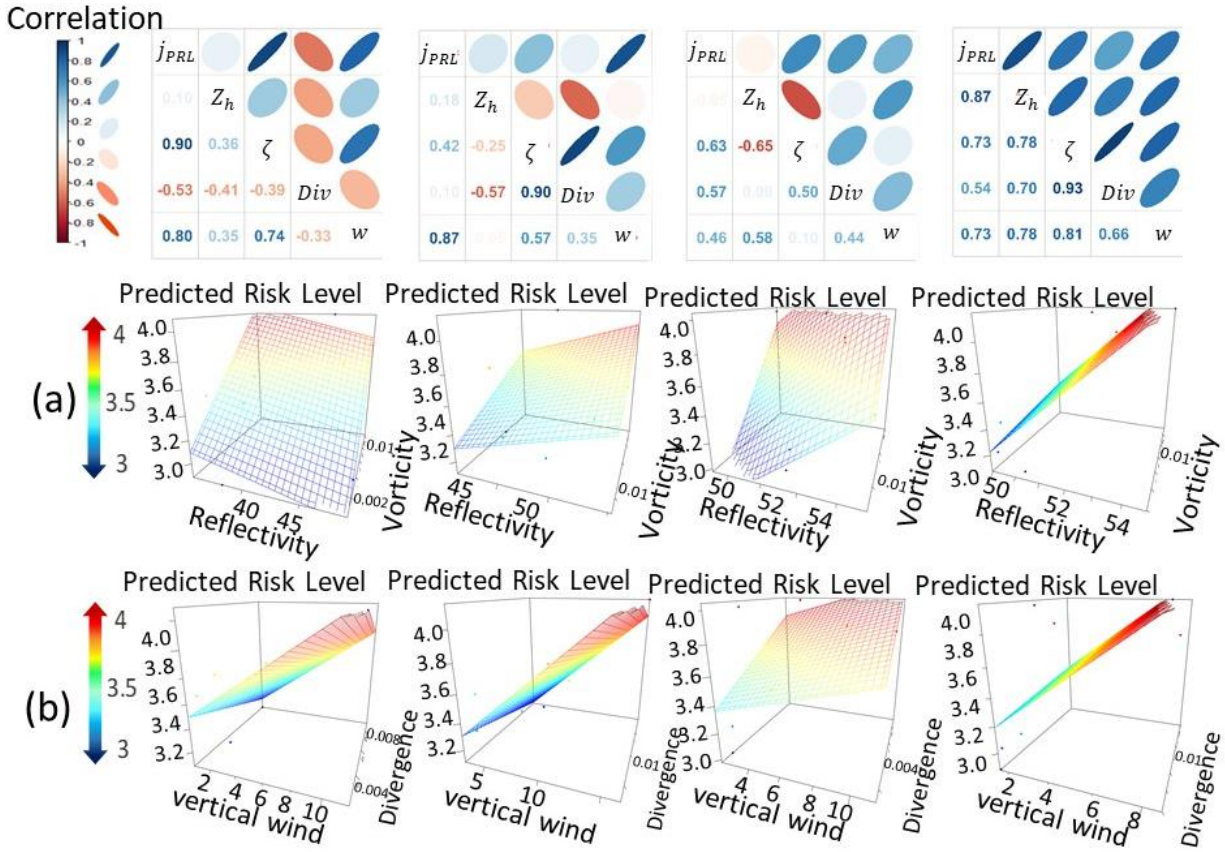

Figure 5.6 The performance of life cycle dependent regressions by correlation, three-dimension scatter and surface plots. By multiple Doppler radar analysis, the relationship between (a) the reflectivity and vorticity, and (b) divergence and vertical wind.

5.4 Conclusion

In this chapter, the relationship is analyzed by reflecting on the physical mechanism. To predict the risk level, the applicability of the quantitative risk prediction method was considered as physical and statistical analyses according to the characteristics of the variables. It could be confirmed that the risk triggered by guerrilla heavy rainfall could be expressed on the life cycle better than rain stage with a time interval of 5 minutes. The usefulness of the life cycle could be explained as the following analyses. First of all, the characteristics of variables according to the

development process are physically analyzed. The predicted risk level was estimated based on the time of the maximum rainfall intensity on the ground by isolated cumulonimbus clouds. With the three-dimensional reflectivity, vorticity, divergence, convergence, and updraft, we found that the value of vorticity pairs, divergence, and convergence increased while the convective cell developed into guerrilla heavy rainfall. Especially, we confirmed that the discrimination of the life cycle reflects clearly the physical aspects, which is that the vorticity, convergence, and vertical wind are related to the predicted risk level of guerrilla heavy rainfall. Then, according to the three-dimension scatter and surface plots, the life cycle and rain stage were compared statistically. In the development and early maturity life cycle, the vorticity, convergence, and vertical wind have a stronger correlation with the predicted risk level than in the early rain stage. When the vorticity is detected in the development of the cumulonimbus cloud, the variables are important for predicting the risk level triggered by guerilla heavy rainfall as the vertical vortex tube is formed by the strong updraft to bring the water vapor. Therefore, it is verified to consider the relationship between predicted risk level and variables (i.e., reflectivity, vorticity, divergence, convergence, and vertical wind) of the life cycle. However, the guerrilla heavy rainfall events are still not enough to be used in various conditions. The data insufficiency could cause overfitting in the analyses. In future research, if more rainfall events are collected, this problem should be solved. Also, the existence of other explanatory variables could find the structure of the cumulonimbus cloud and help the improvement of disaster prevention.

CHAPTER 6

Application of Flash Flood guidance using Weather Radar and Topographic Data

Abstract To alert flash flood warnings, flash flood guidance (FFG) was considered to determine the criteria at which flash floods occur. The flash flood guidance is the amount of precipitation needed in a specific period of time to initiate flooding on the watershed. In this chapter, the flash flood guidance was applied and assessed to alert flash flood events in the Toga River basin, Kobe city. The flash flood guidance was estimated based on threshold runoff and the soil moisture by using the SWMM which is the rainfall-runoff model. In this research, by using topographic (i.e., DEM, land use, cross-section, etc.) and meteorological (i.e., radar rainfall intensity) data, the flash flood guidance was estimated on the mixed land use (i.e., the rural and urban land uses). So, this method is possible to issue flash flood warnings without the need to run the entire hydro-meteorological process in the region where flash floods frequently occur. As a result of the calculation of the flash flood guidance, the value at 10 minutes rainfall duration has the range of 9.97 to 23.89 mm when flash floods occur.

6.1 Introduction

Flash floods caused by heavy rainfall are recognized as one of the most costly and fatal natural disasters in the world (Saharia et al., 2017). Flash floods are often accompanied by other disasters such as landslides, bridge collapses, and casualties. The magnitude of flash floods depends on several natural and human factors, including the duration and intensity of precipitation, soil moisture, land use, soil, and watershed characteristics. The rainfall intensity and soil moisture are the most important effects among the factors (Martínez-Mena et al., 1998; Castillo et al., 2003). The ability of soil conditions to store water affects the likelihood of a sudden increase in surface

runoff and flash floods (Norbiato et al., 2008). Soil moisture is affected by infiltration and runoff as it interacts with the atmosphere through evapotranspiration during heavy rainfalls. Especially, initial soil moisture condition is an important hydrological factor. So, assessing susceptibility to flash floods by considering initial soil moisture conditions is critical in determining the location of river systems that may be affected by flash floods.

Flash floods are characterized by rapid occurrences (within 6 hours after rainfall) and difficult to alert flash flood warning. The rainfall comparison method is one of the flash flood warnings. This method can determine the flash flood occurrence just by comparing the observed rainfall and estimated criteria. The USA National Weather Service regularly develops and relies on flash flood guidance (FFG) (Georgakakos, 2006) calculations to alert flash flood warnings. The flash flood guidance is the amount of precipitation needed in a specific period of time to initiate flooding on a watershed. The flash flood guidance provides usefulness by simplifying the hydrological conditions of the watershed, making it easier to collect precipitation information, and facilitating close cooperation between hydrologists and meteorologists (Norbiato et al., 2008). Therefore, in this chapter, the flash flood guidance was applied and used to alert flash flood events in Toga River, Kobe city.

6.2 Data and Methodology

From 2012 to 2020, the 4 events were collected for calibration and verification of SWMM. Thiessen polygon method was applied to the radar rainfall data to calculate the mean area precipitation on the watershed. GIS data such as Digital Elevation Model (DEM), slope, land use, and impervious area were constructed. This is the basic data necessary for calculating the threshold

runoff and soil moisture. The information was established by the MLIT and from the Geospatial Information Authority of Japan. Also, the cross-section data were collected from Hyogo prefecture.

6.2.1 Estimation of Flash Flood Guidance (FFG)

Figure 6.1 represents the procedure for estimating the flash flood guidance for flash flood warning. In order to obtain flash flood guidance at a specific time (*t*), the estimation of Threshold Runoff (TR) and Soil moisture Deficit (SD) is needed as components of flash flood guidance. The soil moisture conditions were simulated by using a rainfall-runoff model. Also, the threshold runoff was estimated by using topographic data (i.e., digital elevation model, soil map, land use, etc.) and watershed and river characteristic factors (i.e., area of the watershed, river width, river slope, etc.). Figure 6.2 shows the component of flash flood guidance.

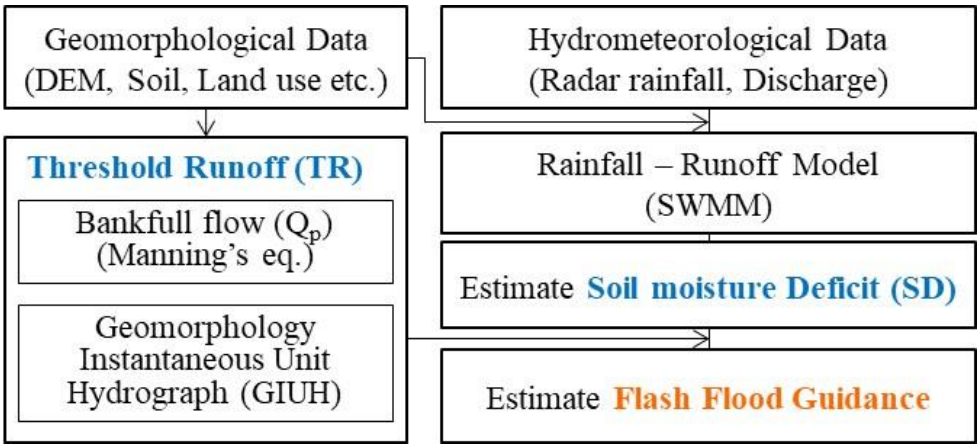

Figure 6.1 Flowchart of Flash Flood Guidance (FFG) estimation.

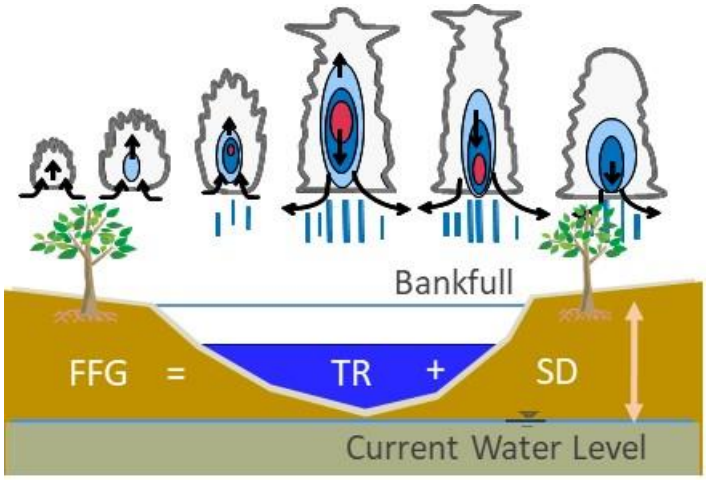

Figure 6.2 The component of Flash Flood Guidance (FFG).

6.2.1.1 Threshold Runoff (TR)

The threshold runoff represents the amount of effective rainfall accumulated during a given time period t_r [hr] over a basin that is enough to cause flooding at the outlet of the draining stream. Effective rainfall is rainfall leading to direct runoff excluding rainfall loss. Threshold runoff values are based on the flood flow Q_p [cms] unit hydrograph peak q_{pR} [cms/km^2/cm] and watershed area A [km^2]. The bankfull flow Q_{bf} [cms] is used as flood flow. The calculations of Q_{bf} and q_{pR} require the channel cross-section parameters. Direct measurements of channel cross-sections are performed through local surveys. The bankfull width B [m], hydraulic depth H [m], and local channel slope S_c [-] can be obtained from on-site measurements. Assuming that watersheds respond linearly to excess rainfall, threshold runoff can be estimated by equating the peak discharge determined from the unit hydrograph over a given duration to the bankfull discharge at the outlet. Mathematically, this is expressed as follows:

$$TR = Q_p/(q_{pR} \cdot A)\,, \tag{6.1}$$

where Q_p [cms] is the flood flow, q_{pR} [cms/km^2/cm] is the unit hydrograph peak for a specific duration t_r [hr], A [km^2] is the watershed area and TR [cm] is the threshold runoff. For estimating threshold runoff, Carpenter et al., 1999 presented the flood flow (Q_p) and the unit hydrograph peak (q_{pR}).

6.2.1.1.1 Flood flow, Q_p

The flood flow Q_p can be calculated either as physically bankfull discharge Q_{bf} by using Manning's equation or statistically as the two year return period flow. The two-year return period flow collects the annual maximum rainfall or flood data. Then, the probability rainfall is calculated by frequency analysis, and the design flood is determined according to the design frequency. However, this method is difficult to use because the available data are not sufficient since most of the watersheds are unmeasured. In this study, the bankfull discharge was computed from channel geometry and roughness characteristics by using Manning's equation for steady, uniform flow (Chow et al., 1988). However, most of the stream flows under the non-uniform flow.

In this chapter, the flow characteristic factors (velocity, water depth, pressure, etc.) are constant in the river section where the cross-sectional shape and slope of the river do not change significantly in the longitudinal directions and are less affected by the upstream or downstream. Then, the flood can be calculated under uniform flow. Also, Henderson, 1966 proved that the resistance equation in turbulent flow and the Manning equation have mathematically the same characteristics. Therefore, when the embankment begins to overflow, the flow can be calculated by applying Manning's equation. Manning's equation for steady, uniform flow is expressed by the following equation,

$$Q_{bf} = A_b \cdot R_b^{2/3} \cdot S_c^{0.5}/n \ , \tag{6.2}$$

$$R_b = \ A_b/P_b \ , \tag{6.3}$$

where Q_{bf} [cms] is the bankfull flow, A_b [m^2] is the cross-sectional area of the flow, R_b [m] is the hydraulic depth, S_c [-] is the local channel slope, n is the Manning's roughness coefficient, P_b [m] is the wetted perimeter of the flow, and D_b [m] is the bankfull hydraulic depth. The subscript b is the state just before the embankment overflows. The streams generally have a very large channel width compared to hydraulic depth. Therefore, when the embankment is full, the bankfull channel width B_b [m] and wetted perimeter P_b [m] show similar values. The flood flow is expressed by the following equation,

$$R_b = \ A_b/B_b = D_b \ , \tag{6.4}$$

$$Q_{bf} = A_b \cdot D_b^{2/3} \cdot S_c^{0.5}/n \ . \tag{6.5}$$

The relationship between channel width B and water depth Y can be approximated in the form of a power function as in the following equation,

$$\mathrm{B} = K \cdot Y^f \ , \tag{6.6}$$

where k is the coefficient of the power function, f is the shape coefficient of the section which has various coefficients depending on the shape of the section. A spherical section, a bowl-shaped section, a parabolic section, a triangular section, and an inverted triangular section are represented

by coefficients of 0, 0.2, 0.5, 1.0, and 1.5, respectively. When the embankment overflows, Equation 6.7 is expressed by integrating the cross-sectional area of the flow A_b [m^2] with respect to the water depth of Equation 6.6 by the following equation,

$$\int B_b \, \mathrm{dy} = A_b = K \cdot {Y_b}^{f+1}/(f+1) \, . \tag{6.7}$$

In general, it is difficult to calculate the hydraulic depth D_b by measuring the cross-sectional area A_b and channel width B. If the hydraulic depth D_b can be expressed as a function of the water depth Y, it can be expressed as Equation 6.8 using Equations 6.6 and 6.7. Also, $A_b D_b^{2/3}$ in Equation 6.5 can be expressed as Equation 6.9.

$$D_b = A_b/B_b = K \cdot {Y_b}^{f+1}/((f+1) \cdot K \cdot {Y_b}^{f}) \; = {Y_b}^{f}/(f+1) \, , \tag{6.8}$$

$$A_b \cdot D_b^{2/3} = B_b \cdot D_b \cdot D_b^{2/3} = A_b \cdot D_b^{5/3} = B_b \cdot [Y_b/(f+1)]^{5/3} \, . \tag{6.9}$$

Therefore, the flood flow is expressed as a function of water depth Y by the following equation,

$$Q_{bf} = B_b \cdot S_c^{0.5}/n \cdot [Y_b/(f+1)]^{5/3}. \tag{6.10}$$

where the n is the Manning's roughness coefficient and has the range from 0.035 to 0.15. When the n is greater than or equal to 0.035, Jarrett, 1984 presents Manning's roughness coefficient equation as a function of local channel slope S_c, and hydraulic depth D_b,

$$n = 0.39 \cdot S_c^{0.38} / [Y_b/(f+1)]^{0.16} \ . \qquad (6.11)$$

6.2.1.1.2 Unit hydrograph peak, q_{pR}

To obtain the peak discharge, the unit hydrograph can be derived using various methods, such as Snyder's synthetic unit hydrograph approach (Chow et al., 1988) or the geomorphologic instantaneous unit hydrograph (GIUH) method (Rodríguez-Iturbe et al., 1979). However, Snyder's synthetic unit hydrograph can calculate a watershed representative unit hydrograph by using a unit hydrograph derived through regional regression analysis, but has disadvantages in that the calculation is complicated, such as the absence of available data and the calculation of empirical parameters for each watershed.

In this study, we used the GIUH method to obtain peak discharge. In order to understand GIUH method, the concept of Instantaneous Unit Hydrograph (IUH) is necessary. An instantaneous unit hydrograph is a hydrograph that shows the flow to the watershed outlet when the unit effective rainfall falls to the watershed over time. The general unit hydrograph has the same duration as the duration of the effective rainfall, but the instantaneous unit hydrograph is a hypothetical concept in which the duration of the unit effective rainfall is close to zero. By combining the instantaneous unit hydrograph and the topographical characteristics, Rodriguez-Iturbe and Valdes, 1979 presented the GIUH method statistically by applying the travel times until the outlet of the watershed when the rainfall particles fall into the watershed. To use the GIUH method, it is assumed that the target watershed follows Horton's and Strahler's law as follows (Geological Survey, 1965). 1) A stream that has no tributaries in the uppermost stream is called a first-order streams. 2) When the i-th order stream join, it becomes the i+1-order stream. 3) When

streams of different orders meet at the junction, the larger order is selected. The relationship between the topographical factors of the watershed is as follows:

1. Law of stream numbers : $N_\omega / N_{\omega+1} = R_B$
2. Law of stream lengths : $L_\omega / L_{\omega-1} = R_L$
3. Law of stream areas : $A_\omega / A_{\omega-1} = R_A$

where R_B , R_L , and R_A are the bifurcation ratio, stream length ratio, and basin area ratio, respectively. R_B is in the range generally 3 to 5, R_L is in the range of 1.5 to 3.5, and R_A is in the range of 3 to 6. ω is the order of streams, N_ω is the number of streams, L_ω is the mean length of streams order, and A_ω is the mean area contributing to stream order.

Rodriguez-Iturbe and Marcelo, 1982 defined the velocity, included in the peak time and peak discharge of IUH suggested by Rodriguez-Iturbe and Valdes (1979), as a function of effective rainfall intensity and rainfall duration. The peak time is expressed as Equation 6.12, and the peak discharge is expressed as Equation 6.13:

$$t_p = C_3 \cdot \Pi^{0.4} \ , \tag{6.12}$$

$$q_{PR} = C_4 / \Pi^{0.4} \ , \tag{6.13}$$

where t_p [hr] is the peak time, q_{PR} [hr^{-1}] is peak discharge, C_3 and C_4 is unit conversion coefficients, and they have values of 0.58 and 0.88 when the United States customary units. Π is a parameter as shown below,

$$\Pi = L^{2.5} / (i \cdot A \cdot R_L \cdot \alpha^{1.5}) , \quad (6.14)$$

$$\alpha = Sc^{0.5} / n \cdot B^{2/3} . \quad (6.15)$$

where i [cm/h] is the effective rainfall intensity, A [km^2] is the drainage area, L [km] is the mainstream length, R_L [-] is Horton's length ratio, S_c [-] is the local channel slope, n [-] is the Manning's roughness coefficient, and B [m] is the top width. In addition, Rodriguez-Iturbe and Marcelo, 1982 converted the peak discharge and time of the IUH into the peak discharge and time of the IUH corresponding to the equivalent excess rainfall of the time duration (t_R). These are expressed as follows:

$$Q_p = 2.42 \cdot i \cdot A \cdot t_R / \Pi^{0.4} (1 - 0.218 \cdot t_R / \Pi^{0.4}) , \quad (6.16)$$

$$t_{PR} = 0.585 \cdot \Pi^{0.4} + 0.75 \cdot t_R . \quad (6.17)$$

The rainfall intensity (i) can be said to be equal to the value obtained by dividing the threshold runoff (TR) by the duration (t_R). So, the peak discharge is expressed as follows:

$$Q_p = 2.42 \cdot TR \cdot A / \Pi^{0.4} (1 - 0.218 \cdot t_R / \Pi^{0.4}) . \quad (6.18)$$

If B and S_c in Equation 6.18 are used as the values for the bankfull flow, the peak discharge of GIUH and Manning's equation are the same. Then, the threshold runoff can be estimated by substituting $i = TR / t_R$. It is a nonlinear function because the variable of threshold runoff includes a term of Π. To estimate the threshold runoff, an approximation was obtained by the Newton-Raphson method.

In this study, as described above, to calculate the threshold runoff, the bankfull overflow was calculated using Manning's equation, and the peak flow in the unit hydrograph was obtained using the GIUH method. This is because these methods have the advantage of being able to accurately extract geomorphological variables with the GIS and extracting parameters on a physical basis.

6.2.1.2 Soil moisture Deficit (SD)

The soil moisture deficit is the amount of soil moisture remaining after subtracting the current soil moisture from the maximum amount of soil moisture. Since the amount of soil moisture and insufficient soil saturation change over time under the influence of rainfall, continuous simulation should be possible. As a method, there is a direct method using lysimeter, neutron probe, Time domain reflectometry (TDR), etc. and an indirect method simulated by a rainfall-runoff model.

6.2.1.2.1 Storm Water Management Model (SWMM)

The urban runoff model has been studied since the 1970s to interpret urban runoff according to the physical changes that urbanization has on watersheds. The urban runoff model is the result of an aim to quantify and model all physical phenomena related to a series of processes from the rainfall to the runoff. The general structure of the urban runoff model consists of design rainfall estimation, watershed loss estimation, characteristics of surface runoff modeling, storm water pipe inflow, sewage pipe estimation, and runoff hydrograph calculation at the pipe end. In general, the criteria for judging the validity of the urban runoff model include the validity of the

assumption that modeled the physical process, the accuracy of the watershed loss, and the error of the simulation for the observed streamflow.

Storm Water Management Model (SWMM) was developed to simulate accurate rainfall-runoff characteristics and water quality in urban watersheds. In 1971, under the support of the US Environmental Protection Agency (EPA), Metcalf and Eddy developed a joint research project with the University of Florida and Water Resources Engineers Inc. of Walnut Creek California (WRE) to simulate flow discharge and water quality in urban watershed sewage systems (EPA, 2004). The SWMM can be simulated in single rainfall and continuous rainfall events. SWMM includes 4 executive blocks, 5 service blocks, and 126 sub-programs. In this research, the SWMM 5.0 version, which can be downloaded free from the US EPA website, was used.

The Executive block is responsible for controlling other executive blocks and transferring data between the blocks. The RUNOFF block applies a nonlinear storage function to the block that performs the initial simulation. The runoff analysis of this model uses data (i.e., land use, rainfall, topography, and antecedent moisture condition) and can consider rainfall, snow cover, surface runoff, and subsurface flow. In the TRANSPORT block, the flow discharge and pollutants in the sewage system are tracked, and infiltration calculation is also possible using kinematic equations based on the calculation results of the RUNOFF block. In order to complement the TRANSPORT block in the EXTRAN block, it is possible to calculate the flow discharge of a Loop network type that could not be calculated with the existing urban runoff model. It is possible to calculate flow discharge by considering the drainage, orifice, weir, pumping station, reservoir, etc. It is designed to work with dynamic and continuity equations. The STORAGE block controls the flow discharge and water quality in the storage tank and evaluates the effectiveness of the treatment filtration.

As the service blocks of SWMM, the Graph block outputs the pollution curve and the hydrograph. The Combine block synthesizes and manages the hydrology and pollution curves in the interface file, so the calculation results are combined with the results of other blocks and applied to other drainage systems. Rain block considers the temporal and spatial distribution of rainfall by using up to 10 rainfall data simultaneously. The Temp block is a block that calculates the temperature. It is used when calculating the snowmelt of the RUNOFF block and is also used as a basic data for calculating evapotranspiration. The Statistic block uses the Weibull function to analyze peak discharge, runoff, duration, pollutants, mean discharge, etc. in a watershed.

Primarily, SWMM is used for urban areas and is a dynamic hydrologic-hydraulic simulation model; however, SWMM also could have applications for drainage systems in non-urban areas (Talbot et al., 2016). Tsai et al. (2017) show that the SWMM simulations can be applied in the pervious area by conceptualizing a drainage system as a series of water and material flows between several environmental compartments. The runoff is estimated by a non-linear reservoir method, considering infiltration, depression loss, storage, and evaporation. SWMM has three methods to simulate infiltration from the surface-watershed to a sub-watershed: Green-Ampt infiltration, Horton infiltration, and Curve Number infiltration. In this research, the Green-Ampt infiltration method was used because this is physically based and easier to use both for a single event and continuous simulation. Three parameters are important as the hydrologic components of the method: saturated hydraulic conductivity, initial moisture deficit, and suction head at the wetting front.

6.2.1.2.2 Estimation of soil moisture deficit

The saturated soil moisture is that the outflow starts when the soil is completely saturated. The soil moisture deficit can be estimated as follows,

$$TSAT = (FC - WP) \cdot Z \,, \tag{6.19}$$

$$SD = TSAT - CSAT \,, \tag{6.20}$$

where *TSAT* [mm] is the soil moisture in the completely saturated state, *FC* is the field capacity, *WP* is the permanent wilting point, *Z* [mm] is the soil depth, *CSAT* [mm] is the current soil moisture, and *SD* [mm] is the soil moisture deficit.

6.2.1.3 Flash Flood Guidance (FFG)

Flash flood guidance is the amount of rainfall needed in a specific period of time to initiate flooding on a small stream. Flash flood guidance and threshold runoff formed a non-linear relationship depending on the amount of moisture absorbed in the soil. If soil moisture is fully saturated and evapotranspiration does not occur, infiltration does not occur and the flash flood guidance is the direct runoff. This can be said to be the same as the threshold runoff, which is the effective rainfall calculated assuming that the soil is saturated. In other words, threshold runoff calculated by GIUH and Manning's bankfull overflow have a constant value for a watershed unless the cross-section of the stream changes. However, since the moisture in the soil is not always completely saturated, rainfall that falls on the watershed causes loss due to infiltration and evaporation. So, flash flood guidance does not always correspond to the direct runoff. Since flash floods occur when the overflows under the current soil moisture condition, direct runoff can occur

only when there is more rainfall equal to the threshold runoff and the insufficient amount of current soil moisture. Therefore, flash flood guidance is calculated in a time series according to the soil moisture condition, and the threshold runoff has a constant value for the watershed.

Since flash floods are caused by localized heavy rainfall of short duration, the loss of soil moisture due to evapotranspiration rarely occurs. Therefore, flash flood guidance can be calculated as the sum of the soil moisture deficit, which is the amount of rainfall required for the soil to become fully saturated, and the threshold runoff, which is the amount of rainfall required to bankull overflow assuming that the soil is saturated. The flash flood guide is determined by the formula:

$$FFG = SD + TR\ , \tag{6.21}$$

where *FFG* [mm] is flash flood guidance, *SD* [mm] is soil moisture deficit, and *TR* [mm] is threshold runoff.

6.3 Results and Discussion

The flash flood guidance on each watershed was calculated using the threshold runoff and soil moisture deficit. The water level that starts the observation was used to evaluate whether the mean area precipitation of radar exceeds the flash flood guidance.

6.3.1 Estimation of Threshold Runoff (TR)

Meteorological influences can significantly affect the timing, location, and severity of flash floods. Rainfall intensity and duration are key considerations when estimating flash flood

occurrence. Also, the hydrological influences cause flash floods significantly. That is why threshold runoff is necessary to estimate flash flood possibility.

6.3.1.1 Establishment of topographic data and classification of watershed

The digital elevation model can separate a basin and the hydrological data (i.e. the area of the watershed, slope, etc.) can be extracted. Through this data, the flow direction and average slope that affect the runoff of the watershed can be calculated. In this study, DEM, land use, and impervious area with a resolution of 5 m, 100 m, and 25 m were collected, respectively. Then, watershed characteristics parameters (i.e., the area of watersheds, slope, stream length) were calculated. Land use was classified into 4 categories (i.e., forest, cropland, urban, and paddy) and used as input data for the rainfall-runoff model. Figure 6.3(a)-(c) shows the digital elevation model, land use, and impervious area in the Toga River basin.

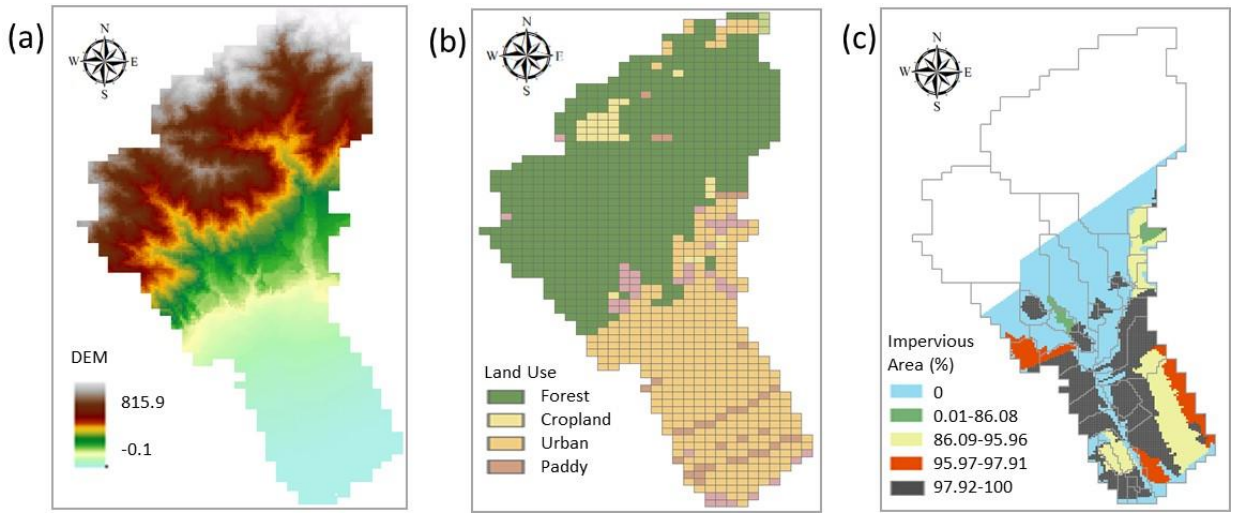

Figure 6.3 Construction of topographical data for threshold runoff and rainfall-runoff model.

In order to estimate the threshold runoff for each watershed, this study used the ArcGIS ArcHydro tool (Maidment, 2002) to divide watersheds from the Toga River basin and extract the streams. First, pre-processing of the raw DEM data was performed with DEM reconditioning operation, and the depression points that obstruct the flow in the watershed were filled to the same height as the surrounding grid, and then the channel section was defined using the stream vector data.

To find out the hydrological characteristics of the surface, the flow direction of all grids in the GRID data expressed as DEM was determined using the Flow Direction function. In this function, using the elevation of the DEM in Figure 6.4(a), the direction in which stream can flow in the 8 adjacent grids is found as shown in Figure 6.4(b). The flow direction was determined as the downstream direction with the steepest slope among the 8 adjacent grids. Therefore, when the steepest downstream slope is determined, the output cell is coded in that direction.

When the flow direction is determined as shown in Figure 6.4(c), the accumulated flow is calculated using the Flow Accumulation function (Figure 6.4(d)). Then, to divide the watersheds, the stream order function was used. The watersheds were divided when the stream order was over than 4. If it was not a natural stream, the stream order was determined as following an artificial channel. Figure 6.5 and 6.6 show the stream order and division of watersheds in the Toga River basin.

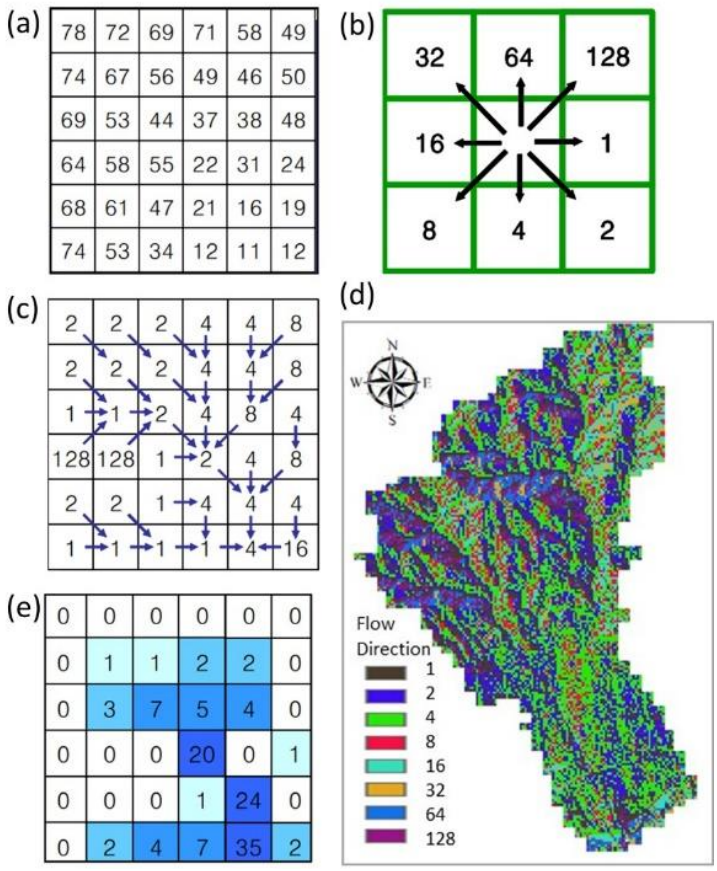

Figure 6.4 The method of flow direction and flow accumulation. The process of stream identification as (a) DEM, (b) direction in which stream can flow, (c, d) flow direction, and (e) flow accumulation.

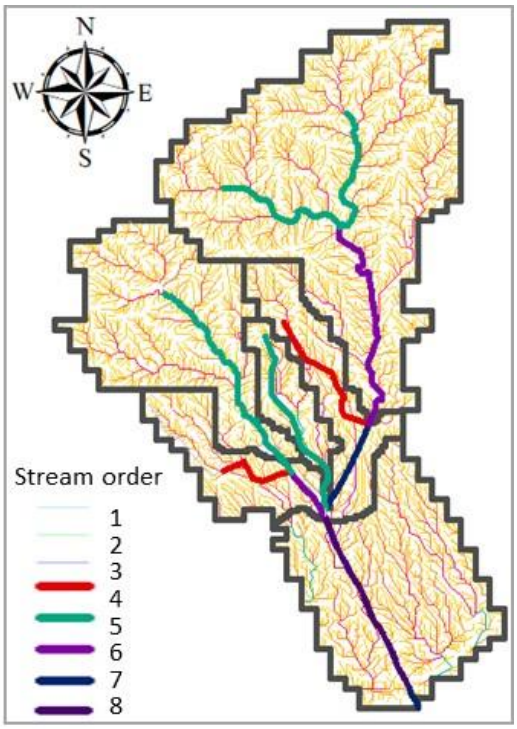

Figure 6.5 The stream order on Toga River basin.

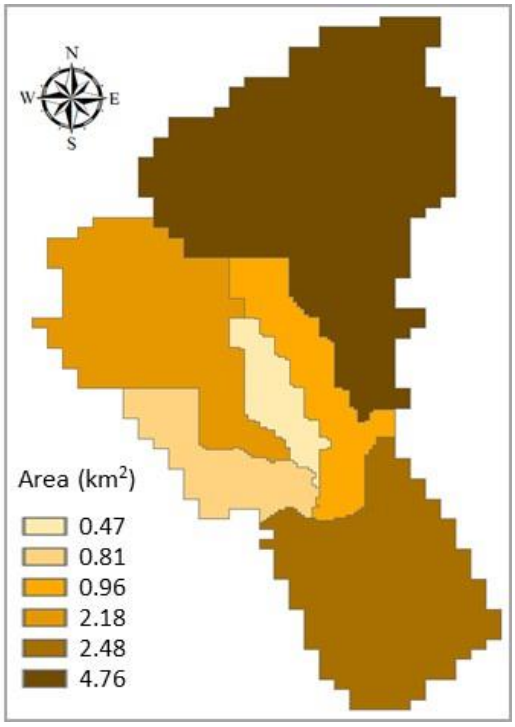

Figure 6.6 The division of watersheds on Toga River basin.

To collect the channel characteristics parameters (the area of stream, width, stream slope and hydraulic depth), the cross-section data of the Toga River basin were collected and analyzed from Hyogo prefecture. The data on the cross-section of the river is composed of natural and artificial cross-sections. The artificial cross-section considers the sewer system that has been prepared for damage of floods in advance. So, it is not suitable for the definition of the threshold runoff. However, the mountainous watersheds in Rokko and Somatani River affect the Toga River. The watershed in Rokko and Somatani River is composed of a natural stream. Also, the threshold runoff in the Toga River was estimated by applying the 50% of high water level. So, in this research, the threshold runoff can be estimated in a mountainous and urban area. Figure 6.7 shows the estimation topographic data with the cross section and longitudinal section on the Toga River basin.

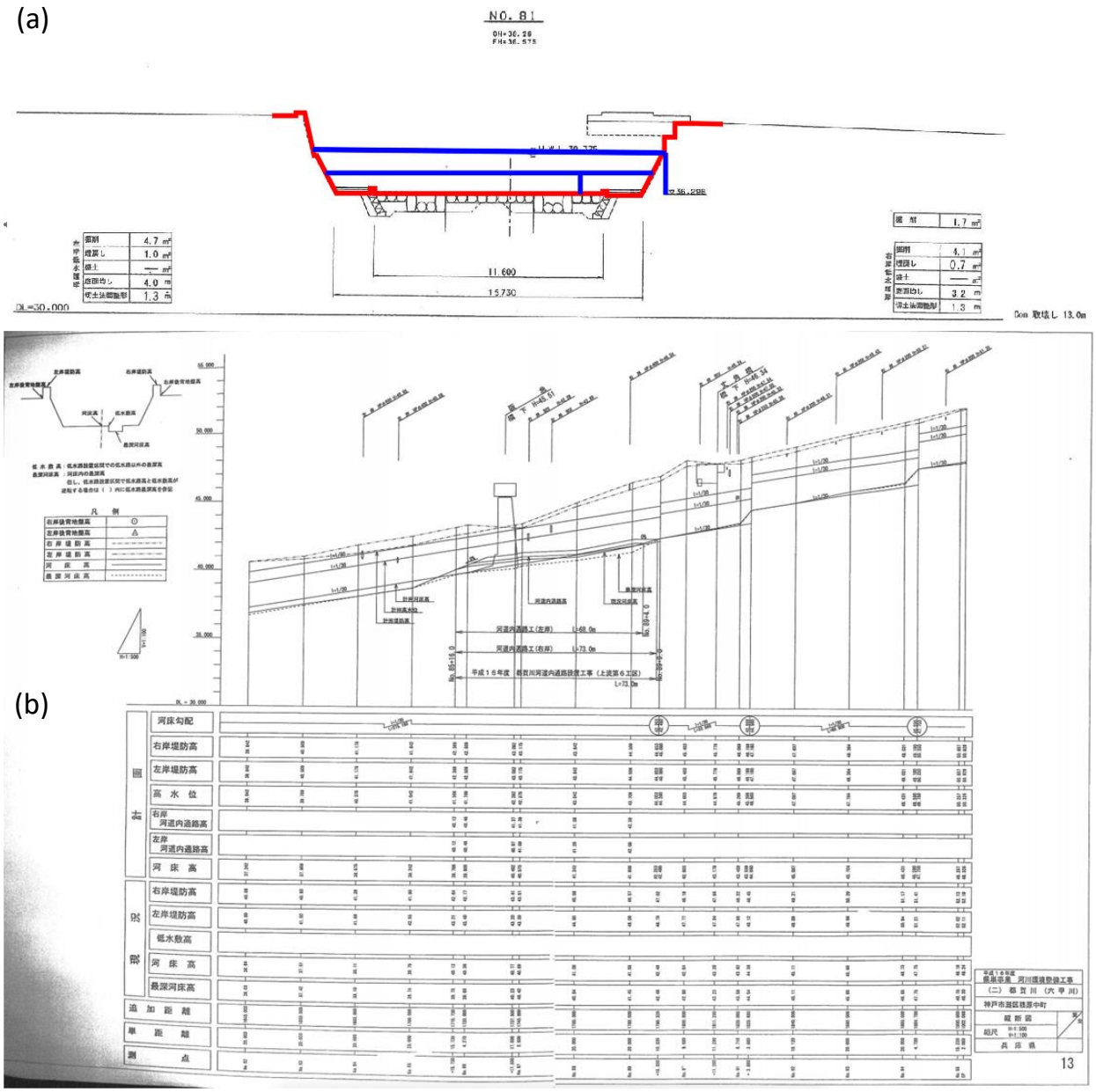

Figure 6.7 Estimation topographic data with (a) the cross section and (b) longitudinal section of No. 81 on the Toga River.

6.3.1.2 The threshold runoff on each watershed

The threshold runoff was calculated with Manning's equation and geomorphologic instantaneous unit hydrograph method using 10 minutes of rainfall observation data. The threshold runoff was reflected by watershed and channel characteristics parameters. As a result, the value of the threshold runoff on 10 minutes of rainfall observation data has the range of 4.05 to 19.48 mm, and the mean and standard deviation were calculated to be 13.43 mm and 6.34, respectively. Figure 6.8 shows the threshold runoff value for each watershed. The streams on 1 and 4 watersheds are small mountainous streams, so these have narrow streams and are highly affected by soil moisture. That is why the value of threshold runoff on 1 and 4 watersheds has a smaller value than the other watersheds.

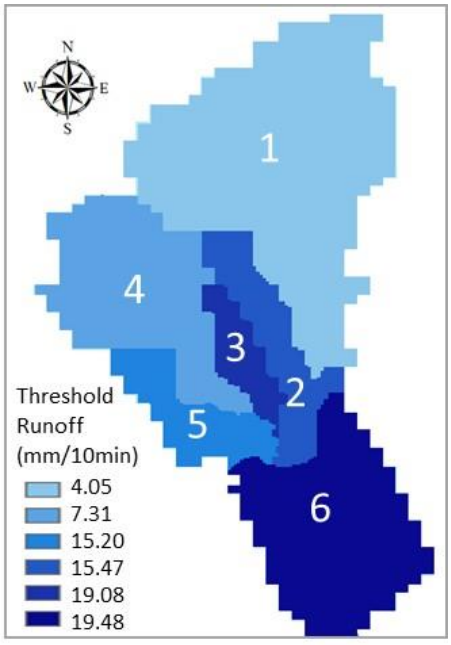

Figure 6.8 Threshold Runoff (TR)

6.3.2 Estimation of soil moisture deficit

The SWMM was constructed using radar rainfall as input data on the Toga River basin. The rainfall datasets were used to conduct event based simulations to analyze the hydrological outputs, including infiltration and runoff. The detailed infrastructure characteristics were needed as input data in the SWMM, such as basins, pipes, manholes, natural channels, pumps, etc. In this research, the SWMM contained 37 watersheds, 37 junction nodes, 16 links consisting of conduits, and an outlet. The Green-Ampt infiltration model, nonlinear reservoir method, and kinematic wave approach were selected to compute the infiltration losses, routing of overland flow, and routing of conduits flow, respectively. Figure 6.9 shows the division of watersheds and networks used to construct the SWMM. The Toga River basin is a mixed land use watershed where the rural and urban land uses affect the flood runoff analysis. In urban flooding, a number of sewage pipe networks and urban rivers are interconnected. To represent the accurate rainfall-runoff characteristics of urban areas, the SWMM integrates inland and river floods. In urban areas, the influence of soil moisture is low because of its high imperviousness. Leach and Coulibaly (2020) aim to identify the feasible imperviousness range to use soil moisture for improving hydrologic forecasting in an urban watershed. According to this research, soil moisture does not need to be considered in the impervious area of 65 - 75% or more. In this study, the effect of soil moisture was considered except for the watershed where the impervious area was 79.7% in the urban area.

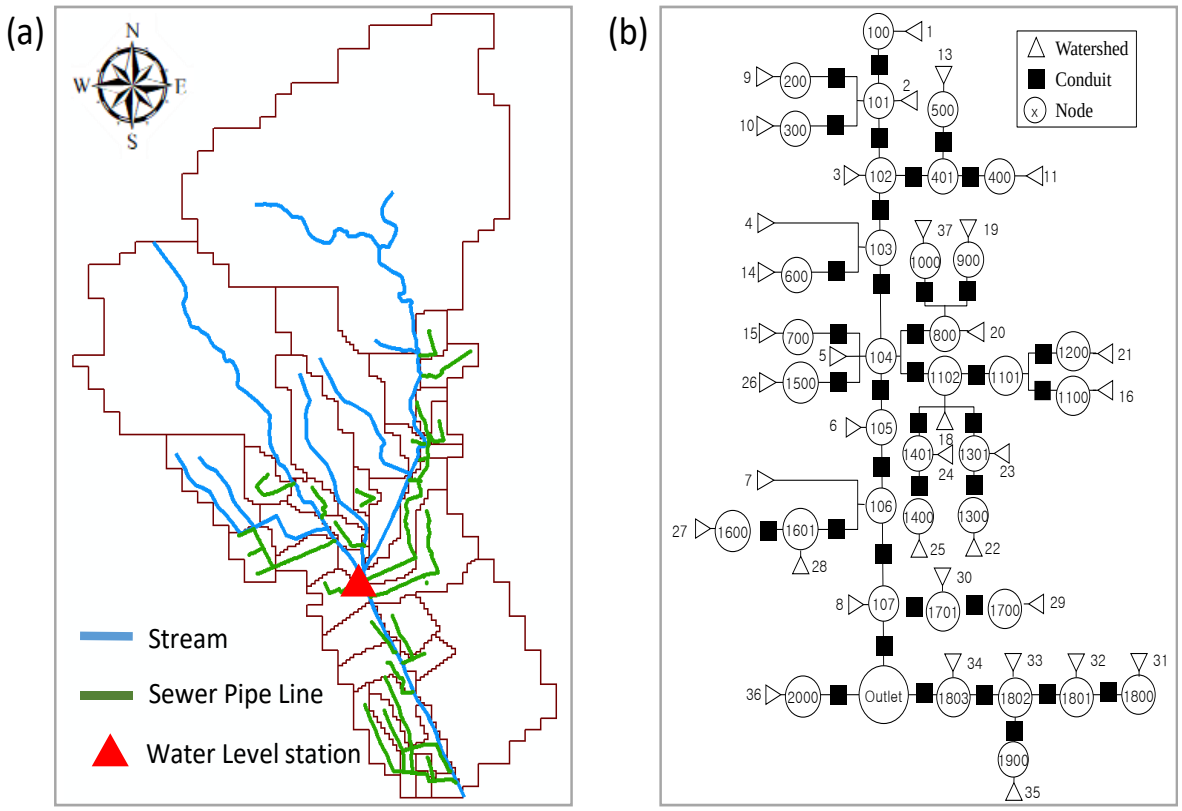

Figure 6.9 Division of watersheds and networks used to construct the SWMM: (a) pipe line (green line) and stream line (blue line); (b) channel network in the Toga River basin.

6.3.2.1 Calibration and verification of SWMM

The rainfall-runoff model is useful to simulate the effect of watershed processes and management on soil and water resources. Four flash flood events were selected to optimize the parameters of the SWMM. Table 6.1 is the list of the flash flood events. Although guerrilla heavy rainfall is the target event, it was selected for the verification because 2 to 3 o'clock on 25th Aug 2013 was shown as the rainfall. By optimizing the parameter, Figure 6.10 and Figure 6.11 present the calibration and verification results from two events each at the water level station (kabutobashi) using the radar rainfall data. The calibrated parameters included the percentage of impervious areas,

the watershed widths, infiltration, storage depth, and Manning's roughness coefficient for the watersheds and channels (Liong et al. 1995; Choi and Ball 2002). The parameter values used for the simulation are listed in Table 6.2.

Table 6.1. List of flash flood events

Calibration		Verification	
No.	Date	No.	Date
1	2012-07-21	1	2013-08-25
2	2020-07-03	2	2014-06-07

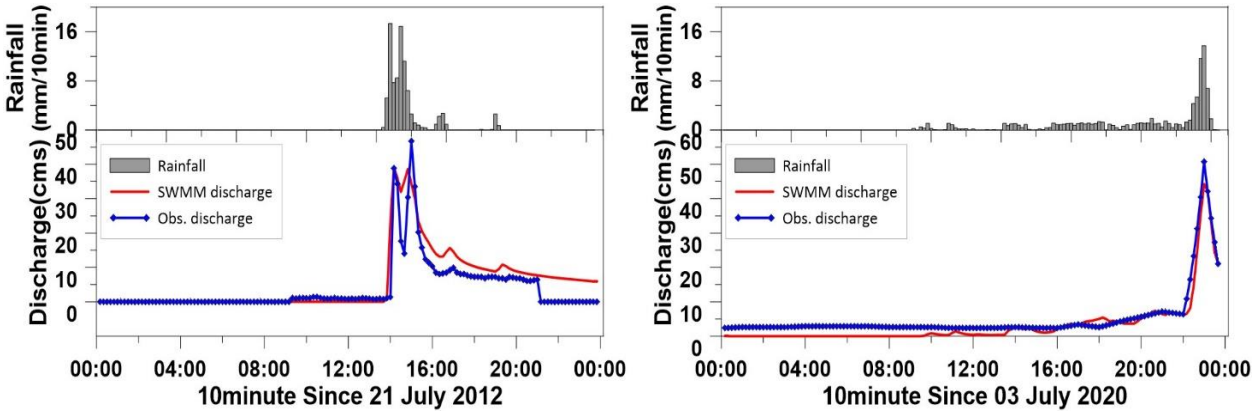

Figure 6.10 Results of model simulation: calibration results (21th July 2012 and 3rd July 2020).

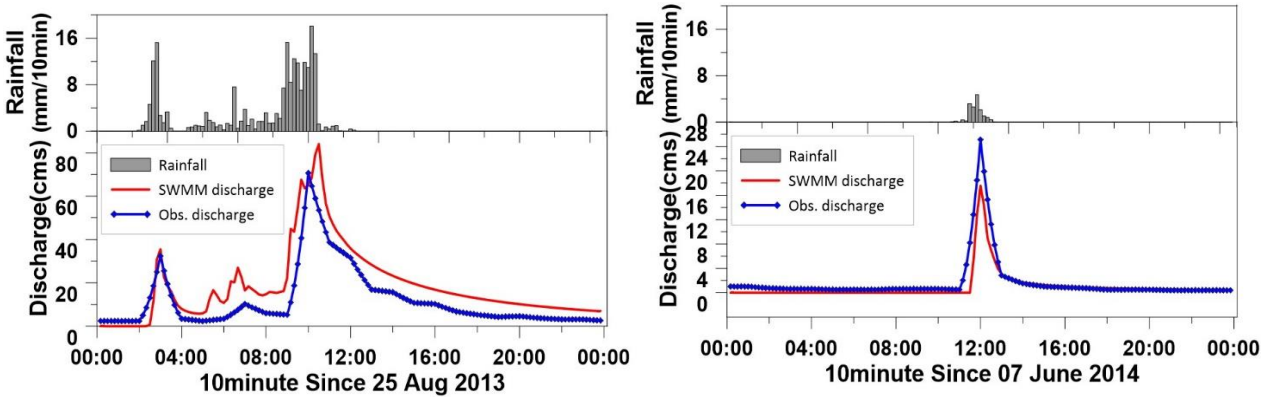

Figure 6.11 Results of model simulation: verification results (25th August 2013 and 7th June 2014).

Table 6.2 SWMM parameters used for the watersheds. Parameter descriptions adapted from Rossman and Huber (2016). The infiltration and aquifer parameters were obtained from Table A.2 in Rossman and Huber (2016). Other parameter values were chosen as they were similar to real-world urban watershed parameters (Liu et al., 2013)

Parameter	Description	Value	Unit
	Sub-catchments		
area	Sub-catchment area	3-500	ha
%Imperv	Impervious percentage of watersheds	0–100	%
Width	Characteristic width of watersheds	30-400	m
Slope	watersheds slope	0-45	%
	Sub-areas		
Nimp	Manning's n for impervious area	0.011	-
Nperv	Manning's n for pervious area	0.1-0.8	-
Simp	Depression storage for impervious area	0.05-1	mm
Sperv	Depression storage for pervious area	0.05-1.5	mm
%Zero	Percent of impervious area without depression storage	25	%
%Routed	Percent of runoff routed from impervious to pervious area	25-75	%
	Infiltration – Green-Ampt		
Psi	Soil capillary suction	166.878- 169.926	mm
Ksat	Saturated hydraulic conductivity	6.604	mm/hr
IMD	Initial soil moisture deficit (porosity – field capacity)	0.2-0.217	–
	Aquifers		
Por	Porosity	0.398-0.501	–
WP	Wilting point	0.135-0.136	–
FC	Field capacity	0.2-0.244	–
Ks	Aquifer saturated hydraulic conductivity	1.5-7.5	mm/hr
Kslp	Slope of the logarithm of hydraulic conductivity vs. moisture deficit	15-27	–
Tslp	Slope of soil tension vs. Moisture content	15	mm

Etu	Fraction of total evaporation available in unsaturated zone	0.2-0.4	–
Ets	Maximum depth evapotranspiration can occur	1.5-10	m
Seep	Deep groundwater seepage rate	0.01-0.04	mm/hr
Umc	Unsaturated zone moisture content at start of simulation	0.244-0.3	–
	Groundwater		
A1	Groundwater flow coefficient	0.08-0.1	–
B1	Groundwater flow exponent	1-5	–
A2	Surface water flow coefficient	0.05-0.1	–
B2	Surface water flow exponent	1-6	–
A3	GW-SW interaction coefficient	0-0.1	–

There are many components that rapidly increase the water level in a stream. Especially, the inflows into the node of streams or sewages have a significant effect on increasing the water level rapidly. So, how much the inflow of streams or sewages into the node was investigated. Then, which of the inflow of streams or sewages affects the risk of flash floods more. Figure 6.12 shows the impact of the stream or sewage inflow on each watershed to the discharge at the confluence. Analysis shows that the larger the area, the greater the inflow. Therefore, it can be seen that the influence of the stream having a large area on nodes (1) and (4) is large. However, the rapid increase in the discharge has a large effect on sewage. So, in mixed land use or urban area, to predict flash floods, a rainfall-runoff model should consider the sewage systems.

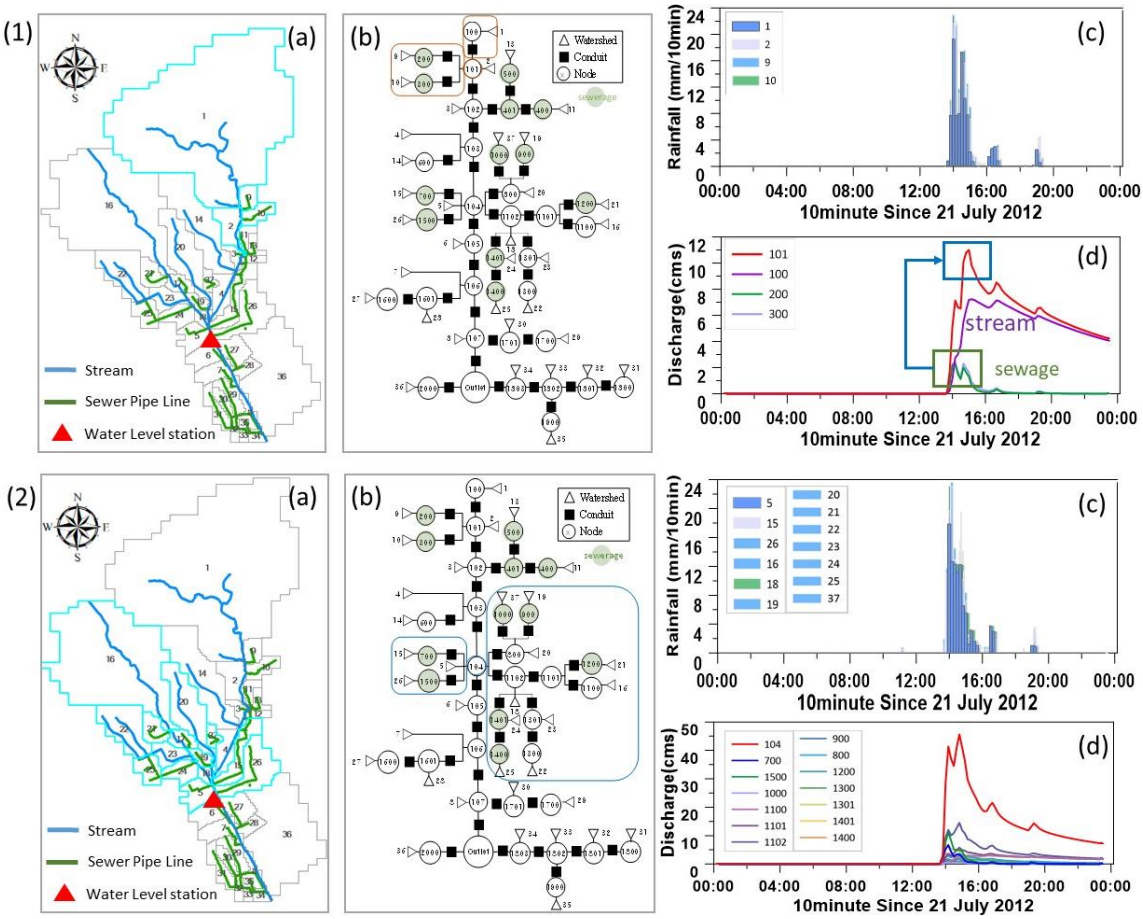

Figure 6.12 The inflows into the node (1) and (2) of streams or sewages: (a) Toga River watersheds correspond to the node; (b) channel network correspond to the node; (c) Mean Area Precipitation; (d) Discharge at the confluence and Inflow of each node.

The calibration of the SWMM was performed at the event based. The results of calibration and verification show that the continuity calculation errors of the surface runoff and flow routing by SWMM are less than ± 1% (meet the error requirements ± 10%). For the evaluation of hydrological model performance, the performance assessment of the SWMM was evaluated using three statistical indices: Nash Sutcliffe Efficiency (NSE), correlation coefficient (R), and RMSE (Root Mean Square Error). The calibration parameters have been iteratively adjusted for each

event until the difference between the simulated and observed discharge time series at each time step is minimized. The efficiency of the model was evaluated with the actual guerrilla heavy rainfall events used for calibration and verification. Performances assessment consists of comparing the observed discharge to the simulated discharge. In this research, the following notations are used: the observed discharge, Q_{obs}; the simulated discharge, Q_{sim}; the average of the observed discharge, $\bar{Q}$; the average of the simulated discharge, $\bar{Q}_{sim}$; *n* the total number of simulation data. The *NSE* can be calculated by the following equation:

$$NSE = 1 - \frac{\sum_{i=1}^{n}(Q_{obs} - Q_{sim})^2}{\sum_{i=1}^{n}(Q_{obs} - \bar{Q})^2} \quad . \tag{6.22}$$

The results will get better when the criterion *NSE* is coming near 1. The result inferior to zero (*NSE* < 0) indicates that the average observed discharge is better than the model. A value of *NSE* ($0.5 \leq NSE \leq 1$) is considered an acceptable value (Moriasi et al., 2007).

The correlation coefficient (*R*) calculates the strength and direction of the linear relationship between observed and simulated discharge. The *R* is given by the Equation 6.23:

$$\mathrm{R} = \frac{\sum_{i=1}^{n}(Q_{obs} - \bar{Q})(Q_{sim} - \bar{Q}_{sim})}{\sqrt{\sum_{i=1}^{n}(Q_{obs} - \bar{Q})^2 \sum_{i=1}^{n}(Q_{sim} - \bar{Q}_{sim})^2}} \quad . \tag{6.23}$$

The range of *R* lies between -1 and 1 which describes how much of the observed dispersion is explained by the simulation. A value of zero means no correlation at all whereas a value of 1 or -1 means that the dispersion of the simulation is equal to that of the observation.

The *RMSE* is given by the Equation 6.24:

$$RMSE = \sqrt{\frac{1}{n}\sum_{i=1}^{n}(Q_{obs} - Q_{sim})^2} \quad . \tag{6.24}$$

It represents the quadratic difference mean and the distance between observed discharge and simulated discharge. When the *RMSE* is nearer to zero, the two considered discharges are similar. The assessments of model performance are represented in Table 6.3.

Table 6.3 Model performance for calibration and verification (NSE, correlation coefficient, and root mean square error)

Type	Event	NSE	Correlation coefficient	RMSE
Calibration	2012-07-21	0.43	0.92	5.67
	2019-09-11	0.90	0.97	2.44
Verification	2014-09-11	0.53	0.93	9.40
	2020-07-30	0.80	0.95	1.61

The indices have been evaluated to assess the performance of the SWMM in simulating the guerrilla heavy rainfall on the event basis. On 21th July 2012, the value of *NSE* is low because SWMM has difficulty simulating the depletion curve. Since the SWMM was simulated for event based, the initial discharge of no rainfall could not consider the previous event. However, this is solved by simulating the SWMM in continuous events. Although the SWMM cannot replicate the guerrilla heavy rainfall event's observed results, the model with calibrated parameters represented the same aspect and peak time as the observation. The *NSE*, *R*, and *RMSE* values of the SWMM

are 0.43-0.90, 0.92-0.97, and 2.44-5.67, respectively. Overall, the SWMM displayed valid results for the guerrilla heavy rainfall events, and the selected parameters were considered suitable.

After calibration, the SWMM was validated using two guerrilla heavy rainfall events that occurred on 25th August 2013, and 7th June 2014. The results from the simulation and the observation show a similar aspect. Moreover, the *NSE*, *R*, and *RMSE* values of the two simulations show that the *NSE* and R values of the two simulations are 0.53-0.80 and 0.93-0.95, respectively, which can indicate that the simulation results fit well with the observations.

6.3.2.2 The soil moisture deficit on each watershed

Using the SWMM model, soil moisture and soil moisture deficit were calculated for each flash flood event. The amount of soil moisture varies according to the topography and soil conditions of each watershed, and it appears to be less than the saturated soil moisture. The actual fully saturated soil moisture of watersheds has the range from 71 to 101.9 mm. Then, the simulated soil moisture was applied to calculate the soil moisture deficit, which is insufficient for the soil to reach full saturation. Soil moisture was calculated for the 37 watersheds of the Toga River basin. Flash flood guidance is most affected by the topographical characteristics of the watershed and the cross-section of the stream. So, using the area weighted average, the value of soil moisture was calculated for 6 watersheds according to the threshold runoff. Figure 6.11 shows the simulated soil moisture on 21th July 2012. The simulated soil moisture for the other flash flood events can be seen in Appendix C.

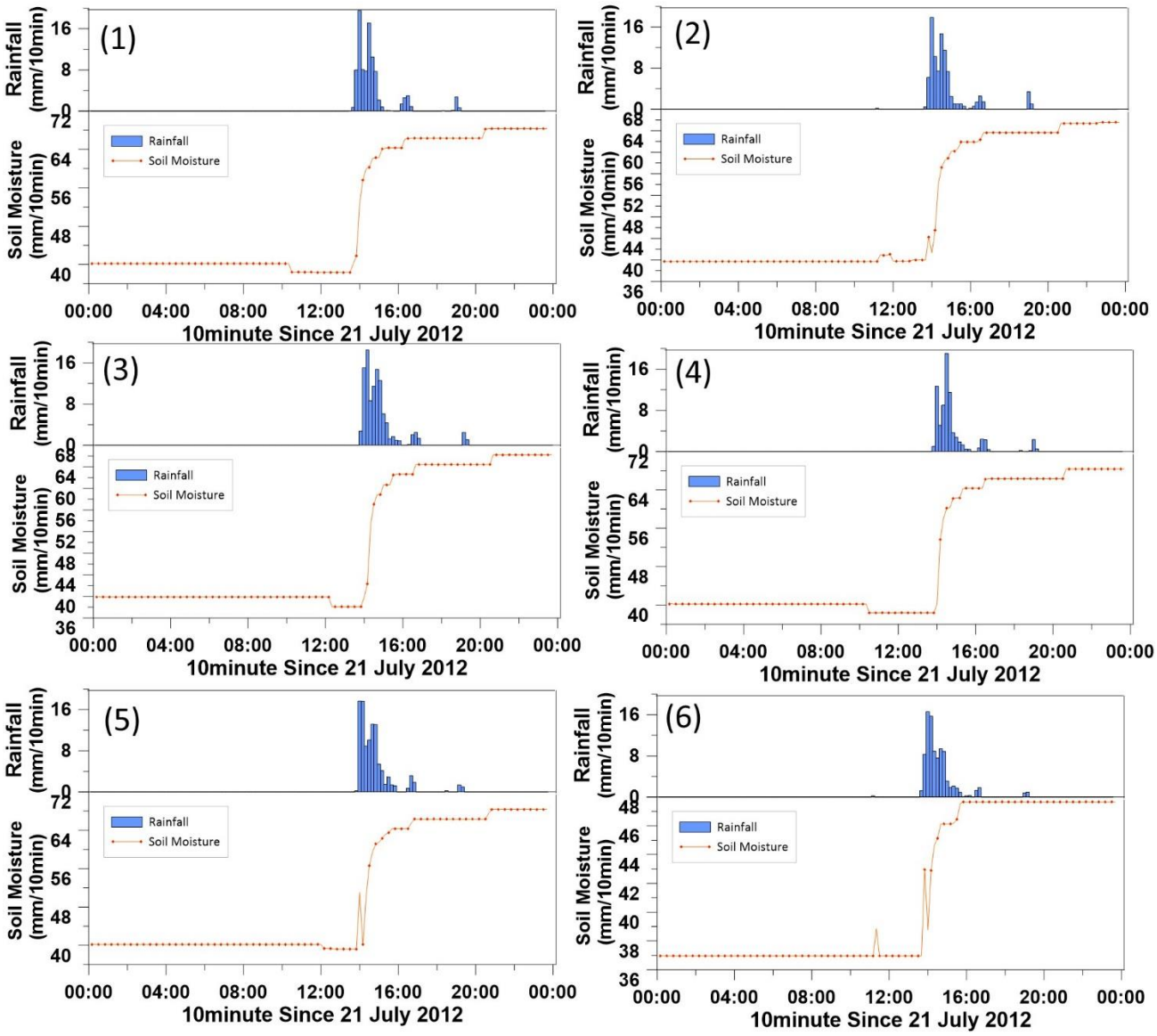

Figure 6.13 The simulations of soil moisture with the SWMM.

Figure 6.12 shows the simulated soil moisture and soil moisture deficit on 21th July 2012. The simulated soil moisture and soil moisture deficit for the other flash flood events can be seen in Appendix C. The simulated soil moisture and soil moisture deficit change values according to the rainfall intensity. This indicates that the soil moisture is calculated by reflecting the characteristics of hydrological and topographic data.

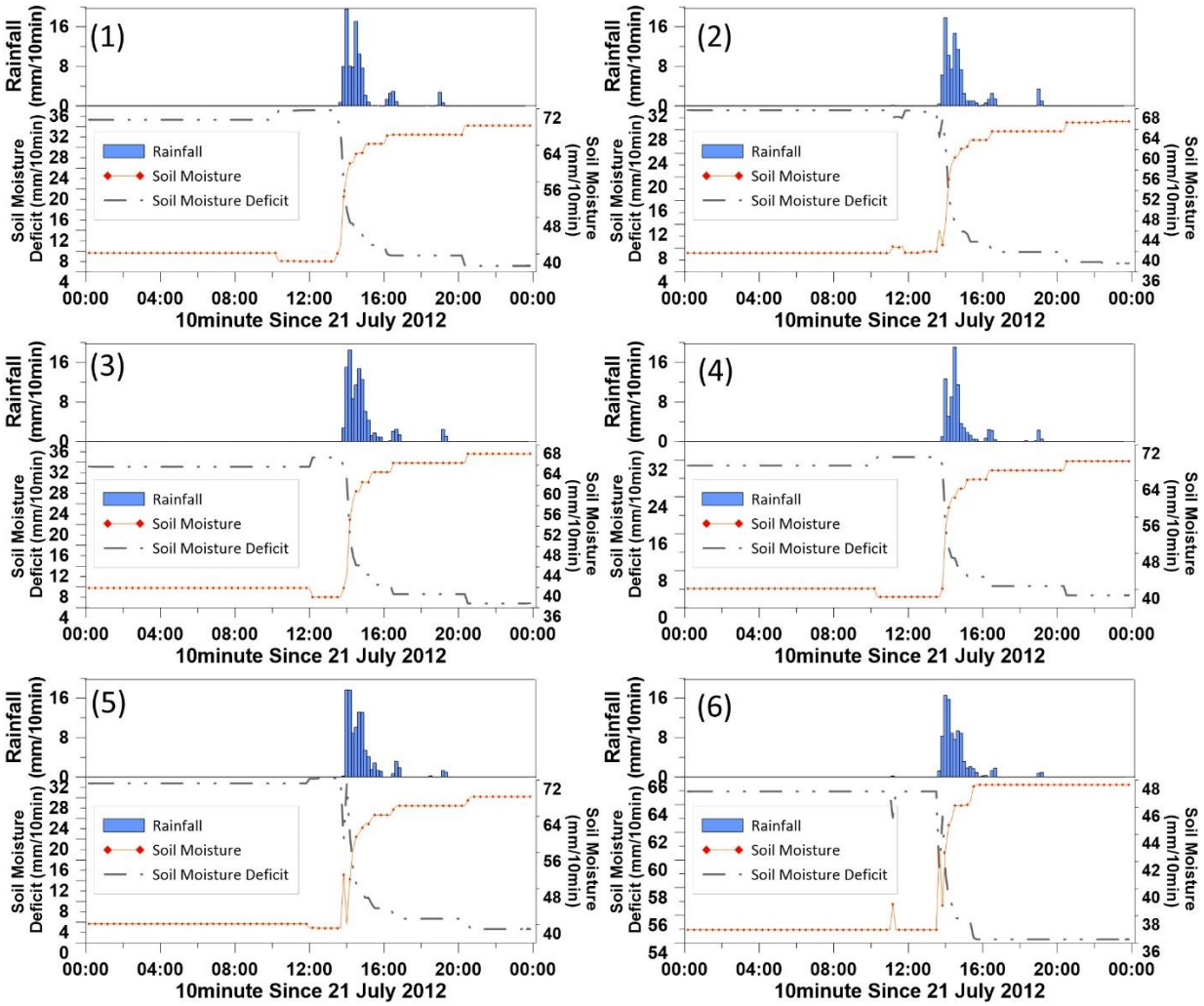

Figure 6.14 Estimation of soil moisture and soil moisture deficit on the watersheds.

6.3.3 Estimation and evaluation of Flash Flood Guidance (FFG)

The threshold runoff and soil moisture deficit were estimated to calculate the flash flood guidance on four flash flood events. The selected flash flood events are the cases that are assumed to have actually occurred. In order to evaluate the flash flood guidance, it was assumed that the actual flash flood occurred when the water level exceeded or closed to half of the needs for

observation (通報水位) designated by the water level observation station. This is because, based on the events reported by the media as flash floods, the watershed is small and flash floods in the mainstream are uncommon. The time at which the rainfall on the watershed exceeded the flash flood guidance was judged as the occurrence of the flash flood. In Figure 6.13, the mean area precipitation of the watershed is indicated by a blue hyetograph and flash flood guidance by solid red lines as representative examples of flash floods with a duration of 10 minutes.

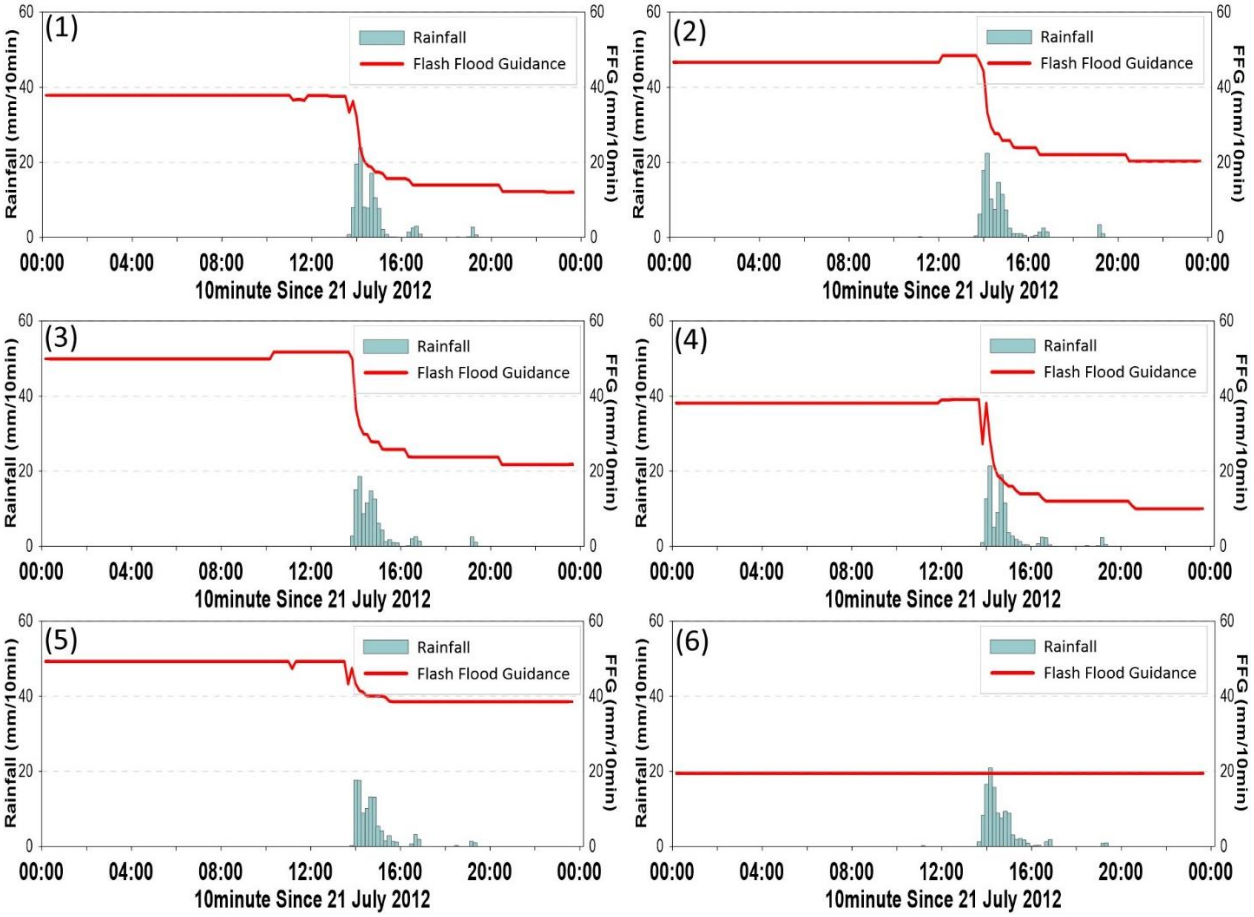

Figure 6.15 Evaluation of Flash Flood guidance on the watersheds.

As a result of analyzing the collected flash flood events, the flash flood guidance of 1, 4, and 6 watersheds exceeded the mean area precipitation. The evaluation results of flash flood guidance for the other flash flood events can be seen in Appendix C. In other flash flood events, it was confirmed that flash floods occurred in 1 and 4 watersheds. When the threshold runoff was estimated, the stream was divided into small mountainous streams and mainstreams considering the channel characteristics of the Toga River basin. In the case of small streams in mountainous areas, the threshold runoff is calculated based on a 0.5 m rise in water level to prevent damage to campers and hikers in the valleys. On the other hand, an artificial embankment is constructed in the mainstream to prevent damage to the human life and property of users using the stream. The threshold runoff was calculated based on the 50% high water level at the mainstream. The small mountainous streams 1 and 4 watersheds have narrow streams and are highly affected by soil moisture. This makes the watersheds vulnerable to flash floods. The flash flood guidance at 10 minutes rainfall duration on the watersheds has the range of 9.97 to 23.89 mm when the flash floods occur. The mean area precipitation exceeded the estimated flash flood guidance for the events assuming a flash flood occurred. This means that the estimated flash flood guidance was reliable and has appropriate flash flood guidance. It will be necessary to collect the flash flood events and review their adequacy.

6.4 Conclusion

In this chapter, the flash flood guidance was applied and assessed for watersheds of the Toga River basin in Japan. The advantage of this method is that it can propose applicable methods for mixed land use (the rural and urban land uses). It is important to know the quantitative criteria

for flash flood warnings as more areas will be prone to flash flooding as a result of increased urbanization. Flash flood guidance was estimated based on threshold runoff and the soil moisture by using the SWMM which is the rainfall-runoff model.

The key advantage of this method is that it is possible to issue flash flood warnings without the need to run the entire hydro-meteorological process in the region where the flash flood was calculated. However, even though the flash flood occurred when the water level exceeded or closed to half of the needs for observation (通報水位) designated by the water level observation station, the mean area precipitation was not exceeded the flash flood guidance on 7th June 2014. In order to supplement the problem, it is necessary to add some preconditions (i.e., soil characteristics, rainfall type, etc.). In addition, since the calculated flash flood guidance reflects only the characteristics of a specific watershed, there is a limit to its application to other watersheds. Therefore, a generalized method of flash flood guidance is needed. This means that the optimal flash flood guidance can be effectively estimated for any watershed. In addition, for not only guerrilla heavy rainfall but also long-duration rainfall, flash flood guidance will be required. Therefore, in order to effectively prepare flash floods, it is necessary to develop an integrated flash flood forecasting system that is divided into short and long-duration rainfall.

The improved quantitative risk prediction method (meteorology) and flash flood warning (hydrology) will be combined in future research. Flash floods happen when meteorological and hydrological circumstances coexist. Therefore, it is expected to bridge the gap between this improved quantitative risk prediction method and the flash flood prediction system.

CHAPTER 7

Concluding Remarks and Future Research

Predicting the guerrilla heavy rainfall is necessary to avoid tragic disasters by comprehensively considering the rainfall-runoff process of flash floods affected by meteorological and hydrological conditions. As the temporal and spatial resolution of radar remote sensing increases, the utilization of radar observation data is expanding. The variables (i.e., reflectivity, vorticity, divergence, and vertical wind) from radar observation and combination with the flash flood guidance method bring new hopes for more accurate prediction of the damage of flash floods by guerrilla heavy rainfall.

In this study, the early detection and quantitative risk prediction method was developed using only radar observation and estimation data to minimize human casualties caused by guerrilla heavy rainfall. In addition, the flash flood guidance method was applied to intuitively judge whether flash floods occurred in the Toga River basin. The occurrence of flash floods by guerrilla heavy rainfall was predicted by using topographical and meteorological data in Japan. That is why this study is valuable. Additionally, this research may suggest ways to improve current flood prediction and warning systems. The process by which the results were obtained is detailed below.

The early detection and quantitative risk prediction method was developed to minimize damage due to the guerrilla heavy rainfall. It shows the relationship among the predicted risk level, reflectivity, and pseudo vorticity within 30 minutes (from rain stage 1 to 6) before the maximum rainfall intensity occurs on the ground. Since reflectivity and pseudo vorticity have different characteristics depending on the rain stage, it is shown that the relationships are required for each rain stage. The correlation between predicted risk level and reflectivity shows positive correlations

that increase as the rain stage develops, except for rain stage 1. The correlation between predicted risk level and pseudo vorticity shows positive correlations at the early rain stage.

In order to discriminate the risk more precisely, the method for improving the accuracy of the quantitative risk prediction was presented. This method considers the performance of added independent variables that have different characteristics depending on the time. It has the potential to improve reliability and accurate risk prediction by adding more explanatory variables (i.e., reflectivity, vorticity, divergence, and vertical wind) with pseudo radar analysis and multiple Doppler radar analysis. The accuracy of multilinear regression was estimated by the receiver operating characteristic analysis. As a result, the most appropriate regression by the relevant variables was composed of reflectivity, vorticity, divergence, and vertical wind by multiple Doppler radar analysis. It is possible to predict the risk of guerrilla heavy rainfall quantitatively with high accuracy of 90% at the early rain stage.

In addition, by reflecting on the development processes of the convective cell, the relationship between the predicted risk level and variables was considered. The accuracy of the quantitative risk prediction was estimated according to the variables that have different characteristics depending on each rain stage and life cycle. The combinations of variables have conditions in common that the vorticity and reflectivity are very important at the early and late rain stage, respectively. We focus on the early rain stage for saving evacuation time to escape from danger because the guerrilla heavy rainfall occurs within a few minutes. So, vorticity is the most explanatory variable to estimate the predicted risk level before the maximum rainfall reaches the ground. The usefulness of the life cycle has been suggested at the early stage with physical and statistical analysis. It demonstrated the availability of life cycle in quantitative risk prediction of guerrilla heavy rainfall.

To alert flash flood warnings for the watersheds of the Toga River basin in Japan, flash flood guidance (FFG) was applied by using hydrological and topographic data. The flash flood guidance is the amount of precipitation needed in a specific period of time to initiate flooding in a watershed. It is necessary to calculate Threshold Runoff (TR) and Soil moisture Deficit (SD). The TR is an effective rainfall that causes a small stream to slightly exceed bank-full when the soil is fully saturated, and the SD is rainfall to get saturated soil conditions by the rainfall-runoff model. It is expected to identify flash flood events accurately. The optimal rainfall values for the flash flood warning threshold were between 9.97 to 23.89 mm per 10min. The advantage of this method is that after estimating the optimal rainfall values, flash flood warnings can be issued without the need to consider the entire hydro-meteorological models.

There are still lots of things to consider for warning flash floods in real-time. To issue the flash flood warning practically in real-time, the quantitative risk prediction (meteorology) and flash flood guidance (hydrology) should be simulated at the same time. Unfortunately, this research is not yet possible to conduct the flash flood prediction in real-time by comprehensively considering meteorological and hydrological circumstances simultaneously. In further research, for combining the quantitative risk prediction (discretized results) and flash flood guidance (continuous results), the flash flood warning system should alert the danger by considering the ensemble of possible flash flood occurrences. Also, depending on the area of watersheds, it is necessary to estimate the concentration time because it could affect the peak discharge.

However, this research is valuable in terms of developing the quantitative risk prediction method and establishing criteria for how much rain is dangerous in the Toga River basin. If further research and analysis on various watersheds and rainfall periods are conducted, this research will propose the accuracy of guerrilla heavy rainfall prediction as useful information for flood

forecasting and warning systems, and will be useful information for flash floods. In addition, for representation of the forecast uncertainty, a range of possible forecast outcomes will be produced to predict the risk in different types of events and a wider range of variables by considering meteorological and hydrological conditions at the same time. It is expected to contribute to the reduction of flash flood damage.

BIBLIOGRAPHY

Ahrens : *Essentials of Meteorology*, An Invitation to the Atmosphere. Brooks/Cole, Cengage Learning, 2012.

Carpenter, T.M., Georgakakos, K.P.: GIS-Based Procedures in Support of Flash Flood Guidance. *Iowa Institute of Hydraulic Research*, University of Iowa, Iowa City, IA, 1993.

Carpenter, T. M., Sperfslage J. A., Georgakakos K. P., Sweeney T., and Fread D. L.: National threshold runoff estimation utilizing GIS in support of operational flash flood warning systems, *Journal of Hydrology*, Vol. 224, pp. 21–44, 1999.

Castillo, V. M., Gomez-Plaza, A., & Martınez-Mena, M. : The role of antecedent soil water content in the runoff response of semiarid catchments: a simulation approach, *Journal of Hydrology*, Vol. 284, No.1-4, pp.114-130, 2003.

Choi, K. S., and Ball, E. B.,: Parameter estimation for urban runoff modelling. *Urban Water*, Vol. 4, No. 1, pp. 31–41, 2002.

Chow, V.T, Maidment, D.R. and Mays, L.W.: *Applied Hydrology*, McGraw-Hill,New York City, New York, USA, 1988.

Collier, C.G., Fox, N.I.: Assessing the flooding susceptibility of river catchments to extreme rainfall in the Kingdom, *Int. J. River Basin Management*, Vol. 1, pp. 1-11, 2003.

Gardner, Martin J., and Douglas G. A. : Confidence intervals rather than P values: estimation rather than hypothesis testing. *British Medical Journal (Clinical research ed.)*, Vol. 292, No. 6522, pp.746-750, 1986.

Gao, J., M. Xue, A. Shapiro, and K. K. Droegemeier: A variational method for the analysis of three-dimensional wind fields from two Doppler radars, *Monthly Weather Review*, Vol. 127, pp. 2128-2142, 1999.

Gregory, J.M., Mitchell, J.F.B.: Simulation of daily variability of surface temperature and prectipitation over Europe in the current and 2xCO2 climates using the UKMO high-resolution Climates model, *Quarterly Journal of the Royal Meteorological Society*, Vol. 121, pp. 1451-1476, 1995.

Hapuarachchi, H.A.P., Wang, Q.J., Pagano, T.C.: A review of advances in flash flood forecast, *Hydrological Process*, Vol. 25, pp. 2771-2784, 2011.

Horton, Robert E. : Erosional development of streams and their drainage basins-hydrophysical approach to quantitative morphology, *Geological Society America*, Vol. 56, No.3, pp. 275-370, 1945.

Houze, R. A., Jr. : Stratiform Precipitation in Regions of Convection: A Meteorological Paradox?, *Bulletin of the American Meteorological Society*, Vol.78, No.10, pp.2179-2196, 1997.

Huber, J. : Partial and part (semipartial) correlation-A vector approach, *The Two-Year College Mathematics Journal*, Vol.12, No.2, pp.151-153, 1981.

Jonkman, S.N.: Global perspectives on loss of human life caused by floods. *Natural Hazards*, Vol. 34, pp. 151-175, 2005.

Katayama, M., Yamaji, A., Nakamura, F., Morita, H., and Nakakita, E. : Development of A System for Early Detection of A Severe Storm. *Advances in River Engineering*, Vol. 21, pp. 401-406, 2015 (Japanese).

Kim, D. S., Maki, M., Shimizu, S., and Lee, D. I. : X-band Dual-Polarization Radar Observation of Precipitation Core Development and Structure in a Multi- Celular Storm over Zoshigaya, Japan, on August 5, 2008. *Journal of the Meteorological Society of Japan*, Vol. 90, No. 5, pp. 701-719, 2012.

Kim H., and Nakakita, E. : Development of the early detection and quantitative risk prediction method on the guerrilla heavy rainfall, *Journal of Japan Society of Civil Engineers*, B1 (Hydraulic Engineering), Vol.76, No.2, pp.175-180, 2020.

Kim H., and Nakakita, E. : Advances in the Quantitative Risk Prediction for Improving the Accuracy on the Guerrilla Heavy Rainfall, *Journal of Japan Society of Civil Engineers*, B1 (Hydraulic Engineering), Vol.77, No.2, pp. I_1321-I_1326, 2021.

Leach, J.M., and Coulibaly, P.: Soil moisture assimilation in urban watersheds: A method to identify the limiting imperviousness threshold based on watershed characteristics, *Journal of Hydrology*, Vol. 587, pp. 124958, 2020.

Liong, S.Y., Chan, W.T., and Shree Ram, J.: Peak-flow forecasting with genetic algorithm and SWMM, *Journal of Hydrologic Engineering*, Vol.8, No. 613, pp. 613–617, 1995.

Liu, G., Schwartz, F.W., Kim, Y., Complex baseflow in urban streams: an example from central Ohio, USA, *Environmental Earth Sciences*, Vol. 70, pp. 3005–3014, 2013.

Maidment, D. R., and Scott Morehouse: *Arc Hydro: GIS for water resources*. ESRI, Inc., 2002.

Martínez-Mena, M., Albaladejo, J., & Castillo, V. M. : Factors influencing surface runoff generation in a Mediterranean semi-arid environment: Chicamo watershed, SE Spain. *Hydrological processes*, Vol. 12, No. 5, pp.741-754, 1998.

Marzban, C. : The ROC curve and the area under it as performance measures, *Weather and Forecasting*, Vol.19, No.6, pp.1106-1114, 2004.

Masuda, A., and Nakakita, E.: Development of a technique to identify the stage of storm life cycle using X-band polarimetric radar. J. Hydraul. Engineers, *Journal of the Meteorological Society of Japan*, Series B, Vol. 70, No. 4, pp. 493-498, 2014 (Japanese).

Miyasaka, T., Hiroaki, K., Tosiyuki, N., Yukiko, I., Izuru, T. : Future projections of heavy precipitation in Kanto and associated weather patterns using large ensemble high-resolution simulations, *Scientific Online Letters on the Atmosphere*, Vol. 16, pp. 125-131, 2020.

Moriasi, D., Arnold, J., Van L. M., Bingner, R., Harmel, R.D., and Veith, T.: Model Evaluation Guidelines for Systematic Quantification of Accuracy in Watershed Simulations, *Transactions of the ASABE*. Vol. 50, 2007.

Norbiato, D., Borga, M., Degli Esposti, S., Gaume, E., Anquetin, S. : Flash flood warning based on rainfall depth-duration thresholds and soil moisture conditions: an assessment for gauged and ungauged basins, *Journal of Hydrology*, Vol. 362, No.3-4, pp. 274-290, 2008.

Nakakita, E., Yamabe, H., and Yamaguchi, K. : Earlier detection of the origin of very localized torrential rainfall. Journal of Hydraulic Engineering, *Japan Society of Civil Engineers*, Vol. 54, pp. 343–348, 2010 (Japanese).

Nakakita, E., Yamabe, H. and Yamaguchi, K. : Early detection and tracking of baby rain cell in the guerilla strom warning using X-band polarimetric radar network, *Annuals of Disaster Prevention Research Institute, Kyoto University*, No.54B, 2011(Japanese).

Nakakita, E., Nishiwaki, R., Yamabe, H. and Yamaguchi, K. : Research on the prognostic risk of baby cell for guerilla-heavy rainfall considering by vorticity with doppler velocity, *Journal of Japan Society of Civil Engineers*, Vol.69, No.4, pp.325-330, 2013 (Japanese).

Nakakita, E., Nishiwaki, R. and Yamaguchi, K. : Detection of a system for early detection of baby rain cell aloft in a storm and risk projection for urban flash flood, *Advances in River Engineering*, Vol. 20, 2014 (Japanese).

Nakakita, E., Sato, H., Nishiwaki, R., Yamabe, H., and Yamaguchi, K. : Early Detection of Baby-Rain cell Aloft in a Severe Storm and Risk Projection for Urban Flash Flood, *Advances in Meteorology*, Article ID 5962356, pp.15, 2017.

Palmer, T.N., Raisanen, J.: Quantifying the risk of extreme seasonla precipitation events in a changing climate?, *Nature*, Vol. 415, pp. 512-514, 2002.

Park, H. S., Ryzhkov, A. V., Zrnic, D., S. : The Hydrometeor Classification Algorithm for the Polarimteric WSR-88D: Description and Application to an MCS. *Weather Forecast*, Vol. 24, No. 3, pp. 730-748, 2009.

Protat, A., and Zawadzki, I. : A Variational Method for Re-al-Time Retrieval of Three-Dimensional Wind Field from Multiple-Doppler Bistatic Radar Network Data, *Journal of Atmospheric and Oceanic Technology*, Vol.16, No.4, pp.432-449, 1999.

Rodriguez-Iturbe, I., Devoto, G. and Valdes, J. B.: Discharge response analysis and hydrologic similarity: The interrelation between the geomorphologic IUH and the storm characteristics, *Water Resources Research*, Vol.15, No.6, pp.1435–1444, 1979.

Rodriguez-Iturbe, I., Gonzalez-Sanabia, M., and Bras, R. L. : A Geomorphoclimatic Theory of the Instantaneous Unit Hydrograph, *Water Resources Research*, Vol. 18, No. 4, pp. 877-886, 1982.

Rossman, L. A.: Storm Water Management Model User's Manual Version 5.0. U.S. Environmental Protection Agency, Washington, DC, EPA/600/R-05/040, 2004.

Rossman, L.A., Huber, W.C.: Storm water management model reference manual volume I–hydrology. *U.S. Environmental Protection Agency*, 231, 2016.

Saharia, M., Kirstetter, P., Vergara, H., Gourley, J. J., Hong, Y., and Giroud, M. : Mapping Flash Flood Severity in the United States, *Journal of Hydrometeorology*, Vol. 18, No.2, pp.397-411, 2017.

Shimizu, S. : Multiple Doppler Radar Analysis for Retriev-ing the Three-Dimensional Wind Field Within Thunder-storms, Doppler Radar Observations, InTech, 2012.

Strahler, A. N.: Quantitative analysis of watershed geomorphology, *Transactions American Geophysical Unionm*, Vol. 38, No. 6, pp. 913-920, 1957.

Talbot, M., McGuire, O., Olivier, C. and Flemin, R.: Parameterization and application of agricultural best management practices in a rural Ontario watershed using PCSWMM, *Journal of Water Management Modeling*, 2016.

Tsai, L.Y., Chen, C.-F., Fan, C.-H. and Lin, J.Y.: Using the HSPF and SWMM Models in a High Pervious Watershed and Estimating Their Parameter Sensitivity, *Water 2017*, Vol.9, No.10, pp. 780, 2017.

Ulanski, S. L. and Garstang, M. : The role of surface diver-gence and vorticity in the life cycle of convective rainfall. Part II: Descriptive model, *Journal of Atmospheric Sciences*, Vol.35, No.6, pp.1063-1069, 1978.

Yoon, S. S. and Nakakita, E. : Application of an X-Band Multiparameter Radar Network for Rain-Based Urban Flood Forecasting, *Journal of Hydrologic Engineering*, Vol. 22, 2015.

Zeng, Z., Yuter, S. E., Houze Jr, R. A., and Kingsmill, D. E.: Microphysics of the Rapid Development of Heavy Convective Precipitation, *Monthly Weather Review*, pp. 1882-1904, 2000.

APPENDIX A

Data Visualization

The Plan Position Indicator (PPI) detects the observation of each elevation angle. Constant Altitude Plan Position Indicator (CAPPI) is the horizontal cross-section data for each specific altitude obtained by interpolating in the vertical direction from PPI. Usually, the obtained PPI is interpolated in the vertical direction. However, the X-MP radar was scanned as three-dimensional observation once every 5 minutes. It is possible to analyze an echo that does not actually exist at the position by interpolation in the vertical direction. It is difficult to comprehend the structure of rapidly changing guerilla heavy rainfall. Therefore, by using the PPI without interpolating the X-MP radar, this research was analyzed with the CAPPI. To represent accurate X-MP radar data, it is necessary to consider the resolution. The resolution of azimuth is one degree and the beam direction is 150 m. As shown in Figure A.1, the altitude H [km] was calculated by the following Equations (A.1) to (A.4) considering the shape of the earth and the refraction of the atmosphere. The distance from the radar to the point below the radar beam is L_d [km], the distances in the longitude and latitude directions are x [km] and y [km], respectively. The distance in the azimuth measured with the radar beam is r [km], the radius of the earth is R_e [km], the elevation of the radar is h_r [km], the observed elevation angle is θ_e [rad], and the coefficient is k = 4/3 considering refraction by the atmosphere. The Equations (A.1) to (A.4) can be expressed as

$$L_d = kR_e \tan^{-1}\left(\frac{r\cos\theta_e}{kR_e + h_r + r\sin\theta_e}\right), \quad \text{(A. 1)}$$

$$H = \frac{r\sin\theta_e + h_r + kR_e}{\cos\left(\frac{L_d}{kR_e}\right)} - kR_e, \quad \text{(A. 2)}$$

$$x = L_d \sin\theta\,, \tag{A.3}$$

$$y = L_d \cos\theta\,. \tag{A.4}$$

It is possible to visualize the PPI without interpolation from the observed radar data. Then, the PPI was transformed into a three-dimensional Cartesian coordinate system. The linear interpolation in the vertical direction was used to insert values at the grids in which the radar beam does not exist. The CAPPI of reflectivity, Doppler wind velocity, and vorticity can be obtained. This CAPPI was used to create vertical cross-sections and three-dimensional images, and to analyze guerilla heavy rainfall and vorticity structures.

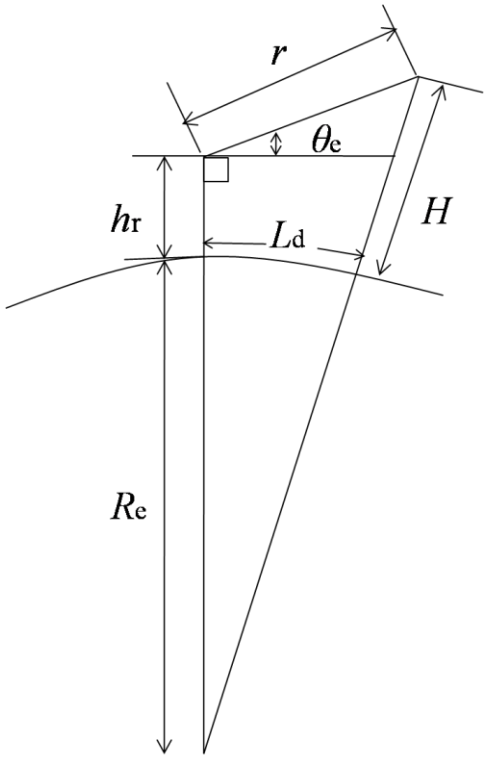

Figure A.1 The angle of elevation, the beam direction, distance from the radar site, and altitude.

APPENDIX B

The three-dimensional development processes of the convective cell

The three-dimensional development processes of convective cells are expressed in the following order of guerilla heavy rainfall events from Figure B.1 to B.6. Table B.1 indicates the list of guerilla heavy rainfall events.

Table B.1 List of guerilla heavy rainfall events

No.	Date
1	2013-08-06
2	2013-08-07
3	2015-08-07
4	2015-08-29
5	2016-08-03
6	2016-08-25
7	2018-08-13

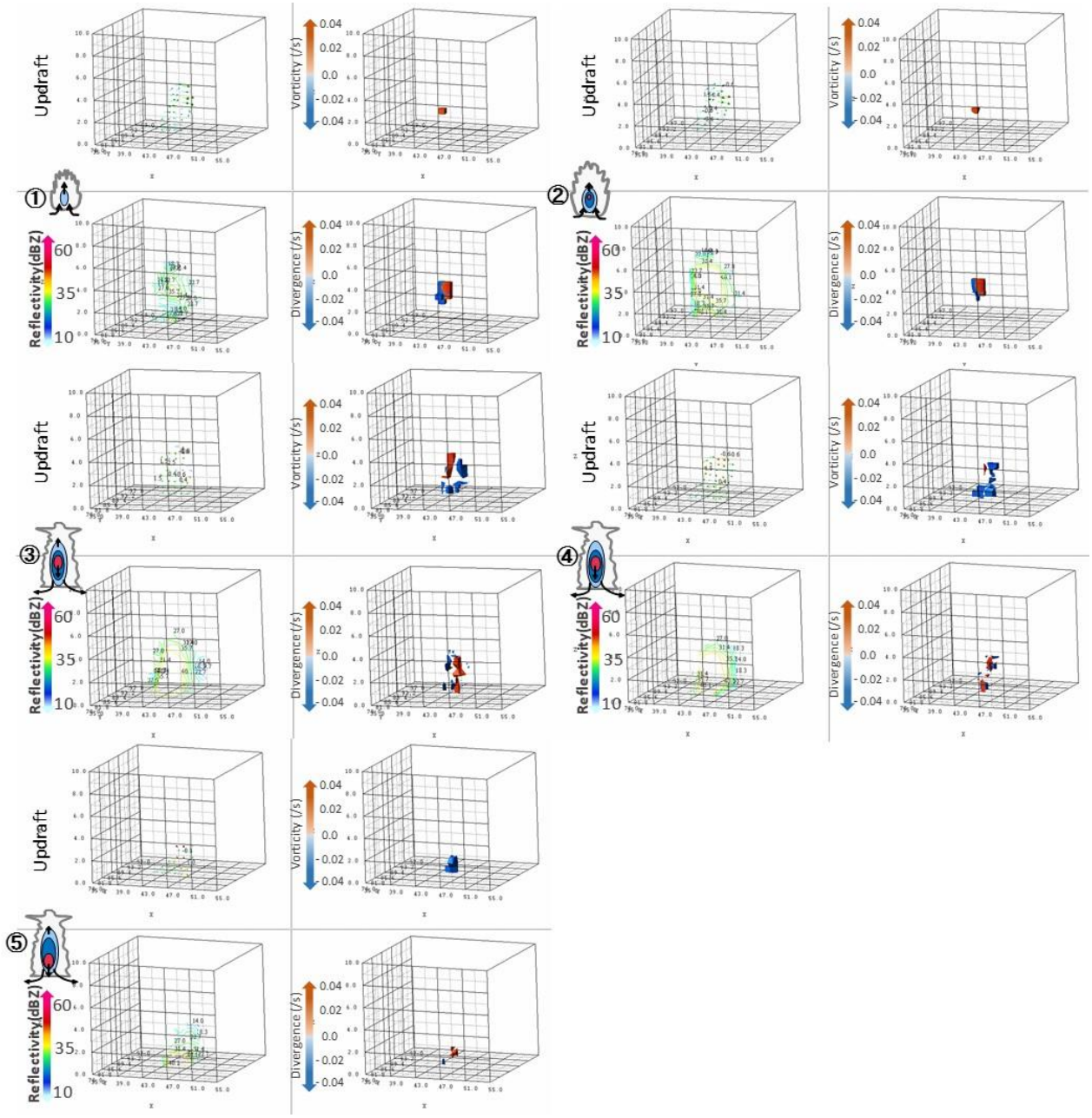

Figure B.1 The characteristics according to the development of the convective cell according to the variables (i.e. radar reflectivity, the vorticity, divergence, and vertical wind) on 6th August 2013.

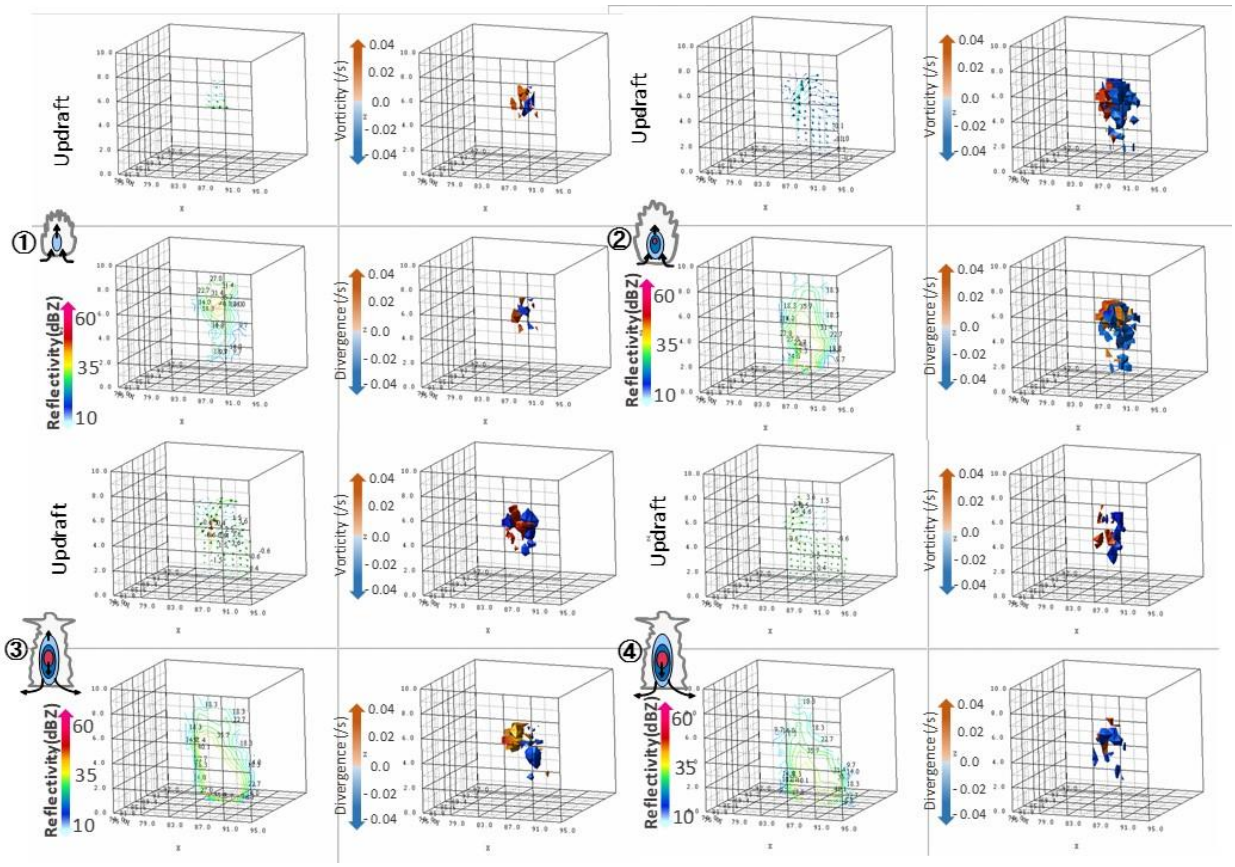

Figure B.2 The characteristics according to the development of the convective cell according to the variables (i.e. radar reflectivity, the vorticity, divergence, and vertical wind) on 7th August 2013.

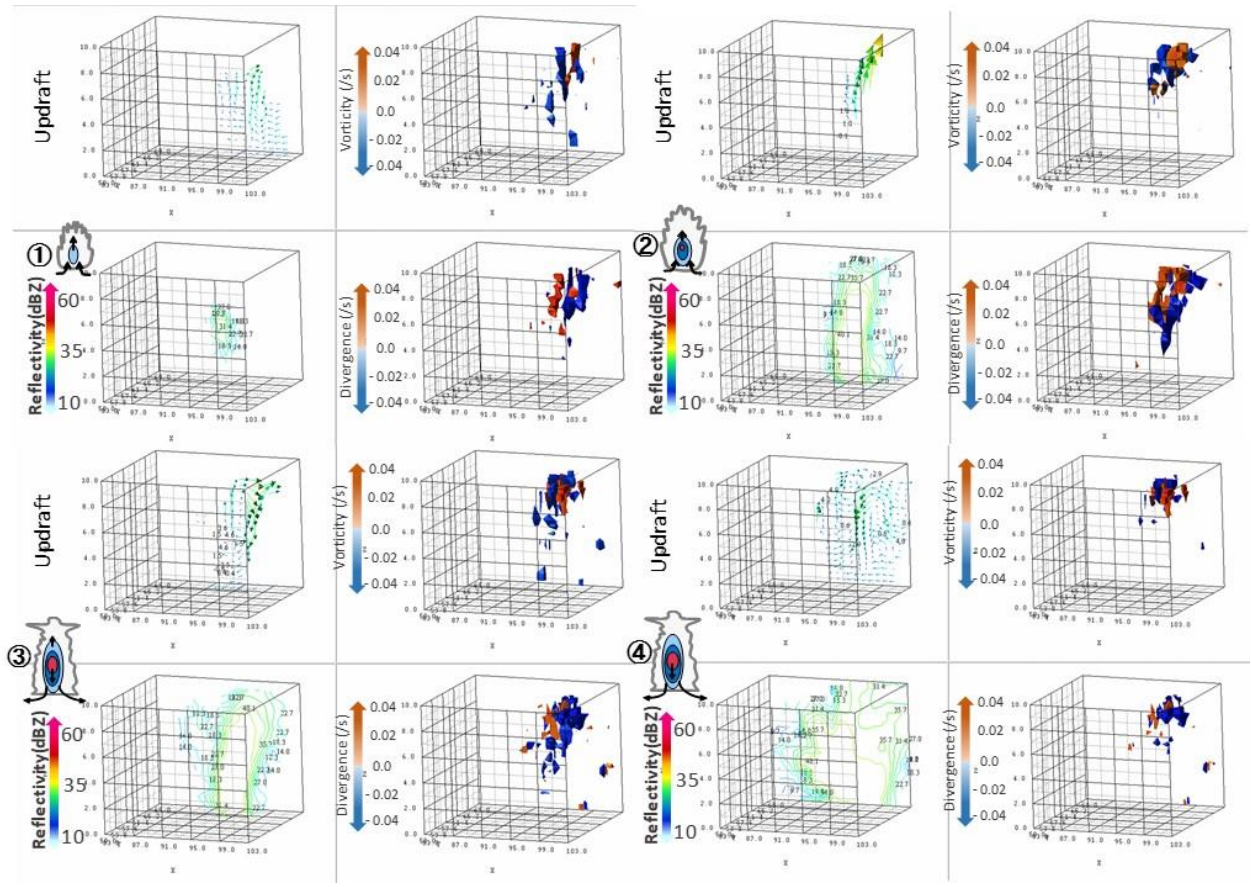

Figure B.3 The characteristics according to the development of the convective cell according to the variables (i.e. radar reflectivity, the vorticity, divergence, and vertical wind) on 7th August 2015.

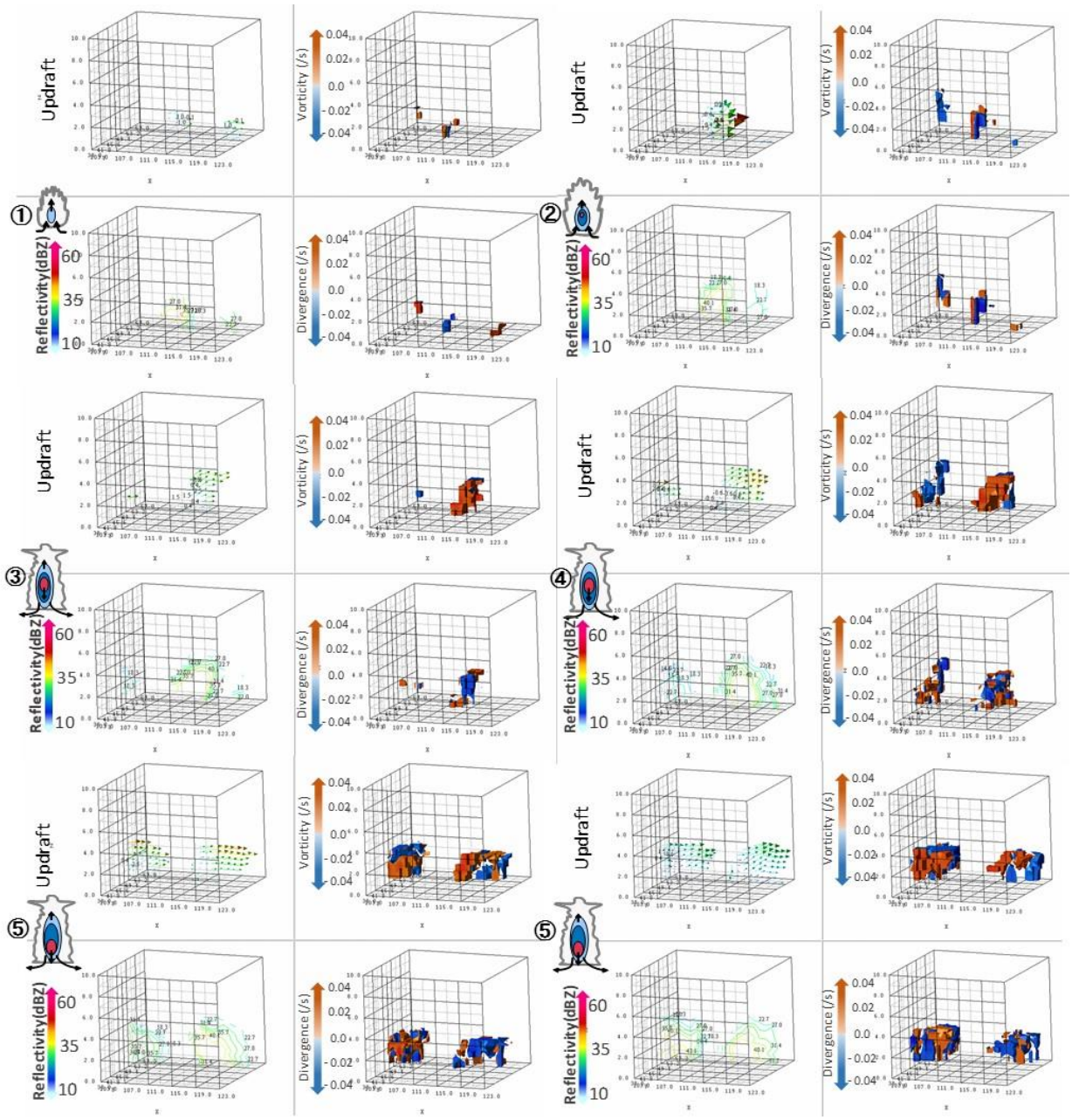

Figure B.4 The characteristics according to the development of the convective cell according to the variables (i.e. radar reflectivity, the vorticity, divergence, and vertical wind) on 29th August 2015.

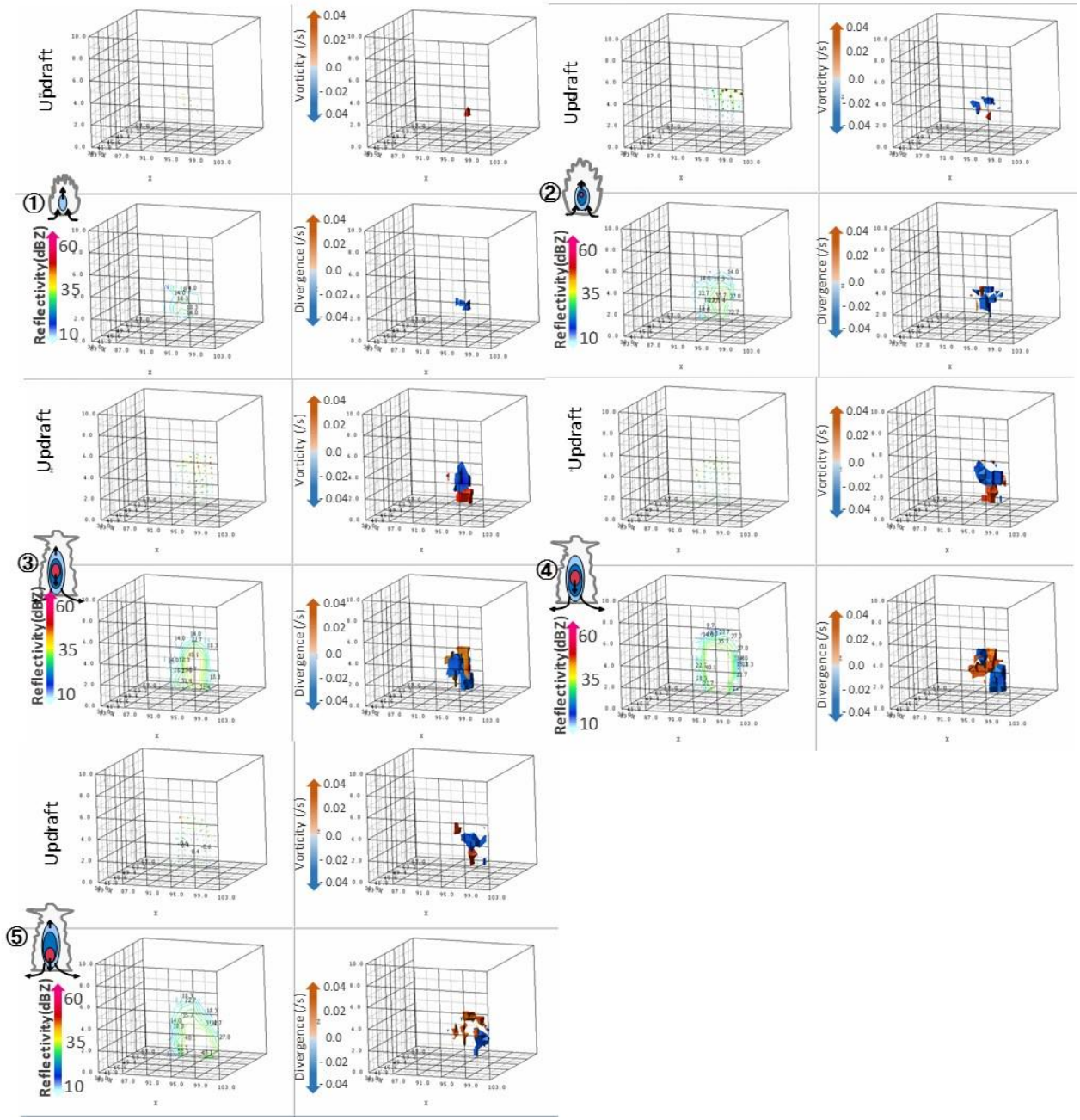

Figure B.5 The characteristics according to the development of the convective cell according to the variables (i.e. radar reflectivity, the vorticity, divergence, and vertical wind) on 3th August 2016.

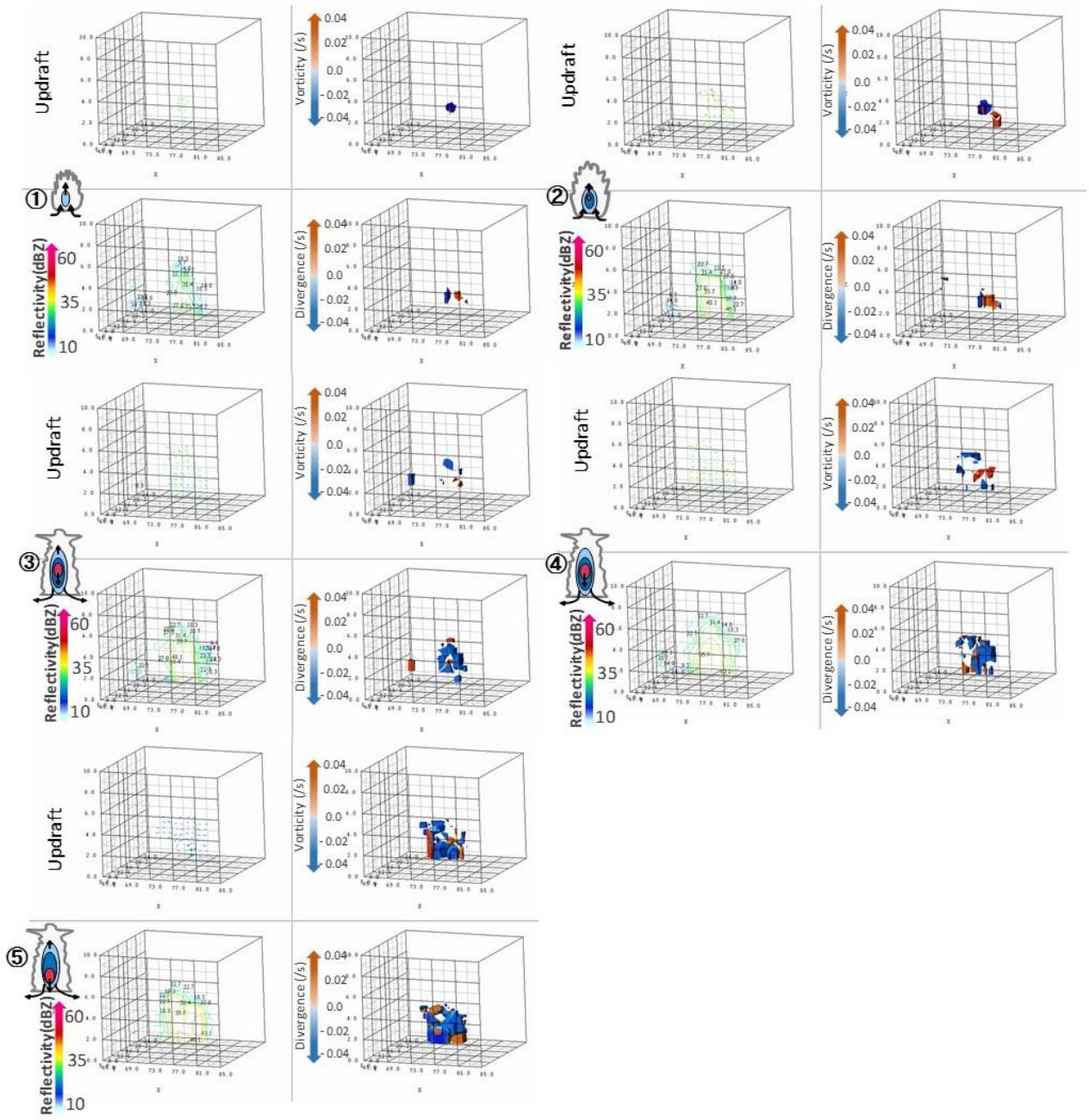

Figure B.6 The characteristics according to the development of the convective cell according to the variables (i.e. radar reflectivity, the vorticity, divergence, and vertical wind) on 25th August 2016.

APPENDIX C

Mean Area Soil Moisture on 6 watersheds in Toga River basin

There are four collected flash flood events. The simulated soil moisture was applied to calculate the soil moisture deficit, which is insufficient for the soil to reach full saturation. Figure C.1 to C.3 show the simulated soil moisture for the flash flood events on watersheds.

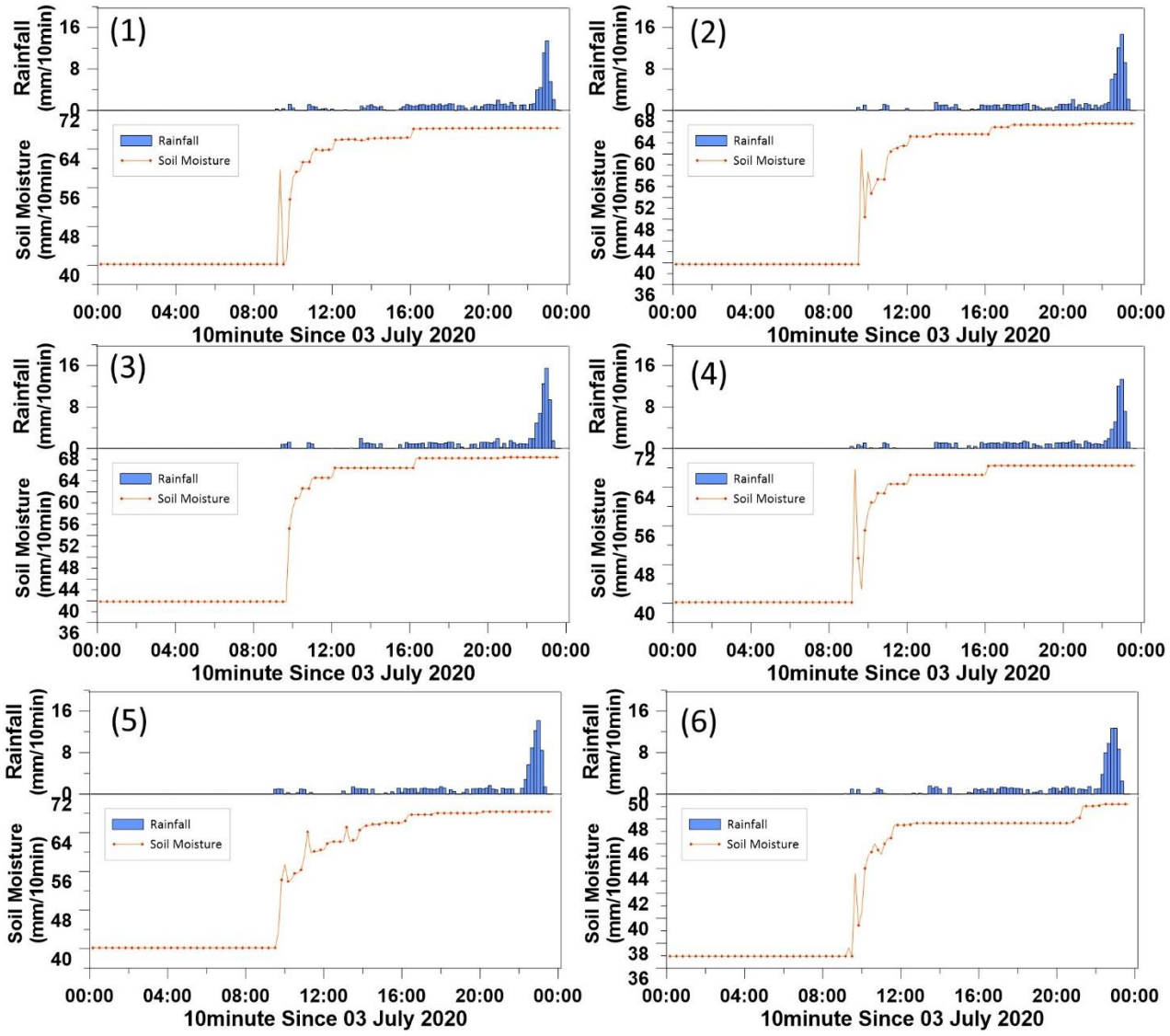

Figure C.1 The simulations of soil moisture with the SWMM on 3rd July 2020.

On 3rd July 2020, the 1, 2, and 6 watersheds are sensitive to the rainfall due to the high permeability. Therefore, it can be confirmed that the soil moisture responds sensitively to the initial rainfall. However, depending on the surrounding conditions, the soil moisture was adjusted.

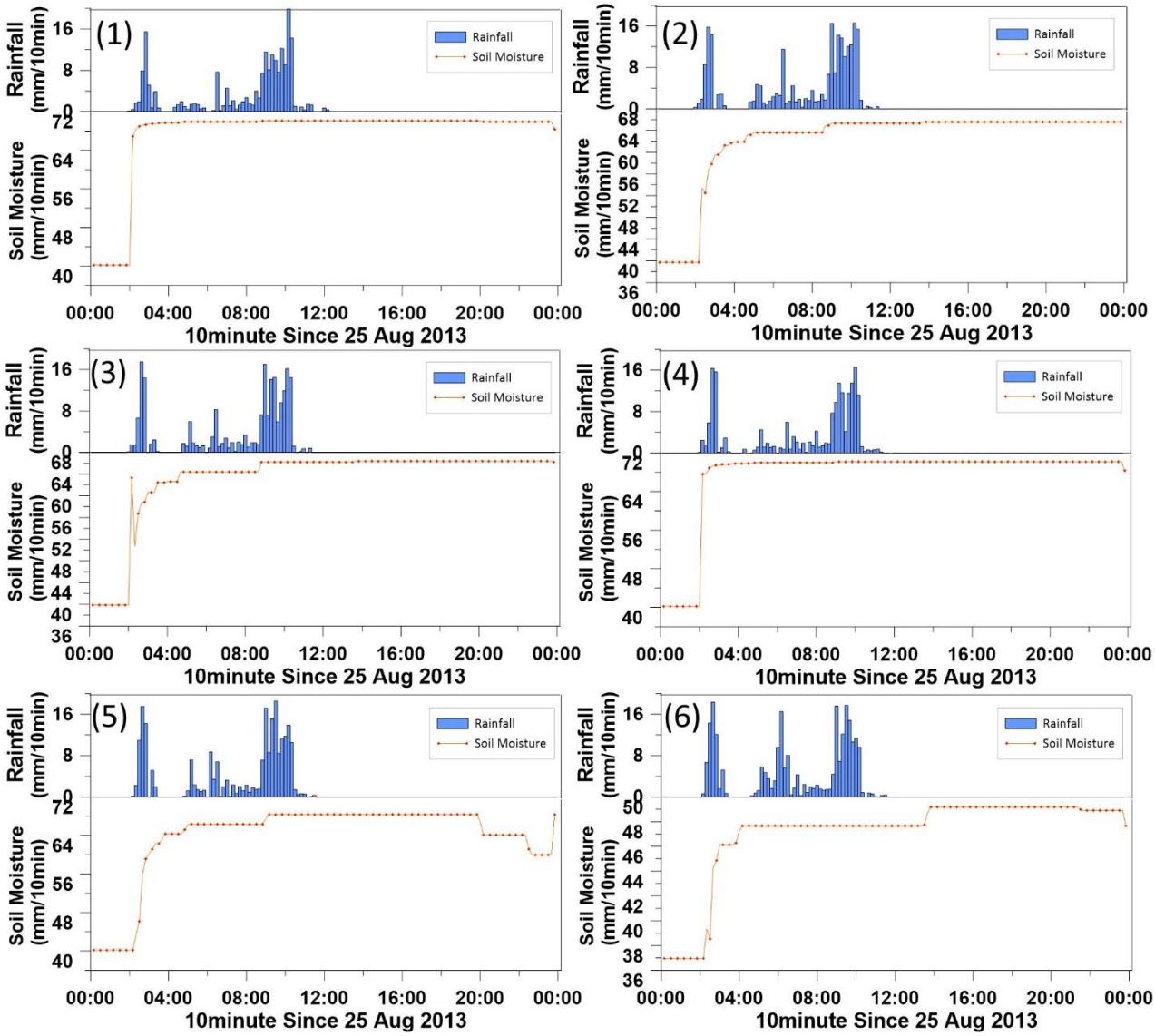

Figure C.2 The simulations of soil moisture with the SWMM on 25th August 2013.

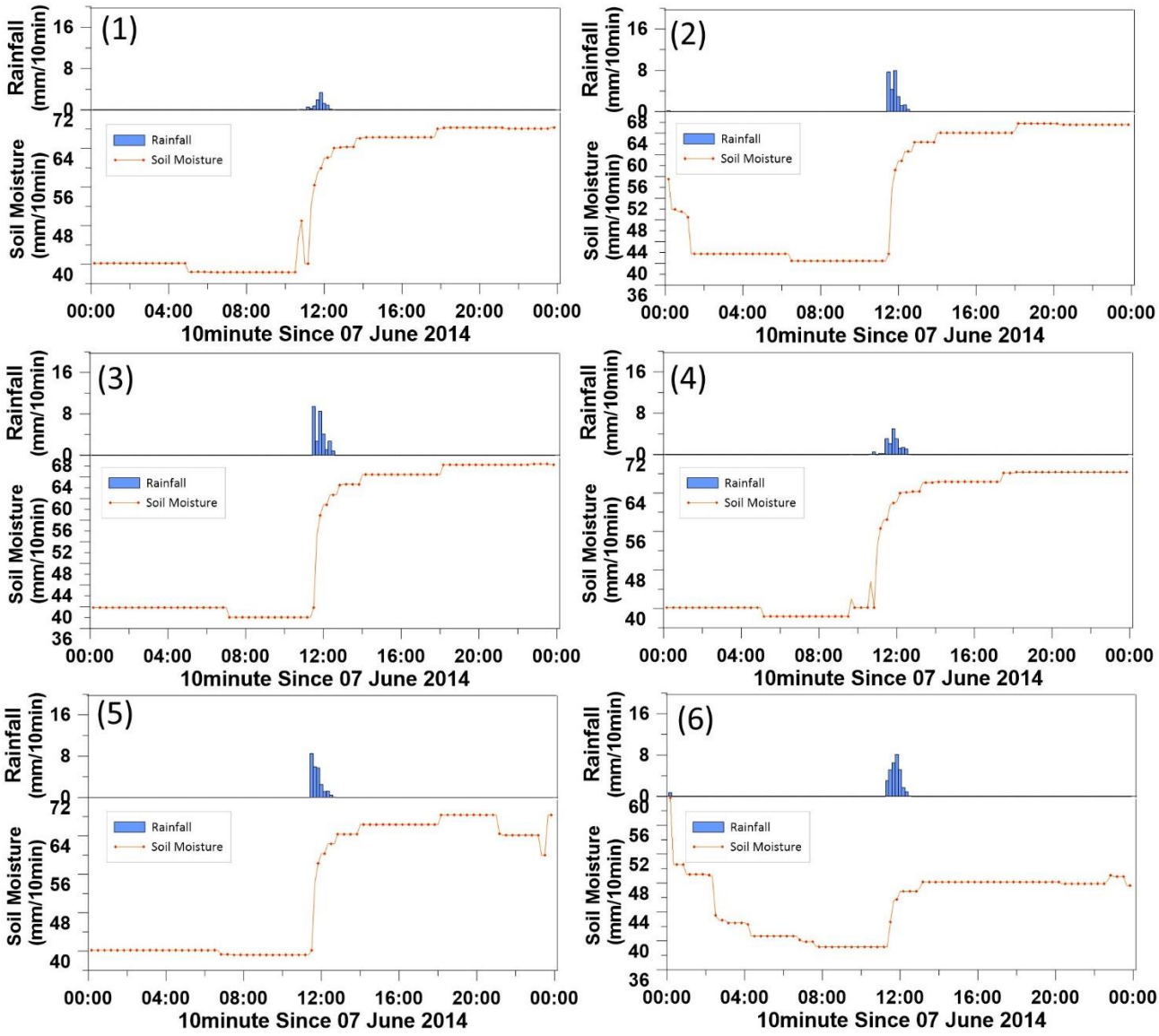

Figure C.3 The simulations of soil moisture with the SWMM on 7th June 2014.

Figure C.4 to C.6 shows the simulated soil moisture and soil moisture deficit for the flash flood events.

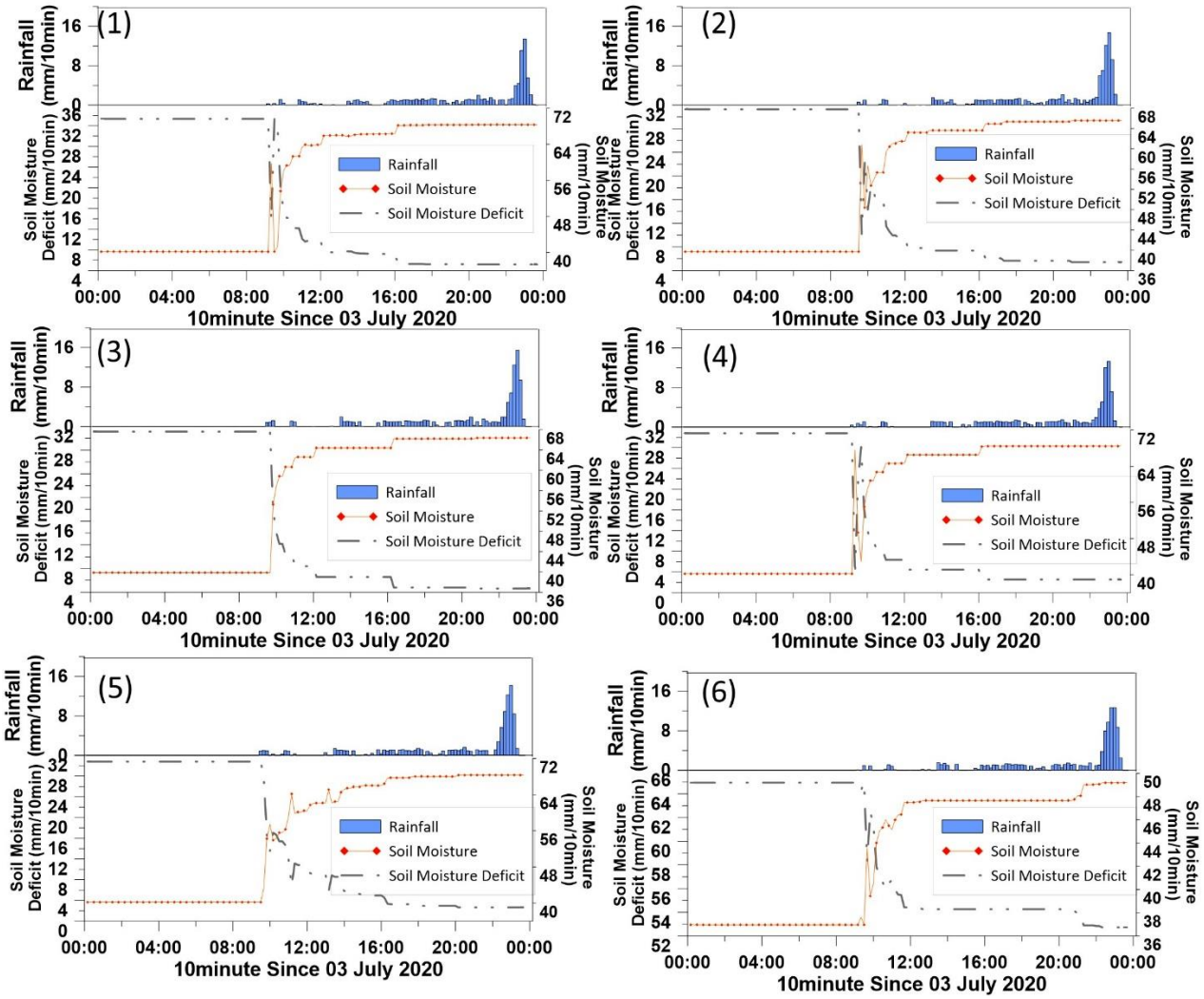

Figure C.4 Estimation of soil moisture and soil moisture deficit on the watersheds on 3rd July 2020.

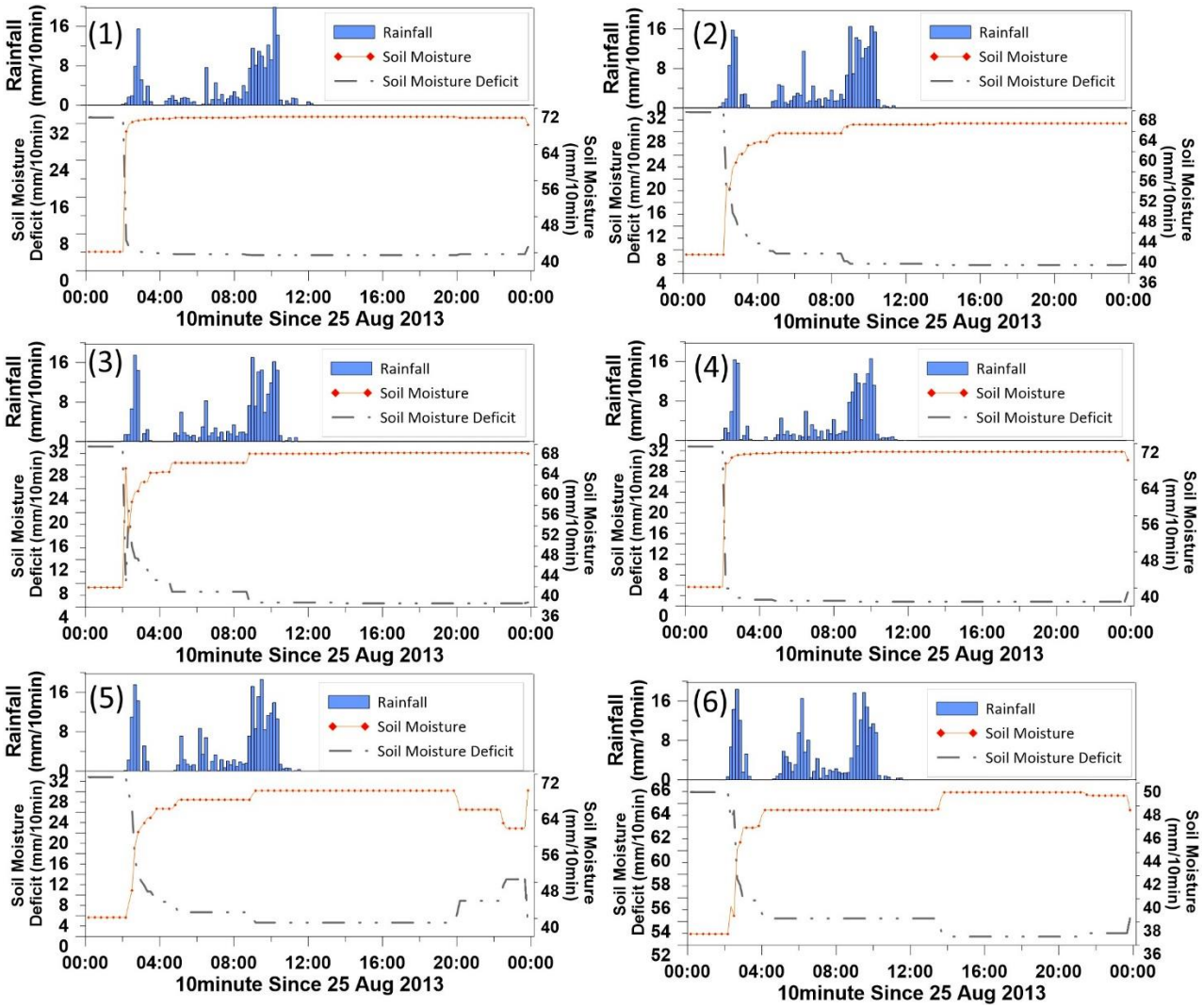

Figure C.5 Estimation of soil moisture and soil moisture deficit on the watersheds on 25th August 2013.

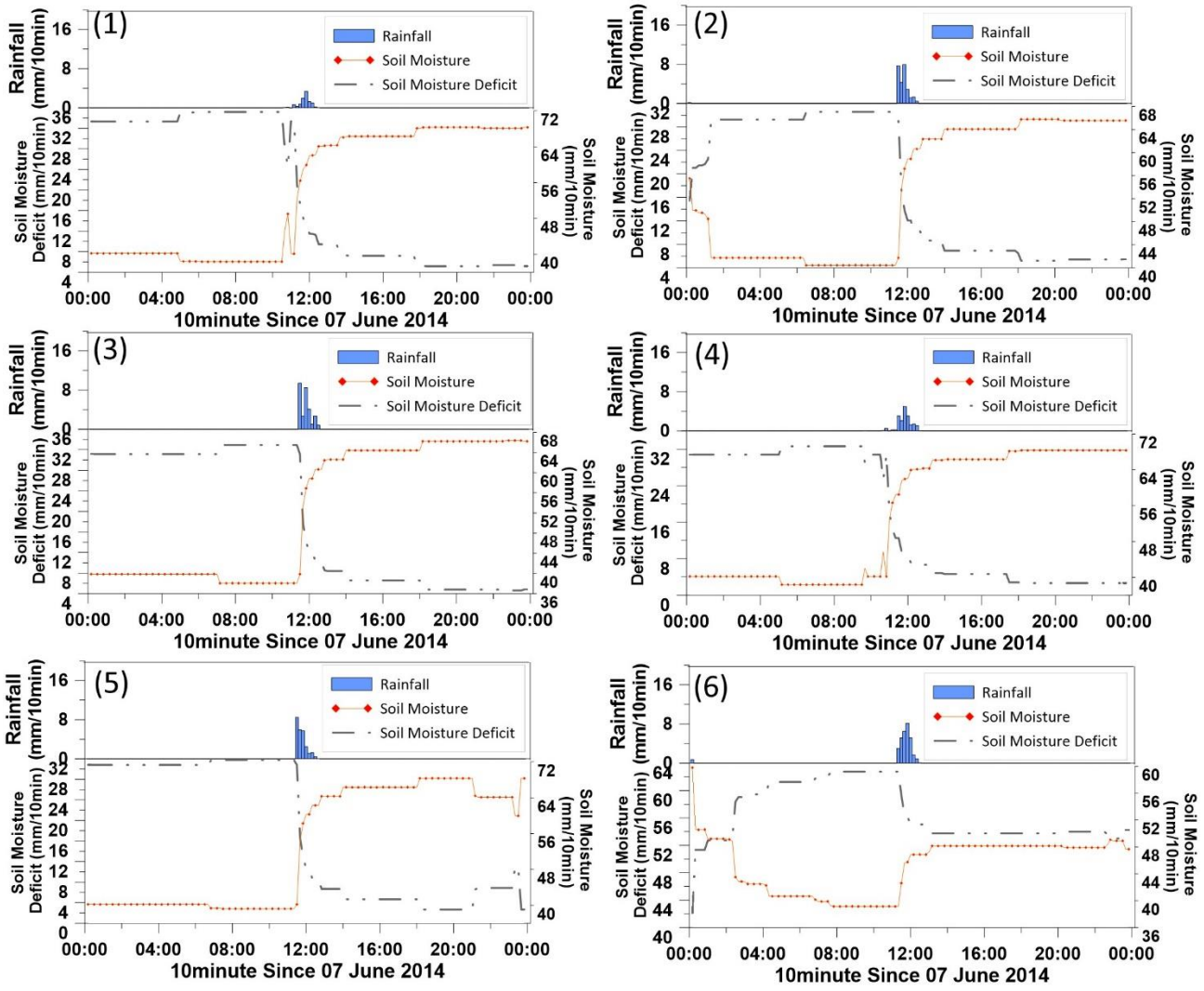

Figure C.6 Estimation of soil moisture and soil moisture deficit on the watersheds on 7th June 2014.

Figure C.7 to C.9 shows the mean area precipitation and flash flood guidance. When the rainfall exceeded the flash flood guidance, it means that the flash flood occurred.

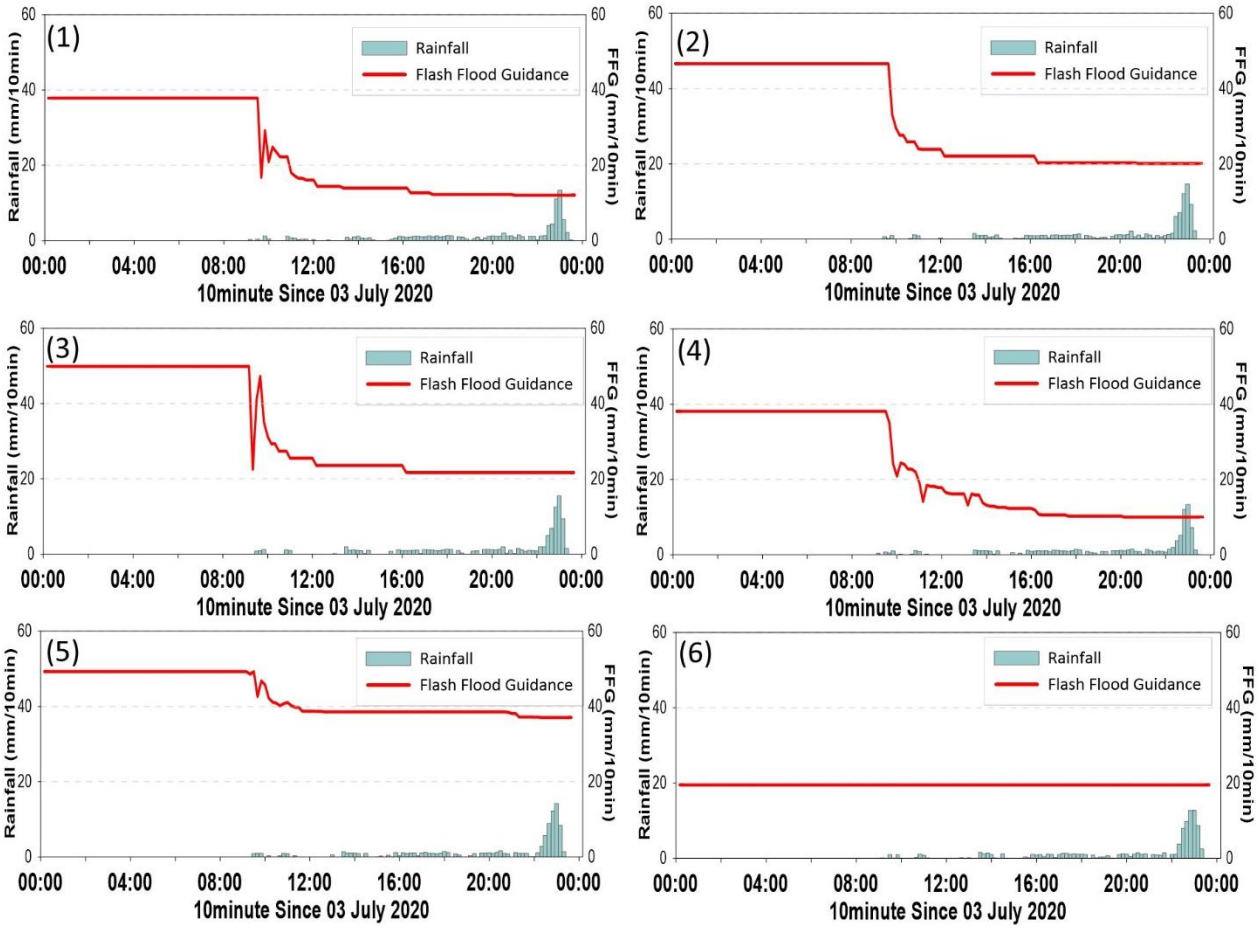

Figure C.7 Evaluation of Flash Flood guidance on the watersheds on 3rd July 2020.

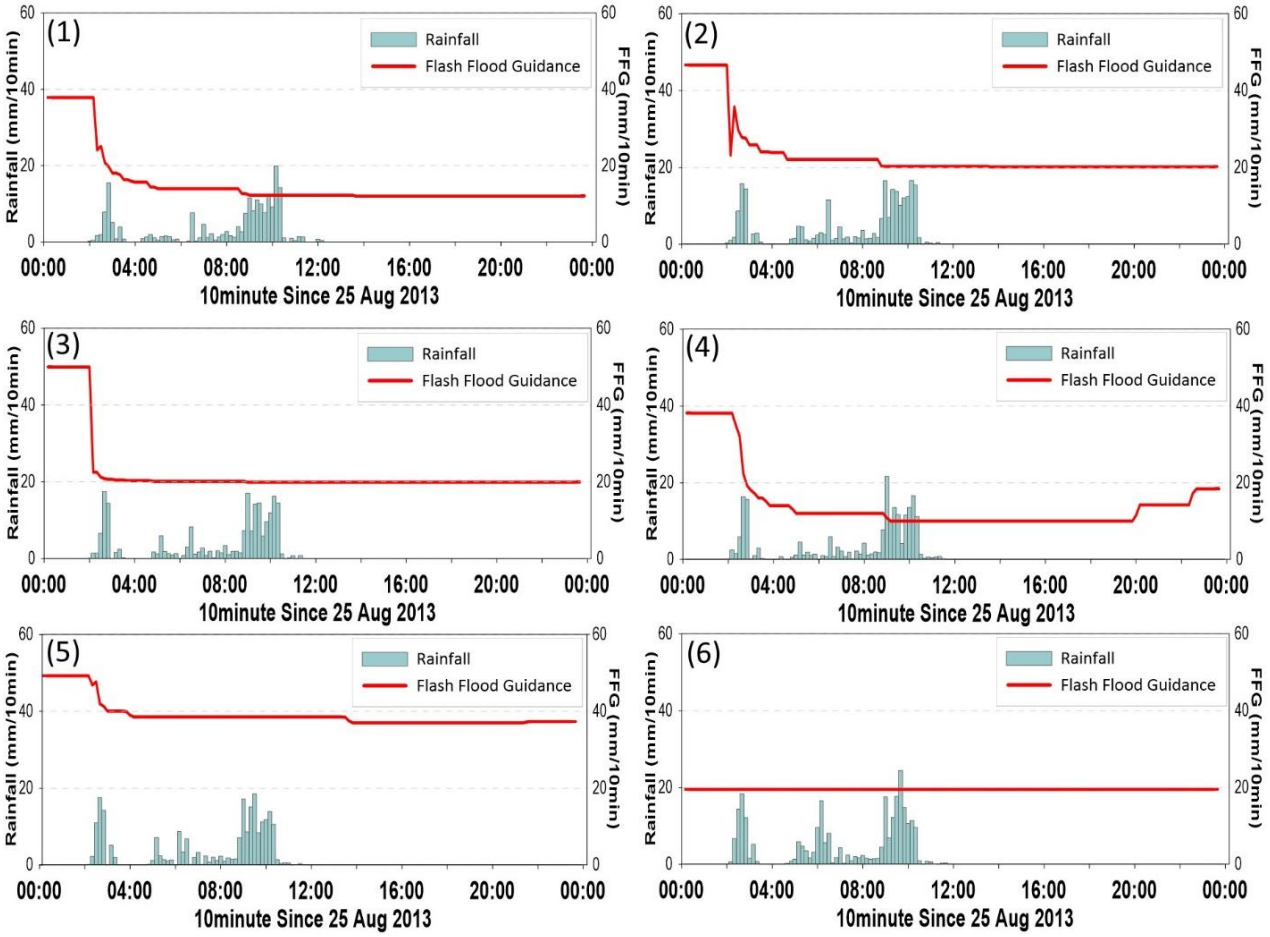

Figure C.8 Evaluation of Flash Flood guidance on the watersheds on 25th August 2013.

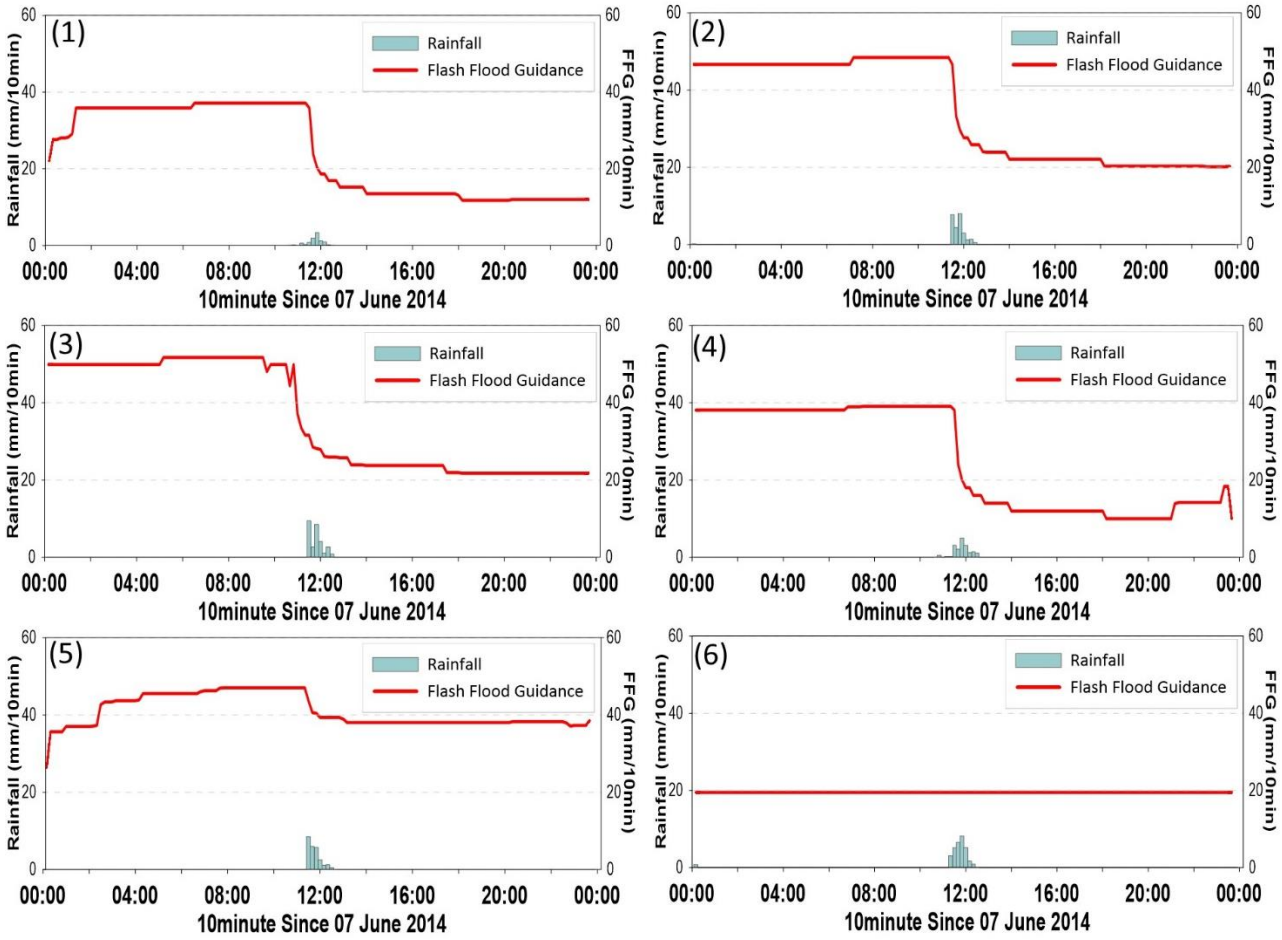

Figure C.9 Evaluation of Flash Flood guidance on the watersheds on 7th June 2014.